DETERMINING CHARGE DISTRIBUTION OF METAL OXIDE SURFACES WITH AFM USING COLLOID PROBE TECHNIQUE

A Thesis Submitted to
the Graduate School of Engineering and Sciences of
İzmir Institute of Technology
in Partial Fulfillment of the Requirements for the Degree of

MASTER OF SCIENCE

in Chemical Engineering

by
Ayşe GÜREL

December 2012
İZMİR

We approve the thesis of **Ayşe GÜREL**

Examining Committee Members:

_____
Prof. Dr. Mehmet POLAT
Department of Chemical Engineering
İzmir Institute of Technology

_____
Prof. Dr. Metin TANOĞLU
Department of Mechanical Engineering
İzmir Institute of Technology

_____
Assoc. Prof. Dr. Ekrem ÖZDEMİR
Department of Chemical Engineering
İzmir Institute of Technology

4 December 2012

_____
Prof. Dr. Mehmet POLAT
Supervisor
Department of Chemical Engineering
İzmir Institute of Technology

_____
Prof. Dr. Mehmet POLAT
Head of the Department of
Chemical Engineering

_____
Prof. Dr. R. Tuğrul SENGER
Dean of the Graduate School of
Engineering and Sciences

ACKNOWLEDGMENTS

First and foremost, I would like to express my gratitude to my supervisor Prof. Dr. Mehmet POLAT for his supervision, academic guidance, encouragement and insight throughout my thesis study.

Secondly, I acknowledge the Scientific and Technological Research Council of Turkey (TÜBİTAK), one of the distinguished institutions of my country, for granting me a graduate scholarship.

I also owe many thanks to Gülnihal Yelken Özek for her valuable helping in the laboratory, experience, motivations, understanding during the study.

I would like to thank to Prof. Dr. Hürriyet Polat for her helping in Particle Size distribution analysis.

I am grateful to Assoc. Prof. Ekrem Özdemir at İzmir Institute of Technology in the Department of Chemical Engineering for his valuable help in Zeta Potential Measurement analysis.

I thank to all my friends, research assistants and technicians in İzmir Institute of Technology for their helps and friendships.

Last but not least, I am indebted the greatest thanks and gratitude to my patient and gentle family, İsmail Gürel, Ayten Gürel and Erdoğan Gürel whom this study is dedicated. Without their unconditional encouragement, support and love, my M.S. studies might have never been completed.

ABSTRACT

DETERMINING CHARGE DISTRIBUTION OF METAL OXIDE SURFACES WITH AFM USING COLLOID PROBE TECHNIQUE

Colloidal systems of micron-sized particles dispersed in a solvent are widely encountered in numerous industries. Homogeneity, dispersibility, rheology and forming characteristics of these systems depend solely on particles-particle interactions which in turn are determined by Van der Waals (vdW) and Electrical Double Layer (EDL) forces.

The vdW forces are not affected by system chemistry. However, the EDL forces, which arise from the charging of on solid surfaces in a solvent, vary significantly with solution chemistry. So, manipulation of electrical forces is used widely in industrial applications to manipulate colloidal systems.

Colloidal particles in solution carry a distribution of positive, negative and neutral charges depending on solution chemistry. Electrophoretic potential mesurements or colloidal titration methods yield only an average charge for the whole population, not the charge distribution on each particle surface. The streaming potential techniques also provide an average charge on the surface.

Currently, there is no accepted technique to determine the charge distribution on solid surfaces. This work aims at using Atomic Force Microscopy (AFM) as a charge probe to achieve exactly this. The work improves on a recent study (Yelken, 2010) which used commercial SiN_4 cantilevers to determine the charge distribution on quartz and sapphire surfaces by replacing SiN_4 cantilevers with custom-made colloid probes of desired material (quartz in this case) to probe the surface. The current work which improves the flexibility and resolution of the method was tested with two quartz and sapphire surfaces under different electrolytic conditions.

ÖZET

METAL OKSİT YÜZEYLERİNİN YÜK DAĞILIMININ KOLLOİD UÇ METODU KULLANILARAK ATOMİK KUVVET MİKROSKOBU İLE BELİRLENMESİ

Mineral, seramik, çevre, biyoloji, boya, ilaç, kozmetik endüstrilerinde sulu çözeltilerde dağılmış kolloidal tanelerin homojenitesi, dagıtılabilirliği, kararlılığı ve şekillendirilebilirliği bu endüstrilerdeki uygulamaların başarısını belirler. Bu özelliklerin kontrolü, sistemi oluşturan tanelerin karşılıklı etkileşimlerinin kontrol edilebilmesine bağlıdır. Sistemdeki diger bileşenlerin (yüzey aktif maddeler, proteinler) tane yüzeylerine adsorpsiyonu da bu etkileşimler tarafından belirlenir.

Van der Waals (vdW) ve Elektriksel Çifte Tabaka (EDL) kuvvetleri, bu etkileşimlerin başlıca bileşenleridir. Tanelerin iç yapısına dayalı olan VdW etkileşimleri bir kolloidal sistem için sabit kabul edilebilir. Tanelerin çözeltide kazandıkları yüzey yükleri tarafından belirlenen EDL kuvvetleri ise çözelti kimyasına bağlı olarak büyük değişimler gösterir. Bu nedenle, EDL kuvvetlerinin manipülasyonu, kolloid sistemlerin kontrolünde kullanılan başlıca yöntemdir.

Sulu çözeltilerde dağılmış metal oksit yüzeylerinde, pH ya bağli olarak, artı ve eksi yükler oluşur. Bu yüklerin oranları yüzeyin yük dağılımını belirler ve tane-tane etkileşiminde önemli rol oynar. Yüzey yüklenmesinin ölçülmesinde kullanılan elektroforetik ya da titrasyon yöntemleri yüzey yük dağılımı degil, sistemin ortalama yük değerini vermektedir. Hali hazırda yüzey yük dağılımını belirlemede kullanılan bir teknik yoktur. Ticari SiN_4 kantilever kullanılarak kuvarz ve safir yüzeylerinde yüzey yükü belirlenmesi çalışması G.Yelken (Yelken, 2010) tarafından gerçekleştirilmiştir. Bu çalışmanın amacı standard AFM ucu yerine, istenen bir malzemeden üretilen küresel AFM uçları ile (Kolloid Prob Metodu) değiştirilerek yöntemin geliştirilmesidir.

Bu çalışmada, alumina ve silika gibi örnek metal oksit yüzeyleri ile silica tozlarından yapılan kolloid problar arasında, farklı çözelti koşullarında, AFM kuvvet ölçümleri yapılmıştır. Bu kuvvetlerden teorik analizlerle elektrostatik bileşenin izole edilmesi sayesinde taranan yüzeyin yük dağılımı elde edilmiştir.

TABLE OF CONTENTS

LIST OF FIGURES

LIST OF TABLES

LIST OF SYMBOLS

A_{ij} Hamaker constant for interaction of particles i and j

a,b Lennard-Jones parameters

b Width of the cantilever (μ)

c Speed of light (2.997925×10^8 m/sec)

c Contact point in force measurement (m)

C_0 Electrolyte concentration of the solution

D Vertical piezo movement in force measurement (m)

e Electronic charge (1.602189×10^{-19} C)

F Faraday constant (9.64845×10^4 C/mole)

F_{AFM} Interaction force between a colloidal probe and flat plate in force measurement ($F_{AFM} = k_n x$; N)

F_{el} Electrostatic pressure between plates (N/m^2)

F_e Dimensionless electrostatic pressure between paltes; $F_e = f_e/2RTC_0$

F_{DLVO} Net interaction pressure between two flat plates (N/m^2)

F_{vdw} Van der Waals interaction pressure between two flat plates (N/m^2)

G_H Free energy of the electrical double layer system when surfaces are separated by a distance of H

G_∞ Free energy of the double layer system when surfaces are separated by a distance of infinity

h Planck's constant (6.626176×10^{-34} J.sec)

h Gap length between two surfaces (m)

h Probe-to-surface separation in force measurement (h=(D-c)-x; m)

H Dimensionless distance between plates; $H = \kappa h$

I Molar electrolyte concentration (M)

k Boltzmann constant (1.380662×10^{-23} J/K)

k_n Spring constant for the cantilever (N/m)

L Length of the cantilever (μ)

M_i Molecular weight of component i (kg/mole)

m_e Rest mass of electron (9.10939×10^{-31} kg)

n_i Refractive index of material i

N_A Avagadro's number

Q_f Quality factor the cantilever oscillations

p Overall pressure between plates (N/m^2)

P Overall dimensionless electrostatic pressure between plates; $P=p/2RTC_0$

R Particle radius (m)

r Radial coordinate

R The gas constant (8.31441J/mol.K)

Re Reynolds number

S_1 Dimensionless surface charge density on plate 1 at separation H; $S_1=\sigma_1{}^2/2\varepsilon\varepsilon_0 RTC_0$

S_2 Dimensionless surface charge density on plate 2 at separation H; $S_2=\sigma_2{}^2/2\varepsilon\varepsilon_0 RTC_0$

$S_{1\infty}$ Dimensionless surface charge density on plate 1 at infinite seperation; $S_{1\infty}{}^2=2\cosh Y_{1\infty} - 2$

$S_{2\infty}$ Dimensionless surface charge density on plate 2 at infinite seperation; $S_{2\infty}{}^2=2\cosh Y_{2\infty} - 2$

T Absolute temperature (K)

x Distance into the solution fromplate 1 located at x=0

x Distance between molecules

x Distance from the surface in the double layer (m)

X Output signal by the photodiode for the overall bending of the cantilever in force measurement (mV)

X_0 Output signal by the photodiode when two surface are not interacting (mV)

X Dimensionless distance into solution from plate 1 located at X=0; $X=\kappa x$

$X_{1,2}$ Dimensionless locations X_1 and X_2 in the diffuse layer with potential Y

X_m The distance of the point where $Y=Y_m$ plate 1

X'_m The distance of the point where $Y=Y_m$ plate 2

Y Dimensionless potential in solution at a point X between the plates

Y_1 Dimensionless surface potential on plate 1 at separation H; $Y_1=zF\psi_1/RT$

Y_2 Dimensionless surface potential on plate 2 at separation H; $Y_2=zF\psi_2/RT$

$Y_{1\infty}$ Dimensionless surface potential on plate 1 at infinite separation; $Y_{1\infty}=zF\psi_{1\infty}/RT$

$Y_{2\infty}$ Dimensionless surface potential on plate 2 at infinite separation; $Y_{2\infty}=zF\psi_{2\infty}/RT$

Y_m Real or imaginary potential at point X_m where dY/dX=0

z Valence of the electrolyte

$\alpha_{0,i}$ Static polarizability of molecule i (1.61×10^{-40} C^2m^2/J for water)

$\alpha^*_{0,i}$ Static polarizability volume of molecule i (1.45×10^{-30} m^3 for water; $\alpha^*_{0,i} = \alpha_{0,i} / 4\pi\varepsilon_0$)

β_{ij} London parameter for molecules i and j ($J.m^6$)

δ Thickness of the interacting plates

ε Relative permittivity (78.5 for water)

ε_0 Permittivity of vacuum (8.854×10^{-12} $C^2/J.m$)

ϕ Integration constant; varies with plate separation H

ϕ_K Energy of Keesom (dipole-dipole) interaction between atoms or molecules (J)

ϕ_D Energy of Debye (dipole-induced dipole) interaction between atoms or molecules (J)

ϕ_L Energy of London (induced dipole-induced dipole) interaction between atoms or molecules (J)

ϕ_{vdw} Energy of van der Waals attraction between atoms or molecules (J)

ϕ_{rep} Energy of electronic repulsion between atoms or molecules

κ Reciprocal thickness of the double layer or Debye-Hückel parameter (m^{-1})

λ_0 Characteristic wavelength of the electronic motion

μ_i Dipole moment of molecule i (6.17×10^{-30} C.m for water)

μ_f Viscosity of fluid in which cantilever vibrates (typically air; 1.79×10^{-5}kg/m.sec)

$\nu_{0,i}$ Frequency of the electron for molecule i (2.1×10^{15} Hz for water)

$\nu_{v,i}$ Characteristic dispersion frequency of material i

ρ_i Density of material i (kg/m^3)

ρ_f Density of fluid in which cantilever vibrates (typically air; 1.23 kg/m^3)

γ_0 A parameter which is equal to $zF\varphi_0/4RT$

σ_1 Surface charge density on first plate at separation h (C/m^2)

σ_2 Surface charge density on second plate at separation h (C/m^2)

σ_{0i} Surface charge density of plate i (C/m^2)

$\sigma_{0i,\infty}$ Surface charge density of plate i at infinite separation (C/m^2)

ω_f Cantilever's fundamental resonance frequency (hertz)

$\Psi(x)$ The value of potential in the double layer at point x between two flat plates (volts)

$\Psi(x)$ Potential in solution at a point X between the plates (volts)

Ψ_{0i} Surface potential of plate i (volts)

$\Psi_{0i,\infty}$ Surface potential of plate i at infinite separation (volts)

Ψ_1 Surface potential on plate 1 at separation h (volts)

Ψ_2 Surface potential on plate 2 at separation h (volts)

$\Psi_{1\infty}$ Surface potential on plate 1 at infinite separation (volts)

$\Psi_{2\infty}$ Surface potential on plate 2 at infinite separation (volts)

CHAPTER 1

INTRODUCTION

1.1. Interactions Among Particles in a Colloidal System

Mineral, ceramic, environment, biology, paints, pharmaceuticals, cosmetics and a variety of industries deal with colloidal systems which are composed of micron sized particles dispersed in solvents such as water, alcohol, oil. Control and manipulation of homogeneity, stability, rheology, transport and forming characteristics of such colloidal systems depend on the mutual interactions among the particles making up these systems. For example, whether the particles in a colloidal dispersion repulse or attract each other will determine if the dispersion will remain dispersed and stable or if the particles will tend to agglomerate. Also, surface active agents (surfactants) or other dissolved species in the same system also interact with the particles depending on the magnitudes of these interactions. Therefore, control and manipulation of the particle-particle interactions, rather of the forces leading to the development of these interactions, is extremely critical in proper handling of all the above applications. For example, the structure, rheology, plasticity and forming behavior of the green ceramic body determine whether the ceramic mold will be filled homogeneusly and properly without minor defects by the green body, hence, the success of all the following steps such as sintering. This directly affects the final outcome and the quality of the ceramic products which tend to move towards high value-added materials of special shapes and properties. However, providing the green body with the desired paste properties listed above requires a good understanding of the interactions taking place among the particles constituting the green body. The presence of numerous dedicated books on particle interactions in ceramic applications points out the importance of the subject (Pugh and Bergstrom, 1994; Holmberg, 2002). This example for the ceramic industry can easily be extended to many other applications ranging from biotechnology to metallurgy.

The interaction among particles develops due to the presence of present forces acting among the particles which constitute a colloidal dispersion. The two most important components of these interactions are van der Waals and Electrical Double

Layer forces. The interplay of these two forces and how they affect the properties of a colloial system is described ingeniously by the well-known DLVO theory (Derjaguin and Landau, 1941; Verwey and Overbeek, 1948).

There are also other forces besides the van der Waals and electrical double layer forces depending on the system. For example, if dissolved surface active species or polymers present in the system and if they are adsorbed on the particles, steric forces develop due to the interaction between these molecules as particles approach. Also, there are so called structural forces which develop due to different interactions between the solvent and the solid so called hydration and hydrophobic forces. For example, structure of water on hydrophillic silica surface is diffferent than that on hydrophobic graphite surface. However, these forces are secondary to both van der Waals and electrical double layer forces since they become effective at very short ranges (in the order of less than 5 nm) and govern not the approach of the particles, but the final magnitude of the contact. Therefore, they could be neglected at ordinary distances where the particles start interacting or the experimental conditions may be selected such that these forces are not present (such as no surface active agents in the solution).

For these reasons, in order to describe interaction among particles of a colloidal system in this manuscript, van der Waals and Electrostatic Forces will be detailed.

1.1.1. Van der Waals Interactions

Van der Waals interaction mainly arises from the fluctuations in the electron densities around individual atoms and molecules which make up the macroscopic bodies.

A theory of van der Waals interactions with respect to macroscopic bodies will be presented. First, the van der Waals interactions between atoms and molecules are discussed. The van der Waals interactions between macroscopic bodies will be taken up next and the relevant theories will be presented.

1.1.1.1. Van der Waals Interactions Between Atoms and Molecules

The interaction between colloidal particles are referred to as “macroscopic interactions” in the literature since these particles are large compared to atomic and

molecular dimensions. A quantitative analysis of this interaction requires a good understanding of the energy of interaction between individual atoms and molecules.

Molecules at small distances, exert strong repulsion on each other because of the overlapping electron probability densities. The energy of this very short-range repulsion can be crudely approximated by $\phi_{rep} \cong \Lambda x^{-n}$. Λ is a constant and n is a large integer between 8 and 18, but is usually taken as 12. Due to this large n value which results in a very sharp drop, ϕ_{rep} is called the Short-Range Repulsion Energy.

There is also an attractive energy operating between atoms and molecules. This attraction is generally called the van der Waals attraction since it was first foreseen by van der Waals in his Gas Law. Van der Waals Attraction originates from different reasons and historically is divided into three Keesom, Debye and London Interactions.

If molecules 1 and 2 have permanent electric dipole moments μ_1 and μ_2 , the force one molecule exerts on the other will depend on the dipole moments, separation between the molecules and the relative orientation of the two dipoles. If all the dipoles are oriented completely randomly, there will be as much attractive interactions as repulsive ones, hence the overall interaction energy will be zero. However, the Boltzmann factor ($e^{-v_0/kT}$) favors attractive orientations which have low energies over the repulsive ones. Due to the involvement of the Boltzmann distribution factor, the dipole-dipole interactions are temperature dependent. The orientation-averaged potential energy of the two permanent dipoles is calculated by Keesom (1921). The resulting equation, called the Keesom Equation is given by:

$$\phi_K = -\frac{2}{3}\frac{\mu_1^2 \mu_2^2}{kT(4\pi\varepsilon_0)^2 x^6} \tag{1.1}$$

For two identical molecules the Keesom Equation becomes:

$$\phi_K = -\frac{2}{3}\frac{\mu^4}{kT(4\pi\varepsilon_0)^2 x^6} \tag{1.2}$$

The permanent dipole moment of one molecule will induce a dipole moment in a second molecule irrespective of whether the second molecule has a permanent dipole moment. The induced dipole is instantaneous compared to the molecular motions due to

thermal agitation. Therefore, the potential energy between a dipole and an induced dipole is independent of temperature. The attractive interaction between the permanent moment of one molecule and the induced moment of the second was calculated by Debye (1920). It is given by the Debye equation:

$$\phi_D = -\frac{(\alpha_{0,2}\mu_1^2 + \alpha_{0,1}\mu_2^2)}{(4\pi\varepsilon_0)^2 x^6} \tag{1.3}$$

For two similar molecules the Debye equation can be written as follows:

$$\phi_D = -\frac{2\alpha_0\mu^2}{(4\pi\varepsilon_0)^2 x^6} \tag{1.4}$$

Even if neither molecule has a permanent dipole moment, there will still be an attractive force between the molecules. This must be so, otherwise gases such as He or N_2 would not condense to form liquids. Since electrons are in a continuous motion around the nuclei, electron density may be concentrated on one side of the molecule at a given instant. This leads to the development of an instantaneous dipole. The instantaneous dipole of a molecule induces a dipole in a nearby molecule. The interaction between the instantaneous dipole moment and the induced dipole moment produces a net attraction. The interaction in these conditions is calculated by the following formula which is given by London equation (1930).

$$\phi_L = -\frac{3}{2} h\left(\frac{\nu_{0,1}\nu_{0,2}}{\nu_{0,1} + \nu_{0,2}}\right)\frac{\alpha_{0,1}\alpha_{0,2}}{(4\pi\varepsilon_0)^2 x^6} \tag{1.5}$$

The London equation is written for two identical molecules:

$$\phi_L = -\frac{3}{4}\frac{h\nu_0\alpha_0^2}{(4\pi\varepsilon_0)^2 x^6} \tag{1.6}$$

The relationship between the refractive index (n_i) with the capacity of the static polarization $\alpha_{0,i}$ is expressed in the following equation:

$$\alpha_{0,i} = \frac{3}{4\pi N_A} \frac{(n_i^2 - 1)}{(n_i^2 + 2)} \frac{M_i}{\rho_i} \tag{1.7}$$

The characteristic frequency of the molecule, $\nu_{0,i}$, is given by the expression:

$$\nu_{0,i} = \frac{1}{2\pi} \sqrt{\frac{e^2}{\alpha_{0,i} m_e}} \tag{1.8}$$

Fluctuations in the electron density which lead to London interactions have frequencies in the ultraviolet range of the electromagnetic spectrum and play an important part in optical dispersion. This is why the London interactions are also called "dispersion interactions" in the literature.

The sum of these three attractive interactions constitutes the van der Waals (vdW) interaction, ϕ_{vdw}. In the literature, ϕ_{vdw} is called long-range interactions because it decays much more slowly compared to ϕ_{rep}. Then, for a pair of identical molecules is given below:

$$\phi_{vdw} = -(\phi_D^{'} + \phi_K^{'} + \phi_L^{'}) x^{-6} = -\left[\frac{\frac{2\mu^4}{3kT} + 2\alpha_0 \mu^2 + \frac{3h\nu_0 \alpha_0^2}{4}}{(4\pi\varepsilon_0)^2} \right] x^{-6} \tag{1.9}$$

If all the terms inside the parenthesis are gathered in a constant β_{11} the attraction energy is presented in the formula:

$$\phi_{vdw} = -\beta_{11}\, x^{-6} \tag{1.10}$$

The force of attraction between two molecules is given as:

$$F_{vdw} = \frac{d\phi_{vdw}}{dx} = 6\beta_{11}\, x^{-7} \tag{1.11}$$

The term β_{11} is called the vdW parameter. At small separations vdW interactions are large but they are usually smaller than chemical binding forces. For large

separations they are weak compared to the electrostatic forces. The contribution of the Keesom (ϕ_K), Debye (ϕ_D) and London (ϕ_L) interactions to the overall vdW interaction is different for different substances. For polar molecules such as water the Keesom interaction is dominant whereas for apolar hydrocarbons the overall interaction energy is almost completely made up of the London contribution.

Lennard-Jones Potential: If the intermolecular potential energy (ϕ) is the sum of the short-range (ϕ_{rep}) and the long-range (ϕ_{vdw}) potentials, we get a function with the form:

$$\phi = \frac{\Lambda}{x^n} - \frac{\beta}{x^6} \tag{1.12}$$

The most widely used intermolecular potential is the Lennard-Jones 6-12 potential where *n* is taken as 12. It is given in the following equation:

$$\phi = a\left[(\frac{b}{x})^{12} - (\frac{b}{x})^6 \right] \tag{1.13}$$

where *a* is the depth of the minimum in potential and b is the intermolecular distance at which ϕ=0. Figure 1.1 presents the Lennard-Jones potential for CH_4 molecule. The values of the a and b parameters for various molecules can be found in Levine (1995) and Atkins (1997). It should be noted that an exponential decay term in the form ($e^{(-x/b)}$) is suggested in order to account for the repulsion energy instead of the ($(b/x)^{12}$) term in molecular dynamics calculations.

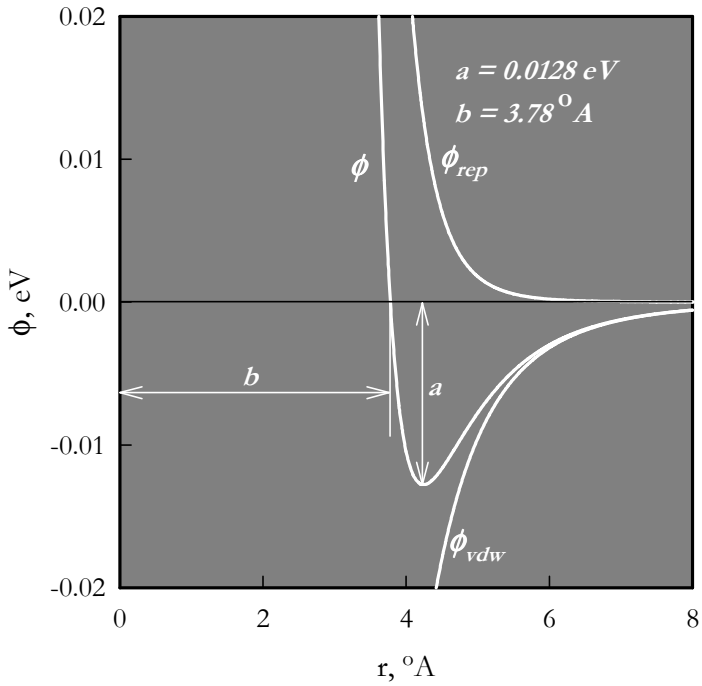

Figure 1.1. Lennard-Jones intermolecular potential for CH_4
(Source: Polat and Polat, 2000-a)

1.1.1.2. Van der Waals Interactions Between Macroscopic Systems

The short-range repulsion interaction is extremely important in molecular dimensions due to its inverse 12^{th} power dependence. However, it has no practical importance for macroscopic bodies which interact through much larger distances. The vdW attraction energy with its inverse 6^{th} power dependence, on the other hand, is felt at much larger distances compared to the electronic repulsion. Hence, it has important implications in the behavior of macroscopic bodies. It should be noted that the Keesom and Debye interactions, which arise when at least one of the molecules has a permanent dipole, can be ignored in the interactions of the macroscopic bodies since their range of action is always small (Gregory, 1970). Hence, only the London interactions need to be considered in the calculation of the vdW constant, β. For this reason β is also commonly called as the London constant in the literature.

‘’Macroscopic bodies” means colloidal structures, macromolecules and substrates in various combinations. Coagulation among particles, adhesion between particles and surfaces, adsorption of surfactant molecules onto various surfaces, adhesion between bubbles and particles and coalescence of oil droplets are important

examples for these interactions. They are extremely important processes in ceramic science, mineral processing, food and drug industry and surface coating processes. The two different approaches have been developed to the calculate of the attractive interaction energy between macroscopic bodies:

The first one was attributed to Hamaker (1937) and is called Microscopic Approach. The second one is named as Macroscopic Approach and develoed by Liftshitz (1956).

Microscopic Approach: Following the theory of London which explains the origins of vdW forces between atoms or molecules, several scientists (Bradley, 1932; de Böer, 1936 and Hamaker, 1937) attempted to utilize it to calculate the attractive forces between macroscopic bodies. Hamaker developed a successful theory based on pairwise summation of intermolecular forces. This theory is called as the Microscopic Approach in the literature since its starting point is microscopic individual intermolecular interactions. The following paragraphs present a detailed discussion on the features of the Hamaker's microscopic theory.

It is based on taking two infinitely wide slabs with thickness δ separated by a distance H and pairwise adding the interection energy for each atom main grup the slabs. An annular ring inside the second slab with inner radius r, thickness dr and width dh (Figure 1.2). The number of atoms in the ring is is calculated by the formula below:

$$N_2 = 2\pi r \left(\frac{\rho_2 N_A}{M_2}\right) dr dh \tag{1.14}$$

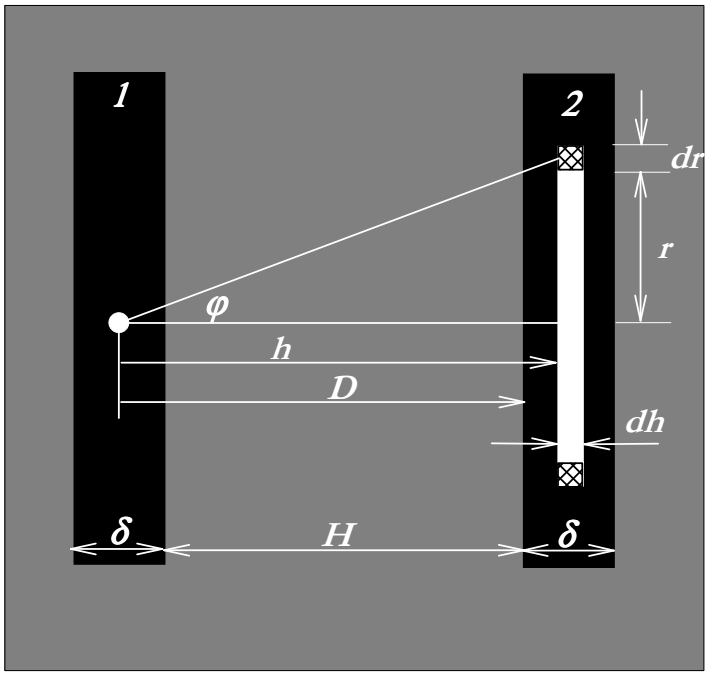

Figure 1.2. The geometry for the calculation of the attractive interaction energy between two infinite slabs (Source: Polat and Polat, 2000-a)

Here, $\rho_2 N_A/M_2$ is the number of atoms per unit volume of the slab. Then, according to Equation 1.11, the force between a single atom in slab 1 and all the atoms inside the annular ring in slab 2 is given by:

$$F_{12}^{'} = 12\pi r\left(\frac{\rho_2 N_A}{M_2}\right) Cos\varphi\, \beta_{12}\, x^{-7} dh dr \tag{1.15}$$

From the geometry of the slabs, $x = \sqrt{r^2 + h^2}$ and $\mathrm{Cos}\varphi = \mathrm{h}/(\mathrm{r}^2 + \mathrm{h}^2)^{0.5}$ can be calculated. Then, the force between a single atom in slab 1 and all the atoms in slab 2 is given as:

$$F_{12}^{'} = 12\pi\left(\frac{\rho_2 N_A}{M_2}\right)\beta_{12}\int_{r=0}^{\infty} r\left[\int_{h=D}^{D+\delta} \frac{h}{(r^2+h^2)^4} dh\right] dr \tag{1.16}$$

Integrating the above equation with respect to the distance h gives:

$$F_{12}^{'} = -2\pi(\frac{\rho_2 N_A}{M_2})\beta_{12}\int_{r=0}^{\infty}\left[\frac{1}{r^2+(D+\delta)^2}-\frac{1}{r^2+D^2}\right]dr \tag{1.17}$$

Another integration with respect to the radius r yields:

$$F_{12}^{'} = \frac{\pi}{2}(\frac{\rho_2 N_A}{M_2})\beta_{12}\left[\frac{1}{D^4}-\frac{1}{(D+\delta)^4}\right] \tag{1.18}$$

The force of interaction between all the atoms in slab 1 and all the atoms in slab 2 is:

$$F_{vdw} = \int_{H}^{H+\delta} F_{12}^{'} d\forall_1 \tag{1.19}$$

or

$$F_{vdw} = \frac{\pi}{2}(\frac{\rho_1 N_A}{M_1})(\frac{\rho_2 N_A}{M_2})\beta_{12}\int_{H}^{H+\delta}\left[\frac{1}{D^4}-\frac{1}{(D+\delta)^4}\right]dD \tag{1.20}$$

The solution of the above equation is the force of interaction per unit area of the slabs between the two infinitely wide slabs separated by distance H:

$$F_{vdw} = \frac{\pi}{6}(\frac{\rho_1 N_A}{M_2})(\frac{\rho_2 N_A}{M_2})\beta_{12}\left[\frac{1}{h^3}+\frac{1}{(h+2\delta)^3}-\frac{2}{(h+\delta)^3}\right] \tag{1.21}$$

For infinitely thick slabs ($\delta \rightarrow \infty$) this equation simplifies to

$$F_{vdw} = \frac{A_{12}}{6\pi h^3} \tag{1.22}$$

where the constant A is called the Hamaker Constant and it is calculated as below:

$$A_{12} = \pi^2(\frac{\rho_1 N_A}{M_2})(\frac{\rho_2 N_A}{M_2})\beta_{12} \tag{1.23}$$

The potential energy of interaction is obtained by integrating Equation 1.22 once more with respect to distance from H to infinity:

$$V_{vdW} = \int_{H}^{\infty} F_{vdw}\, dx \tag{1.24}$$

The resulting equation is in the form:
for slabs of thickness δ:

$$V_{vdW} = -\frac{A_{12}}{12\pi}\left[\frac{1}{H^2} + \frac{1}{(H+2\delta)^2} - \frac{1}{(H+\delta)^2}\right] \tag{1.25}$$

for slabs with infinite thickness:

$$V_{vdW} = \frac{A_{12}}{12\pi H^2} \tag{1.26}$$

It is important to note that Equation 1.11 which gives the attraction energy between two molecules is the starting point in the calculation of the interaction energy between macroscopic bodies. This simply means that colloidal and interfacial processes such as flocculation, adsorption, adhesion and spreading have the same molecular roots with such phenomena as boiling, evaporation, deviation from the ideal gas law.

Scaling-up of the Molecular Interaction Energy: An important question regarding the foregoing analysis is whether the scaling up of the molecular interaction energy to macroscopic dimensions is an accurate assumption. In order to answer this when take two identical spheres A and B of radius R_1 interacting through a gap X_1. Then, the long-range interaction energy will simply be in the form:

$$\phi_{vdw}^{AB} = \beta \int_{V_A}\int_{V_B} X^{-6} dV_A dV_B \tag{1.27}$$

Now, when take another couple of identical spheres C and D with radius R_2 interacting through the gap X_2 such that $R_2 = f R_1$ and $X_2 = f X_1$. That is, both the radii of the spheres

and the gap for the second case are f times larger than the first. The energy of interaction for this case will be:

$$\phi_{vdw}^{CD} = \beta \int_{V_C} \int_{V_D} (fX)^{-6} dV_C dV_D \tag{1.28}$$

$$\phi_{vdw}^{CD} = \beta \int_{V_C} \int_{V_D} (fX)^{-6} d(\frac{4}{3}\pi R_2^3)_C d(\frac{4}{3}\pi R_2^3)_D \tag{1.29}$$

$$\phi_{vdw}^{CD} = \beta \int_{V_C} \int_{V_D} (fX)^{-6} d\left[\frac{4}{3}\pi (fR_1)^3\right]_C d\left[\frac{4}{3}\pi (fR_1)^3\right]_D \tag{1.30}$$

$$\phi_{vdw}^{CD} = f^{-6} f^3 f^3 \beta \int_{V_C} \int_{V_D} X^{-6} dV_A dV_B \tag{1.31}$$

It is easy to see that:

$$\phi_{vdw}^{CD} = \phi_{vdw}^{AB} \tag{1.32}$$

This is an important result since it shows that the interaction energy between smaller bodies (molecules) can be scaled up to larger sizes (macromolecules, particles, etc.).

Macroscopic Approach: The Hamaker treatment of vdW interaction between macrobodies suffers from three restrictions:

(a) the assumption of pairwise additivity of molecular interactions; Event though perfectly accurate for the rarefied systems such as gases, pairwise additivity may result in erroneous results in condensed systems. Most probable source of the error is the screening effect. Hamaker's theory does not distinguish between the surface and the bulk molecules. However, the interactions between the two molecules inside the bulks of macrobodies may be screened by the surface molecules significantly.

(b) the neglect of the separating medium; Hamaker theory does not directly include the effect of the molecules of the intervening medium. Depending on the type of the medium, even the sign of the interaction energy may change.

(c) the neglect of the retardation effect.

All of these shortcomings were remedied in a more comprehensive theory by Liftshitz (1956). The theory of Liftshitz was generalized by Dzyaloshinski, Liftshitz and Pitaevski (1961) and is also called as the DLP theory. The most important feature of the theory is that it is entirely based on measurable bulk properties rather than molecular parameters as in the Hamaker's theory. For this reason it is named as the Macroscopic Approach. The bulk properties, which are the basis of the theory, are the dielectric properties of the matter. The development of the theory involves advanced statistical mechanical and quantum field theoretical arguments which can not be repeated here. The form of the Liftshitz equation, which gives the non-retarded force for two dissimilar plates 1 and 2 separated by medium 3 for separation small distances (<20 ^{o}A) is as follows:

$$F_{132} = \frac{h}{8\pi^2 H^3}\int_0^\infty \sum_{n=1}^{\infty}\left[\frac{1}{n^3}\left(\frac{\varepsilon_1(i\xi)-\varepsilon_3(i\xi)}{\varepsilon_1(i\xi)+\varepsilon_3(i\xi)}\right)\left(\frac{\varepsilon_2(i\xi)-\varepsilon_3(i\xi)}{\varepsilon_2(i\xi)+\varepsilon_3(i\xi)}\right)\right]^n d\xi \qquad (1.33)$$

It is important to note that the effect of the medium is automatically included in the Liftshitz theory. For the two plates interacting through vacuum, the ε3(iξ) value for the medium should simply be replaced by the dielectric constant of vacuum, which is medium 1. For practical purposes only the first two terms of Equation 1.33 (n=1 and n=2) are enough since this corresponds to 98% of the exact value of the integral. Even neglecting the second term (n=2) provides an accuracy of 87% (Israelachvili, 1972).
If the whole integral is ϖ, the resulting equation is:

$$F_{132} = \frac{h\varpi_{132}}{8\pi^2 H^3} \qquad (1.34)$$

The product hϖ is named as the Liftshitz-vdW constant in the literature. It is important that both this equation and the Hamaker's equation for the plate-plate interaction energy (Equation 1.21) have the same functional dependence on H. If we equate Equations 1.21 and 1.34, it can be seen that there is a direct relationship between the Hamaker and Liftshitz vdW constants:

$$A = \frac{3}{4\pi} h\varpi \qquad (1.35)$$

Hamaker Constants: The predictions of the general Liftshitz theory and the Hamaker's approach for the interaction energy between two plates have the same dependence on the distance of separation. Therefore, an accurate determination of the vdW interaction energy decrease to properly determining the Hamaker constant for the system in question. Various methods have been used to determine the Hamaker constant. They can be classified under three general category: 1) From molecular parameters 2) From bulk material parameters and 3) From experiments

A comprehensive compilation of Hamaker constants for a variety of materials are displayed in Table A.1 (Appendix A). The data includes the method of determination and the references in which they first cited for vacuum and water as the separating medium. (London, 1930; Eisenschitz and London, 1930; Slater and Kirkwood, 1931; Moelwyn and Hughes, 1961; Renne and Nijboer, 1967; Gregory, 1970; Visser, 1972).

It is clear from Table A1 the Hamaker constants, hence the magnitude of the vdW interaction energy, changes significantly deppending on whether the gap separating the macroscopic bodies is simply vacuum or contain another phase such as water. Therefore, an effective Hamaker constant A_{132} must be utilized for the two bodies 1 and 2 separated by a gap containing medium 3. The most commonly used method to determine A_{132} is to assume that the two particles interact through a pseudo-chemical reaction where the two particle-medium pairs (1-3 and 2-3) produces one particle-particle (1-2) and one medium-medium (3-3) pairs (Figure 1.3).

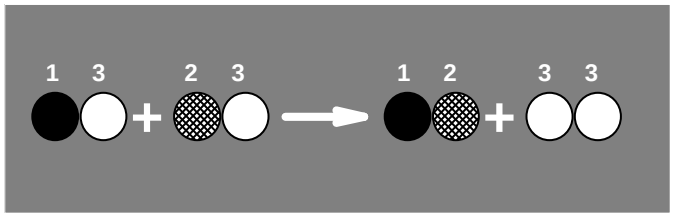

Figure 1.3. The thermodynamic path taken for calculating the effective hamaker constants (Source: Polat and Polat, 2000-a)

The change in the potential energy for such a process is illustrated in the following formula.

$$\Delta\phi = \phi_{12} + \phi_{33} - \phi_{13} - \phi_{23} \tag{1.36}$$

Since the energy of interaction between two colloidal particles is a direct function of the Hamaker constant for a given distance, the change in the potential energy can be written in terms of the Hamaker constants:

$$A_{132} = A_{12} + A_{33} - A_{13} - A_{23} \tag{1.37}$$

The value A_{132} is called the effective Hamaker constant. The interaction between the two materials i and j can be represented by the geometric mean of the interaction between i-i and j-j pairs to a good approximation as (Fowkes, 1967):

$$A_{ij} = \sqrt{A_{ii} A_{jj}} \tag{1.38}$$

Krupp (1967) has shown that this relationship holds within 95% accuracy. Then, combining Equations 1.37 and 1.38 give:

$$A_{132} = (\sqrt{A_{22}} - \sqrt{A_{33}})(\sqrt{A_{11}} - \sqrt{A_{33}}) \tag{1.39}$$

For the case where the two particles are identical (A_{11}=A_{22}), the effective Hamaker constant becomes A_{131} and is equal to:

$$A_{131} = (\sqrt{A_{11}} - \sqrt{A_{33}})^2 \tag{1.40}$$

Retardation Effect in vdW Interactions: If the two atoms are widely separated, time of the travel of electromagnetic field between them may be comparable with the fluctuation period itself. That is, when the reflected electromagnetic field is received by the first atom, its dipole may no longer be in phase with its neighbor. In this case, the inverse 6^{th} –order dependence should be expected to change. Since the propagation time for the electromagnetic radiation between two bodies is a function of x/c and the time it takes for an electron complete its orbit around the atom is $2\pi/\nu_0$, it is required that the retardation effect will be negligible if the molecular distance x is much smaller compared to the characteristic wave length. That is:

$$x << 2\pi c/\nu_0 = \lambda_0 \tag{1.41}$$

Casimir and Polder calculated ϕ_{vdw} for all x values (Casimir and Polder, 1948).

$$\begin{aligned} &\text{For} \quad x << \lambda_0 \quad \rightarrow \quad \phi_{vdw} = -\beta x^{-6} \\ &\text{For} \quad x >> \lambda_0 \quad \rightarrow \quad \phi_{vdw} = -\beta x^{-7} \end{aligned} \tag{1.42}$$

Casimir and Polder correction can be given as (Overbeek, 1952):

$$\phi_{vdw} = -\frac{3}{4}\frac{h\nu_0\alpha_0^2}{(4\pi\varepsilon_0)^2 x^6} f(p) \tag{1.43}$$

The dimensionless function f(p) is given as follows:

$$f(p)=1.01- 0.14p \text{ for } 1<p<3$$

where $p=2\pi x/\lambda 0$; (1.44)

$$f(p)=2.45/p- 2.04/p2 \text{ for } 3<p<\infty$$

It should be noted that the error is less than 10% at separations smaller than 100 nm, where the energy of interaction is most significant. However, in this study that the retardation effect will be ignored here because distance less than 20 nm.

1.1.2. Electrostatic Interactions

When two plates with a double layer of each own approach each other, they interact electrostatically. The magnitude of the energy of electrostatic interaction as a function of the interplate separation can be obtained from the changes in the osmotic pressure or free energy between the plates. A priori in defining the system for this purpose is the fact that the surfaces should be assumed to carry either constant surface potential or constant surface charge. Nevertheless, finding exact solutions is not possible without making certain approximations. Exact solutions are possible if one is

willing to use tables (Verwey and Overbeek, 1948; Overbeek, 1952) or numerical integration (Chan et al., 1980; Chan and Mitchell, 1983; Barouch and Matijevic, 1985). Below the details of how the energy of electrostatic interaction between two double layers with constant potential will be presented assuming that the Debye-Hückel approximation (φ0<25 mV) holds (Hogg et al., 1965). According to the Gouy-Chapman model of the electrical double layer, for low surface potentials (Debye-Huckel Approximation), the potential variation in the double layer in the x-direction is given as:

$$\frac{d^2\varphi}{dx^2} = \kappa^2\varphi \tag{1.45}$$

where ;

$$\kappa^2 = \frac{F^2}{\varepsilon\varepsilon_0 RT} I \tag{1.46}$$

Two flat plates with respective surface potentials $\varphi_{0,1}$ and $\varphi_{0,2}$ and H distance apart. The boundary conditions for this system are $\varphi=\varphi_{0,1}$ @ $x=0$ and $\varphi=\varphi_{0,2}$ @ $x=H$. Solution of the above equation with these boundary conditions gives the potential distribution between the plates as a function of distance (Figure 1.4).

$$\varphi_{12} = \varphi_{0,1}\, Cosh\kappa x + \left(\frac{\varphi_{0,2} - \varphi_{0,1}\, Cosh\kappa H}{Sinh\kappa H}\right) Sinh\kappa x \tag{1.47}$$

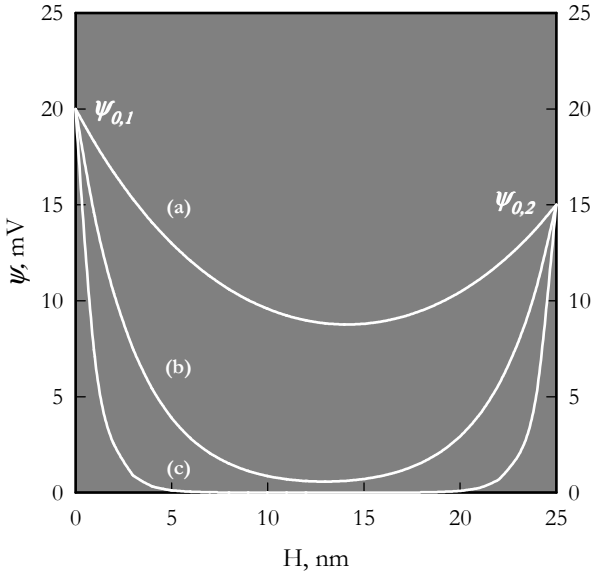

Figure 1.4. Change of electric potential between two flat plates 25 nm apart and of dissimilar surface potentials as a function of distance; (*(a) C_o=0.001 M,; (b) C_o=0.01 M,; (c) C_o=0.1 M*)(Source: Polat and Polat, 2000-b)

The potential energy of electrostatic interaction (V'_{el}) is equal to the change in free energy of the double layer system when the plates are brought together from infinity to a distance H.

$$V'_{el} = \Delta G = G_H - G_\infty \tag{1.48}$$

When the surface potential is constant and small, the free energy of a single double layer is given by (Verwey and Overbeek, 1948):

$$G = -\frac{1}{2}\sigma^s \varphi_0 \tag{1.49}$$

The free energy of the two interacting double layers (G_H) is equal to the sum of the free energies of the separate double layers:

$$G_H = -\frac{1}{2}(\sigma_1^s \varphi_{0,1} + \sigma_2^s \varphi_{0,2}) \tag{1.50}$$

The surface charge density at a plane surface is given by the folloiwng equation.

$$\sigma^s = -\varepsilon\varepsilon_0 \left(\frac{d\varphi}{dx}\right)\Big|_{x=0} \tag{1.51}$$

Electrostatic Potential Energy Between Parallel Plates: Taking the derivative of Equation 1.47 and replacing in Equation 1.51 gives:

$$\sigma_1^s = -\varepsilon\varepsilon_0\kappa(\varphi_{0,2}\cos ech\ \kappa H - \varphi_{0,1}\coth\ \kappa H) \tag{1.52}$$

$$\sigma_2^s = \varepsilon\varepsilon_0\kappa(\varphi_{0,2}\coth\ \kappa H - \varphi_{0,1}\cos ech\ \kappa H) \tag{1.53}$$

Substituting for $\sigma_1{}^s$ and $\sigma_2{}^s$ in Equation 50 gives:

$$G_H = \frac{\varepsilon\varepsilon_0\kappa}{2}\left[2\varphi_{0,1}\varphi_{0,2}\cos ec\ \kappa H - (\varphi_{0,1}^2 + \varphi_{0,2}^2)\coth\ \kappa H\right] \tag{1.54}$$

Then, as the separation of the plates becomes large:

$$G_\infty = -\frac{\varepsilon\varepsilon_0\kappa}{2}(\varphi_{0,1}^2 + \varphi_{0,2}^2) \tag{1.55}$$

Thus, from Equation 1.48

$$V_{el}^{'} = \frac{\varepsilon\varepsilon_0\kappa}{2}\left[(\varphi_{0,1}^2 + \varphi_{0,2}^2)(1 - \coth\ \kappa H) + 2\varphi_{0,1}\varphi_{0,2}\cos ech\ \kappa H\right] \tag{1.56}$$

Equation 1.56 expresses the electrostatic potential energy of interaction per unit area between two parallel, infinite, flat double layers as a function of the surface potential of each plate, and the separation between the plates.

Electrostatic Potential Energy Between Spherical Particles (Derjaguin's Approximation): Hogg et al. (Hogg et al., 1966) used Derjaguin's approximation, to calculate the interaction between double layers on spherical particles. In Derjaguin's approximation the thickness of the double layer is assumed to be small compared to the

particle size (κ^{-1}<<R). Hence, spherical particles may be assumed contain of infinitely thin parallel rings each with its own double layer stacked on top of each other. If each ring can be considered to be a flat plate with an area $2\pi rdh$ as $h \to 0$, the differential interaction energy for a given ring can be written as (Figure 1.5).

$$dV_{el} = 2\pi r V_{el}^{'} dh \tag{1.57}$$

where V'_{el} is given by Equation 1.56. The overall energy of interaction between the spherical double layers is then the sum of the interactions due to the each ring and is represented by the following formula.

$$V_{el} = \int_0^{\infty} 2\pi h V_{el}^{'} dh \tag{1.58}$$

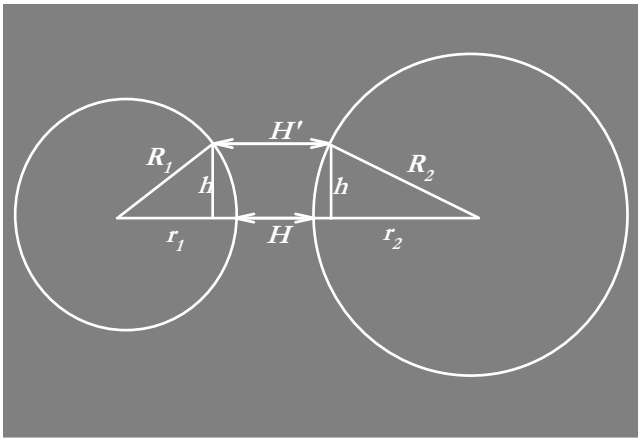

Figure 1.5. The geometry for the calculation of the electrostatic interaction energy between two spherical particles (Source: Polat and Polat, 2000-b)

From the geometry of Figure 1.5:

$$H'-H = (R_1 - r_1) + (R_2 - r_2) = (R_1 - \sqrt{R_1^2 - h^2}) + (R_2 - \sqrt{R_2^2 - h^2}) \tag{1.59}$$

$$H'-H = R_1 + R_2 - \sqrt{R_1^2 - h^2} - \sqrt{R_2^2 - h^2} \tag{1.60}$$

Differentiating with respect to H gives:

$$dH = \left(\frac{1}{R_1\sqrt{1-h^2/R_1^2}} + \frac{1}{R_2\sqrt{1-h^2/R_2^2}}\right)hdh \tag{1.61}$$

Since $h \to 0$

$$dH = \left(\frac{1}{R_1} + \frac{1}{R_2}\right)hdh \tag{1.62}$$

$$hdh = \left(\frac{R_1 R_2}{R_1 + R_2}\right)dH \tag{1.63}$$

Inserting Equation 1.56 and 1.63 in Equation 1.58 gives:

$$V_{el} = \pi\varepsilon\varepsilon_0\kappa\left(\frac{R_1 R_2}{R_1 + R_2}\right)\int_H^\infty \left[(\varphi_{0,1}^2 + \varphi_{0,2}^2)(1 - \coth\ \kappa H) + 2\varphi_{0,1}\varphi_{0,2}\cos ech\,\kappa H\right] dH \tag{1.64}$$

Solution of the integral results:

$$V_{el} = \pi\varepsilon\varepsilon_0\kappa\left(\frac{R_1 R_2}{R_1 + R_2}\right)(\varphi_{0,1}^2 + \varphi_{0,2}^2)\left[\frac{2\varphi_{0,1}\varphi_{0,2}}{(\varphi_{0,1}^2 + \varphi_{0,2}^2)}\ln\left(\frac{1+e^{-\kappa H}}{1-e^{-\kappa H}}\right) + \ln(1-e^{-2\kappa H})\right] \tag{1.65}$$

This is a general solution for interaction between constant potential double layers surrounding dissimilar colloidal particles and is good up to around 50-60 mV [Hogg et al., 1966]. As to the validity of Derjaguin's approximation, it is good for $\kappa R > 5$. For similar particles ($\varphi_{0,1}=\varphi_{0,2}$ and $R_1=R_2$), the above equation simplifies to:

$$V_{el} = 2\pi R\varepsilon\varepsilon_0\kappa\varphi_0^2\left[1 + \ln(1-e^{-\kappa H})\right] \tag{1.66}$$

1.1.2.1. Formation of Electrostatic Charging on Solid Surfaces in Water: Electrical Double Layer (EDL)

In response to the charging of a colloidal particle in liquid, an ionic environment spontaneously develops around it on the liquid side. These two charged regions (one on the particle and the other on the solution side) are called *the Electrical Double Layer, EDL* (Figure 1.6). Accumulation of charge in solution side of the *EDL* requires a finite thickness because of interplay between electrostatic interactions and the thermal disturbance. Therefore, while the charges on the particle are confined to the surface, charges on the solution side show a diffuse character.

The greatest concentration of excess charge *(Counter Ions)* will be adjacent to the surface where the electrostatic forces are largest and most able to overcome the thermal process. Actually, some of the counter ions will form a firmly attached layer around the surface of the colloid. This layer of counter-ions is known as *the Stern layer*.

Additional counter ions are still attracted by the surface, but now they are repelled by the Stern layer as well as by other counter ions that are also trying to approach the colloid. Hence, progressively lesser concentration of counter ions will be found at greater distances from the surface. This dynamic equilibrium is named *the diffuse layer* of counter ions (Polat et al., 2009).

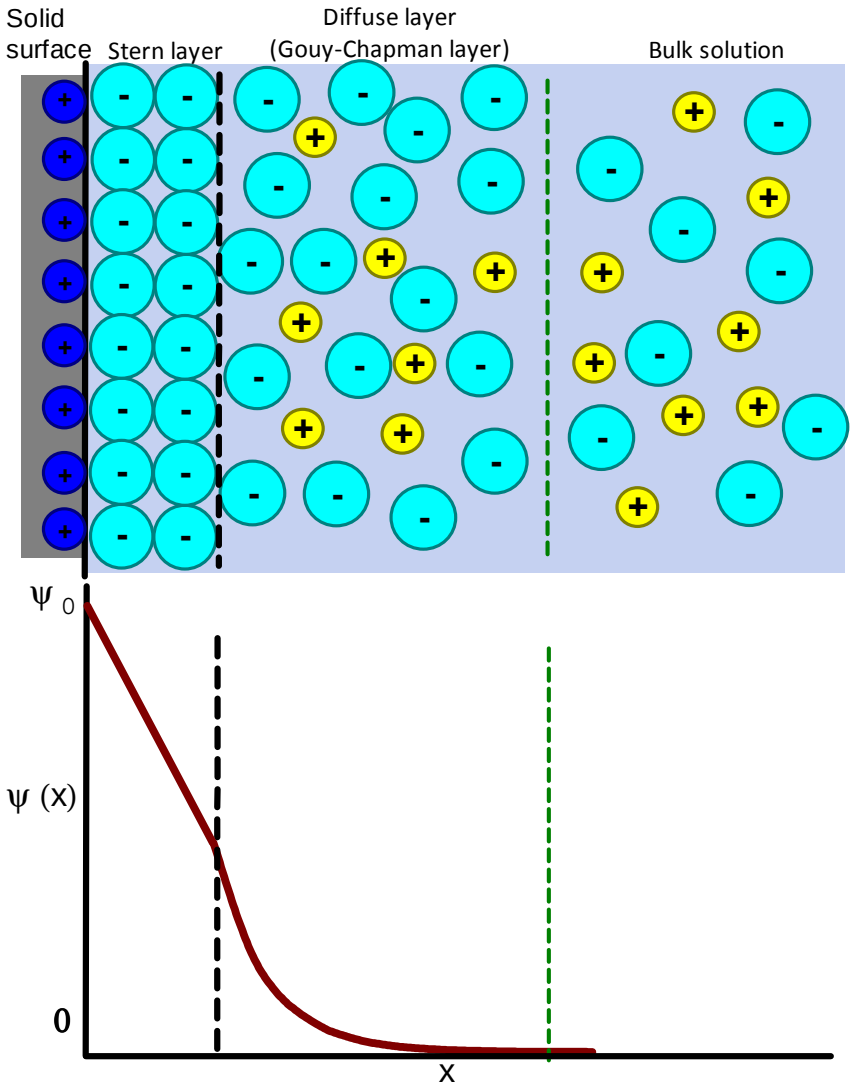

Figure 1.6. Development of a diffuse layer of charge in response to spontaneous charging of a solid in liquid (the electrical double layer, EDL) and the change of potential $\psi(x)$ in the EDL as a function of distance x from the solid surface (Source: Polat et al., 2009)

1.1.2.2. Gouy-Chapman Model of EDL

Even though the charge on the solid is confined to the surface, the same may not be true for the charges in solution. Especially for low concentrations of electrolyte, it may take a significant thickness of solution to accumulate the excess charge to counter balance the surface charge. A finite thickness would arise essentially because there is an interplay between the tendency of charges on the solid to attract or repel the carriers according to polarity and the tendency of the thermal process to randomize them. Hence, this model involves a diffuse layer of charge in the solution side of the double layer. The greatest concentration of excess charge (*counter ions*) will be adjacent to the

surface where the elctrostatic forces are largest and most able to overcome the thermal process. Progressively lesser concentrations will be found at greater distances as those forces are weakened. The problem was first formulated by Gouy (1910) and Chapman (1913) and named as the Gouy Chapman model.

When assume that the solution is divided into laminae, parallel to the surface and of thickness *dx*, that all of this laminae are in thermal equilibrium with each other. The ions of any species *i* are not at the same energy level in various laminae, because the electrostatic potential ψ varies with distance. The laminae can be regarded as the energy states with equivalent degree of degeneracy. Hence, the number concentration of species in two laminae have a ratio determined by a Boltzmann factor. A reference laminae is far from the surface where every ion is at its bulk concentration $n_{i,0}$ $[m^{-3}]$, then the population in any other lamina $[m^{-3}]$ is given by following formula (Polat, 1999).

$$n_i(x) = n_{i,0} \exp(-\frac{z_i e_0 \psi(x)}{kT}) \tag{1.67}$$

The potential at an arbitrary *x* location ($\psi(x)$) is measured with respect to the bulk solution. In this equation *k* is the Boltzmann constant $(1.38066x10^{-23}\ J/K)$. The charge density per unit volume (C/m^3) at a distance *x* from the surface is given by:

$$\rho(x) = \sum_i z_i e_0 n_i(x) \tag{1.68}$$

The summation is carried out for all species of ion present and the valence z_i may take positive or negative values. Combining equations 1.67 and 1.68 gives the change in the charge density as a function of the potential and the bulk concentration of species i.

$$\rho(x) = \sum_i z_i e_0 n_{i,0} e^{-\frac{z_i e \psi(x)}{kT}} \tag{1.69}$$

This equation can be viewed as a model in which the thermal and electrostatic effects are merged into a Boltzmann type distribution. In electrostatics, r(x) is related to the potential y(x) by the Poission equation:

$$\rho(x) = -\varepsilon\varepsilon_0 \frac{d^2\psi(x)}{dx^2} \tag{1.70}$$

Inserting equation 1.69 into 1.70 yields:

$$\frac{d^2\psi}{dx^2} = -\frac{F}{\varepsilon\varepsilon_0}\sum_i z_i C_{i,0} e^{-\frac{z_i F\psi}{RT}} \tag{1.71}$$

where $C_{i,0}$ is the concentration of the i^{th} species of ion in bulk solution in moles/m^3. This equation is known as the Poison-Boltzmann equation.

Boundary condition: dy/dx =y = 0 at x=∞

$$(\frac{d\psi}{dx})^2 = \frac{2RT}{\varepsilon\varepsilon_0}\sum_i C_{i,0}\left[e^{-\frac{z_i F\psi}{RT}} - 1\right] \tag{1.72}$$

For a symmetric electrolyte ($z = z^+ = -z^-$), summation results:

$$\frac{d^2\psi}{dx^2} = \frac{2zFC_0}{\varepsilon\varepsilon_0} sinh(\frac{zF\psi}{RT}) \tag{1.73}$$

Equation 1.73 can be written in dimensionless using dimensionless quantities.

$$\kappa = \sqrt{\frac{2z^2F^2C_0}{\varepsilon\varepsilon_0 RT}}\,, \; = zF\psi/RT \quad \text{and} \quad X = \kappa x$$

The equation becomes:

$$\frac{d^2Y}{dX^2} = sinh\, Y$$

This nonlinear differential equation in one dimension is an expression of how the potential Y varies with distance X between the two plates separated by a gap H (Figure

1.7). Though it is the basis of any quantitative study on the interactions between two such surfaces. Equation 1.73 does not lend itself to a simple analytical solution.

$$(\frac{dY}{dX})^2 = sign(Y)\,(2\cosh\, Y + \phi) \tag{1.74}$$

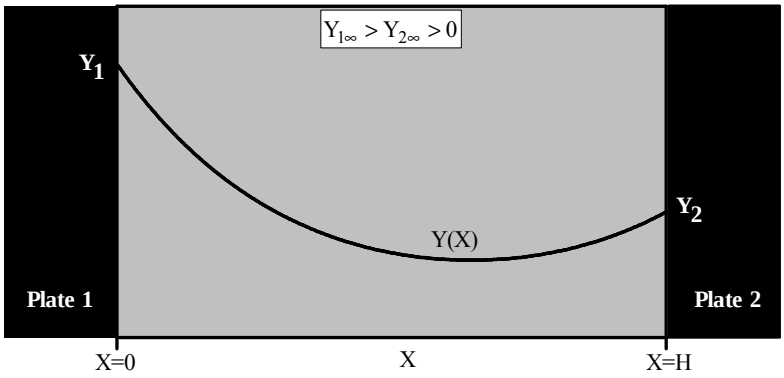

Figure 1.7. Change of potential Y as a function of X between two plates.
(Source: Polat and Polat, 2010)

Equation 1.74 is valid for surfaces with potentials of any magnitude and sign interacting through symmetrical electrolyte solutions. The first integration constant ϕ varies as H changes.The sign(Y) takes into account that integral of sinh(-Y)=coshY. The charge density, σ , of any one of the plates, is equal in magnitude but opposite in sign to the net excess charge in solution:

$$\sigma_0 = -\int_0^\infty \rho(x)dx \tag{1.75}$$

Combining with the Poisson equation 71 gives:

$$\sigma_0 = \varepsilon\varepsilon_0 \int_0^\infty \frac{d^2\psi(x)}{dx^2}dx \tag{1.76}$$

By integrating the above equation and applying the boundary conditions and recognizing that $d\psi(x)/dx=0$ at $x=\infty$ the following equation obtained.

$$\sigma^s = \varepsilon\varepsilon_0 \frac{d\psi(x)}{dx}\bigg|_{x=0}^{x=\infty} = -\varepsilon\varepsilon_0 \frac{d\psi(x)}{dx}\bigg|_{x=0} \tag{1.77}$$

Combining equation 1.77 with equation 1.73 under the condition that $\psi=\psi_0$ at x=0 yields:

$$\sigma_{0,\infty} = \sqrt{8\varepsilon\varepsilon_0 RTC_0}\,\sinh\left(\frac{zF\psi_{0,\infty}}{2RT}\right)$$

$$S_{0,\infty} = \sinh\left(\frac{Y_{0,\infty}}{2}\right) \tag{1.78}$$

The above equation gives the total net charge in the diffuse layer and is equal to the opposite of the surface charge. By integrating and applying the boundary conditions mentioned in Figure 1.7 and expressing in terms of dimensionless quantities yield:

$$S_1 = -\frac{dY}{dX}\bigg|_{x=0} = \frac{\sigma_1}{\sqrt{2\varepsilon\varepsilon_0 RTC_0}}$$

$$S_2 = -\frac{dY}{dX}\bigg|_{x=H} = \frac{\sigma_2}{\sqrt{2\varepsilon\varepsilon_0 RTC_0}} \tag{1.79}$$

Combining these definitions with Equation 1.74 and evaluating at infinite separation where dY/dX ≡ 0 and Y ≡ 0 is satisfied for each plate demonstrate that ϕ=-2 when the plates are not interacting (at infinite separation). Since the potentials and charge densities on the plates satisfy $Y_1= Y_{1\infty}$, $Y_2= Y_{2\infty}$, $S_1 = S_{1\infty}$, and $S_2 =S_{2\infty}$ under such conditions, it can be seen from Equation 1.74 and 1.79 that:

$$S_{1,\infty}^2 = 2\cosh Y_{1\infty} - 2$$

$$S_{2,\infty}^2 = 2\cosh Y_{2\infty} - 2 \tag{1.80}$$

The surface potentials or charge densities at infinite separation can be estimated experimentally using such techniques as zeta potential measurements or colloidal titration procedures. Evaluation of equation 1.74 on the solid/solution interface on both plates (X ≡ 0 and X ≡ H) shows that a general relationship can be obtained for the first integration constant ϕ in terms of surface potentials and surface charge densities:

$$\phi = S_1^2 - 2\cosh Y_1 = S_2^2 - 2\cosh Y_2 \tag{1.81}$$

Equation 1.81 hold at all seperations but the magnitude of ϕ will be different for different plate seperations. Though Y_1, Y_2, S_1, and S_2 have specific values at a given plate separation, they will change in relation to each other as H changes depending on the charging mechanism of the surfaces. For example, for constant-potential surfaces Y_1 and Y_2 will be equal to the surface potentials at infinite separation ($Y_{1\infty}$ and $Y_{2\infty}$) for all H whereas S_1 and S_2 must adjust as the planes approach. Conversely, S_1 and S_2 will always be equal to the surface charge densities at infinite separation ($S_{1\infty}$ and $S_{2\infty}$) for constant-charge surfaces while Y_1 and Y_2 will have to vary during the approach.

1.1.2.3. Electrostatic Pressure Between Two Interacting Plates

Charging of the surfaces leads to a pressure force experienced by the interacting plates as they approach each other. The analysis of this force has been done by Werwey and Overbeek analyzed this force and found that osmotic and electrostatic are effective factors. The osmotic pressure force acting on a volume element of liquid (per unit volume) along the x-axis can be given as:

$$F_{os} = -\frac{dp_{os}}{dx} \tag{1.82}$$

If the volume element is within a potential field, it will also experience an electrostatic force called the Maxwell stress. The x component of this force is equal to

$$F_{el}{}' = -\rho\left(\frac{d\psi}{dx}\right) \tag{1.83}$$

At equilibrium, overall force balance on the volume element along the x-direction will require that:

$$\frac{dp_{os}}{dx} + \rho\,(\frac{d\psi}{dx}) = 0 \tag{1.84}$$

Substituting ρ(x) from Poisson Equation gives:

$$dp_{os} - \varepsilon\varepsilon_0(\frac{d^2\psi}{dx^2})(\frac{d\psi}{dx}) = 0 \tag{1.85}$$

Recognizing that $(\frac{d^2\psi}{dx^2})(\frac{d\psi}{dx}) = \frac{1}{2}\frac{1}{dx}(\frac{d\psi}{dx})^2$ yields

$$\frac{dp_{os}}{dx} - \frac{\varepsilon\varepsilon_0}{2}\frac{1}{dx}\left(\frac{d\psi}{dx}\right)^2 = 0 \tag{1.86}$$

Which gives:

$$p_{os} - \frac{\varepsilon\varepsilon_0}{2}(\frac{d\psi}{dx})^2 = \text{constant} = p \tag{1.87}$$

It can be seen from Equation 1.87 that the difference between the osmotic pressure and the Maxwell stress is always equal to a constant pressure at a given separation of the plates. The osmotic pressure component can be evaluated further by rewriting Equation 1.84 as in the follwing:

$$dp_{os} + \rho\, d\psi = 0 \tag{1.88}$$

If q(x) is substituted using Equation 1.69 for a z:z electrolyte, the resulting expression is in the form:

$$dp_{os} = -z_i FC_0 \,(e^{-\frac{zF\psi}{RT}} - e^{\frac{zF\psi)}{RT}})d\psi \tag{1.89}$$

$$dp_{os} = 2z_i FC_0 \ sinh(\frac{zF\psi}{RT})d\psi \tag{1.90}$$

The excess osmotic pressure between the plates can be found by setting the osmotic pressure in the bulk liquid (where there are no electrostatic effects; $\psi \equiv 0$) to zero and integrating Equation 1.90 between a point in bulk and any point between the plates with pressure p_{os} and potential $\psi(x)$:

$$p_{os} = 2RTC_0 \left[\cosh(\frac{zF\psi}{RT}) - 1)\right] \tag{1.91}$$

Combining Eqs 87 and 91 gives:

$$p_{el} = 2RTC_0 \left[\cosh(\frac{zF\psi}{RT}) - 1\right] - \frac{\varepsilon\varepsilon_0}{2}\left(\frac{d\psi}{dx}\right)^2 \tag{1.92}$$

In terms of dimensionless quantities, it becomes

$$P_{el} = \frac{p}{2RTC_0} = [\cosh\ Y - 1] - 0.5(\frac{dY}{dX})^2$$

Equation 1.92 gives the net pressure force between the two plates as a function distance from each plate. Since the two pressures must balance each other, the net pressure between the two plates must always be equal to a constant value, P for a given plate separation H. Since the pressure will be constant at any point within the liquid separating the plates, its evaluation at one of the plates is sufficient. Doing so for plate 2 and expressing in terms of

dimensionless quantities determines the magnitude of the double layer pressure at a given separation of the plates:

$$P_{el} = [\cosh Y_0 - 1] - \frac{S_0^{\,2}}{2} \tag{1.93}$$

It should be noted that the pressure value obtained from Equation 93 is meaningful only if it is paired to the distance H between the two plates (Polat and Polat, 2010).

1.1.2.4. Debye-Hückel Approximation

The best known solution of the Poission-Boltzmann equation is known as the Debye-Hückel approximation (Debye and Hückel, 1923). In this treatment, the exponential in the Poission-Boltzmann equation is expanded in series and only the first two terms are taken into account. The condition for this assumption is that the electrical term zFψ is small compared to the thermal term RT.

$$\frac{d^2\psi}{dx^2} = -\frac{F}{\varepsilon\varepsilon_o}[\sum_i z_i C_{i,0} - \sum_i z_i C_{i,0} \frac{z_i F\psi}{RT}] \tag{1.94}$$

Since the solution is electro-neutral, the first summation over all ionic species in solution must be zero. Therefore;

$$\frac{d^2\psi}{dx^2} = (\frac{F^2}{\varepsilon\varepsilon_o RT} \sum_i z_i^2 C_{i,o})\psi \tag{1.95}$$

If the collection of terms within the pharantesis is dumped into a parameter κ, the above equation becomes:

$$\frac{d^2\psi}{dx^2} = \kappa^2\psi \tag{1.96}$$

Where

$$\kappa = (\frac{F^2}{\varepsilon\varepsilon_o RT})^{\frac{1}{2}} (\sum_i z_i^2 C_{i,o})^{\frac{1}{2}} = (\frac{F^2}{\varepsilon\varepsilon_o RT})^{\frac{1}{2}} \sqrt{I} \tag{1.97}$$

The parameter κ is called the Debye-Hückel parameter and it plays a prominent role in the elecrical double layer systems. If concentration of the electrolyte in water at 25 ^{o}C is given in moles/liter, the Debye-Hückel parameter is calculated in nanometers as:

$$\kappa(nanometers) = 3.2864\sqrt{I} \tag{1.98}$$

Equation 1.96 is a linear, homogeneous second-order differential equation. It has the general solution:

$$\psi(x) = c_1 e^{-\kappa x} + c_2 e^{\kappa x} \tag{1.99}$$

Double layer, of which plates do not interact with each other ($h=\infty$), has surface profile as $\psi_{01,\infty}$ ve $\psi_{02,\infty}$ and potential profile as $\psi_1(x)$ *ve* $\psi_2(x)$**.** When the double layer interact each other the potential profile change like ψ_{01} at $x=0$ and ψ_{02} at $x=h$. Double layer has only one potential profile $\psi(x)$ (Figure 1.8). This boundary condition helps to calculate c_1 ve c_2 constants:

$$c_1 = \frac{\psi_{01}\, e^{\kappa h} - \psi_{02}}{e^{\kappa h} - e^{-\kappa h}}$$

and (1.100)

$$c_2 = -\frac{\psi_{01}\, e^{-\kappa h} - \psi_{02}}{e^{\kappa h} - e^{-\kappa h}}$$

$$\psi(x) = \psi_0 e^{-\kappa x} \tag{1.101}$$

The above equation is called the *Debye-Hückel solution* of the potential profile in the double layer. It can be seen that the potential, which has a ψ_0 value at the surface decreases exponentially as one moves from the surface, into the solution. At a distance of κ^{-1} it will drop to a value of ψ_0/e (Polat, 1999).

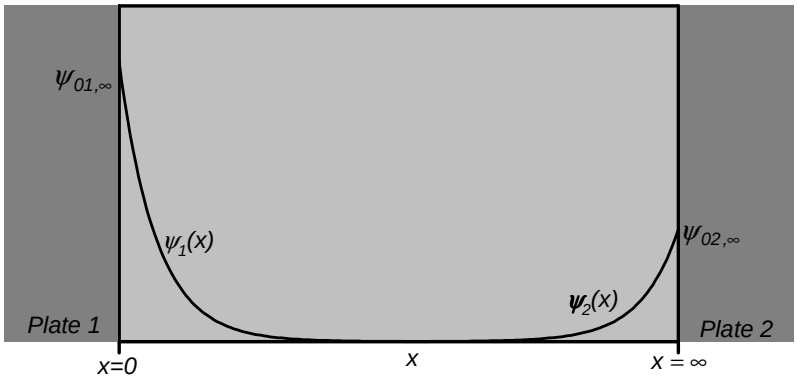

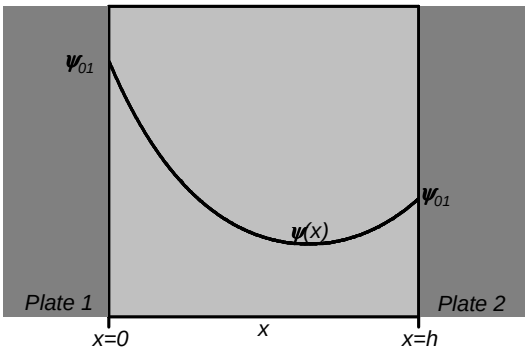

Figure 1.8. Changing of potential profile $\psi(x)$ of interacting two layer at $x=\infty$ and $x=h$

1.1.2.5. Analytical Solution of Poisson–Boltzmann Equation for Interacting Plates

Polat and Polat (2010) recently have developed an analytical solution for interacting parallel plates which carry varying potentials. These equations are perfectly valid for low and high surface charge conditions. Constant charge and constant potential surfaces are provided in Appendix B.

1.1.2.6. Constant Charge and Constant Potential Surfaces

When the surface and bulk ions come to equilibrium faster than the rate of approach of surfaces, a balance between these ions is preserved. Since the surface potential is determined by this balance, it remains constant during the interaction. These surfaces are called Constant Potential Surfaces.

If the surface and bulk ions cannot achieve thermodynamic equilibrium during the approach, the balance between these ions cannot be maintained and the potential will vary during the course of approach. In these types of system, what remains constant during the approach is the surface charge. These surfaces are called Constant Charge Surfaces.

1.1.3. The DLVO Theory

Accurate theoretical calculations of force curves for constant potential and constant charge surfaces are important in determining the surface charge of surface potential from the AFM force data. If one can accurately calculate the theoretical force curve for electrostatic interaction only them one can equate it to the measured force curve to estimate the surface charge at that point on the surface.

Derjaguin and Landau (Derjaguin and Landau, 1941) and Verwey and Overbeek (Verwey and Overbeek, 1948) were the first to develop independently the theory describing the interactions of two parallel, infinite, flat double layers. The theory is known as the DLVO theory in colloid science. The theoretical force calculations calculations carry out based on the DLVO theory, assuming that the net force of interaction (F_{DLVO}) per unit area of the interacting plates was a sum of van der Waals (F_{vdW})and double layer forces (F_{el}).

The van der Waals interaction given by:

$$F_{vdw} = \frac{A_{12}}{6\pi h^3} \tag{1.102}$$

For calculating the electrostatic pressure force (F_{el}) , a full analytical solution of the Poission-Botzman equation given in following. The algorithm for both constant surface potential and constant surface charge system is given as:

$$F_{cp}(h) = \frac{-\varepsilon\varepsilon_0\kappa^2}{2}\left[\frac{\psi_1^2 + \psi_2^2 - 2\psi_1\psi_2\cosh(\kappa h)}{\cosh(\kappa h)^2 - 1}\right] \tag{1.103}$$

$$F_{cc}(h) = \frac{-1}{2\varepsilon\varepsilon_0}\left[\frac{2\sigma_1\sigma_2\cosh(\kappa h) + (\sigma_1^2 + \sigma_2^2)}{\sinh(\kappa h)^2}\right] \tag{1.104}$$

The net force of interaction (F_{DLVO}) per unit area of the interacting plates:

$$F_{DLVO}(h) = F_{cc/cp}(h) + F_{vdW}(h) \tag{1.105}$$

Total interaction pressure (F_{DLVO} in Pa; between two plates) converts through Derjaguin approximation to total interaction force (F_{AFM} in N; between a spherical tip and a flat surface).

$$F_{AFM}(h) = 2\pi r \int_{h}^{\infty} F_{DLVO}(h)dh \tag{1.106}$$

CHAPTER 2

MATERIALS

The main materials were metal oxide substrate like quartz and sapphire surfaces and quartz colloidal probe. Detailed information about these materials was provided in the following.

2.1. Metal Oxide Surfaces

Within this study, the crystal structure of metal oxide surfaces were smooth at the atomic level (SiO_2 and Al_2O_3) were supplied. During the entire study, these surfaces need to be renewed on a regular because of wear, breakage, contamination. They also must be standard in mineralogical. The substrates used in characterization work:

a) Z-Cut quartz surface is smooth at the atomic level ,10x10x1mm,(MTI, California, USA)

b) 0001 Sapphire surface is smooth at atomic level α-alumina 10x10x1mm, (MTI, California,USA)

The crystal surface were tabulated in Table 2.1.

Table 2.1. Details of Single-crystal surfaces used in characterization work (Source: http://www.mtixtl.com)

	Single crystal Al_2O_3 (Sapphire)	Single crystal SiO_2 (Quartz)
Size	10 x 10 x 0.1 mm	10 x 10 x 0.1 mm
Orientation	<0001>; +/-0.5^o	Z cut; 30^o ~ 42.75^o ±5 min.
Polished Surface	On one side; EPI polished Ra<5Å	On one side ; EPI polished Ra<10Å
Crystal Structure	Hexagonal a=4.758 Angstrom c=12.99 Angstrom	Hexagonal a= 4.914 Angstrom c = 5.405 Angstrom
Melt point	2040 ^{o}C	1610 ^{o}C
Density	3.97 g/cm^3	2.684 g/cm^3
Growth Method	Czochralski(CZ)	Hydrothermal
Purity wt%	>99.99%	>99.99%
Hardness	9 Moh's	7.0 Moh's
Thermal expansion (10^{-6}/ ^{o}C)	7.5x10-6 (/ ^{o}C)	a_{11}: 13.71(/ ^{o}C) ; a_{33}: 7.48 (/ ^{o}C)
Thermal Conductivity	46.06 @ 0 ^{o}C; 25.12 @ 100 ^{o}C; 12.56 @400 ^{o}C W/(m.K))	0.0033 cal/cm/ ^{o}C
Thermoelectric Constant	9.4 @300K at A axis 11.58@300K at C axis	1200 mV/^{o} C@300 ^{o} C
Index of Refraction	1.771	1.544

2.2. Metal Oxide Powders

Silica and alumina powder were supplied nin order to use in characterization techniques and to prepare colloid probe. Powders used in the study as follows:

a) Silica Powder (Origin: The spherical silica is commercially names SO-E6 was supplied Admatech, Japan)
b) Alumina Powder (Origin: The spherical alumina is commercially AO-802 was supplied Admatech, Japan)

Detailes of the powders used in the work are presented in Table 2.2.

Table 2.2. Details of powders
(Source: Admatechs)

	Al_2O_3-Powder	SiO_2-Powder
Purity (Wt%)	>99.9	>99.9
Fe (ppm)	35	8
Si (ppm)	43	-
Al (ppm)	-	40
Ca (ppm)	<10	<2
Na (ppm)	<5	<0.1
K (ppm)	<5	<0.2
pH	5.3	5.2
Moustire	<0.5	<0.03

2.3. Other Materials Used in the Thesis

Force measurements were made in a liquid media. Liquid refers to a ratio of a specific set of pure water solution of the electrolyte concentration. KCl was used to prepare the solution and was obtained from Sigma Aldrich (Stock No. 12636).

Ultra-pure water was used in the preparation of Electrolyte concentrations and all the cleaning processes.

Silicone cantilever (Code: TL-FM-20) was used to prepare collidal probes obtained from Nanosensors (California, USA). The width of these cantilevers range

from 0.215 to 235 micrometers and their length varies between 28-35 micrometers. They have 0.5-9.5 N/m spring constant range.

Probe colloid particles were attached on the cantilever using epoxy type of Araldite 2011 adhesive obtained from Huntsman company.This adhesive has chemical and waterproof properties and can be applied on ceramics, glass, plastic material.

In addition, micro pipettes were used to capture the colloidal particles that have 5micrometers inner diameter (Microsupport company code is MP-005).

Colloidal particles were fixed on the membrane filter with a hole diameter of 0.2 micrometers to catch up by micro pipette.

Finally, tungsten needle was used to apply adhesive on cantilever, 0.125 mm diameter and 50 mm length with 1 micron tip, obtained from Academic Instruments (Bradenton, Florida, USA).

2.4. Characterization of Powders

Powders was used to prepare colloid probe should be identified.In addition surfaces were used in force measurement should be characterized to examine results. Therefore, characterization techniques as particle size distribution, SEM, XRD, BET, FTIR, Zeta potential were employed in this work.

2.4.1. Particle Size Distribution

Determination of particle size distribution of particles is important for forming colloidal probe. Particle size distribution measurements were measured on the Malvern Mastersizer. The size distributions were given in Figure 3.1 and 3.2. According to these distributions, the median particle size of SiO_2 powder was 1.95 micrometers while the median particle size of Al_2O_3 powder was 0.78 micrometers. However, at least some populations of particles are up to 10 micrometers size.

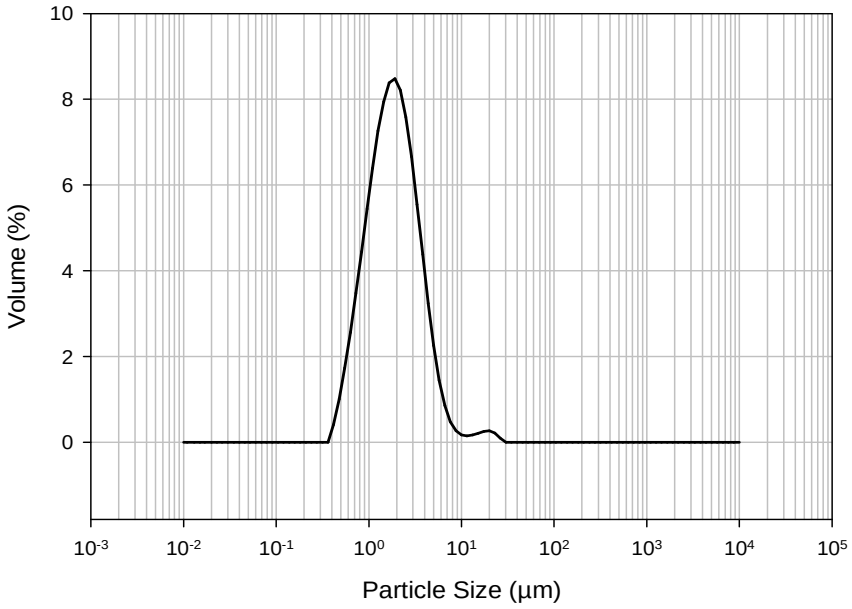

Figure 2.1. The particle size distribution of SiO_2 powder

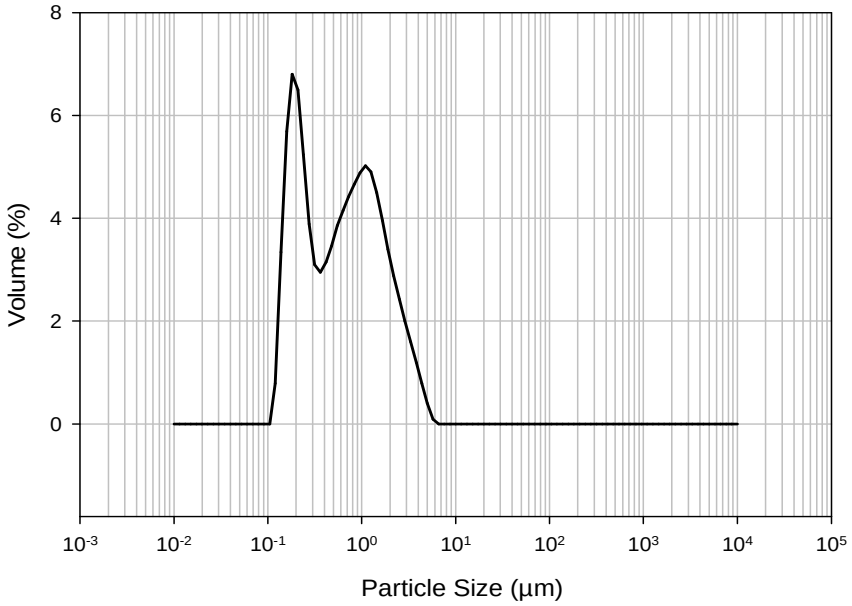

Figure 2.2. The particle size distribution of Al_2O_3 powder

2.4.2. SEM Micrographs

Although SiO_2 powder of average size 1.95 microns, the powder has a wide distribution range (Figure 2.1 and 2.2). The smallest and the biggest sizes of the

particles were observed from SEM 0.27 μm and 3.02 μm, respectively in Figure 2.3. The particles were nonporous and spherical shaped.

The mean particle size of Al_2O_3 powder is 0.78 μm in Figure 2.2. According to the SEM images in Figure 2.4 the particles size is changing from 0.1-10 μm. The smallest and the biggest sizes of the particles were observed from SEM 0.16 μm and 2.37 μm respectively in Figure 2.4. The particles of Al_2O_3 powder were nonporous and spherical shaped (Yelken, 2011). In summary, the particles of Al_2O_3 and SiO_2 powders are suitable for colloid prob due to their nonporous and spherical shaped and particle size.

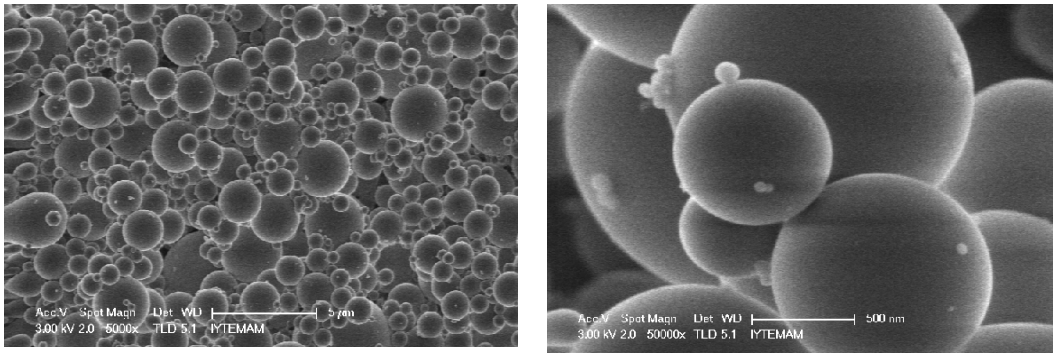

Figure 2.3. SEM micrograph of SiO_2 powder
(Source: Yelken, 2011)

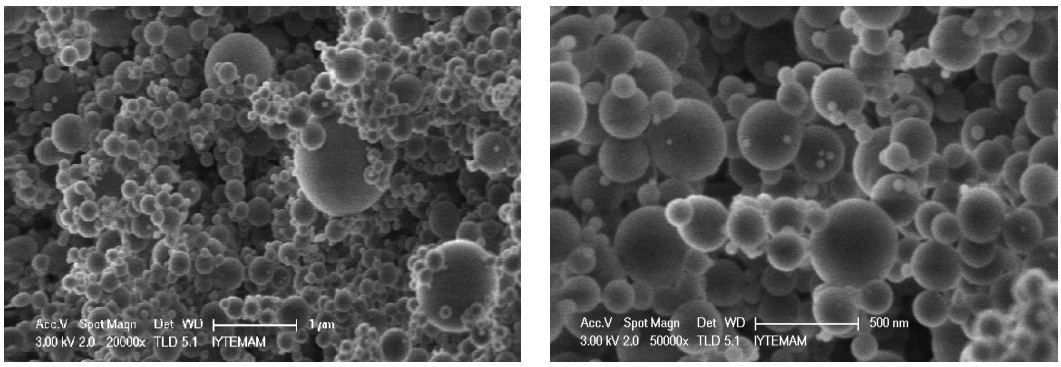

Figure 2.4. SEM micrograph of Al_2O_3 powder
(Source: Yelken, 2011)

2.4.3. BET Surface Area Measurements

Brauner-Emmett-Teller (BET) theory is a rule for the physical adsorption of gas molecules on a solid surface and serves as the basis for an important analysis technique for the measurement of the specific surface area of a material. BET analysis

of powder was measured on Micromeritics Gemini V, in Materials Research Center, IZTECH. Surface area of alumina powder is analyzed as 7.34 m^2/g. However, the silica powder could not be analyzed by N_2 adsorption because of low surface area (Yelken, 2011). In the literature, the BET for the same silica has been reported as 1 m^2/g (Kosmulski, 2009).

2.4.4. Zeta Potential Measurements

The zeta potential is a method of the potential difference of a solution. Any solid surface in a solution gain a charge due to the surface adsorption processes that develope potantial profile of solution. This potential causes electrostatic interactions between the surfaces and plays an extremely important role in both biological and inorganic systems. Zeta potential measurement gives detailed information about how granular structures are dispersed in solution and their stability (Israelachvili, 1977). Zeta potential measurements were carried out by Malvern Nano ZS in de-ionized water or in electrolyte solutions (Department of Chemical Engineering, Iztech).

Zeta potential measurement with 0.1% by wt SiO_2 powder was obtained in 10^{-3} M KCl solutions and ultra-pure water. Figure 2.5 shows that zeta potential values of powder has a quite different potential with different pH values. This result allign with the related literature (Kosmulski, 2009). Figure 2.6 shows zeta potential profile of 0.1% by wt Al_2O_3 powder in 10^{-3} M KCl solutions and ultra-pure water. It's clear that Al_2O_3 powder has different surface potential with different pH values. The related literature also confirms this result (Kosmulski,2009).

Zeta potential measurements is important to confirm the potential values which are obtained from made the AFM force measurement,and to demonstrate the accuracy of the method.

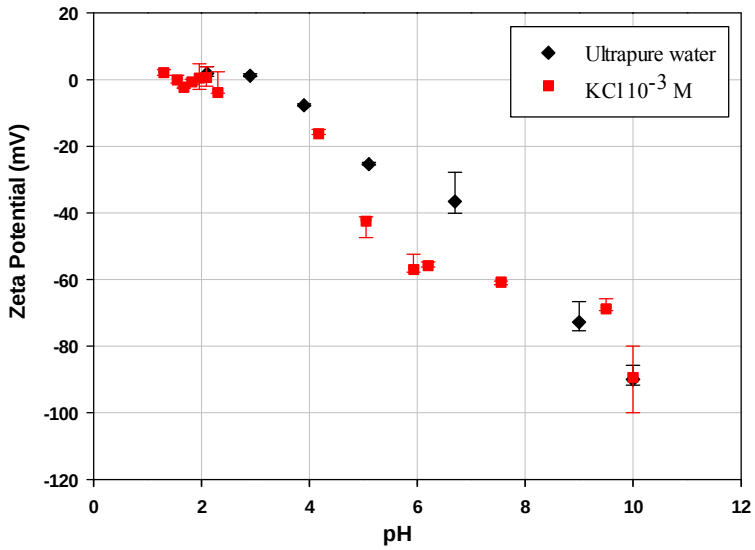

Figure 2.5. Zeta potential of SiO_2 powder in 10^{-3} M KCl solution and ultra-pure water

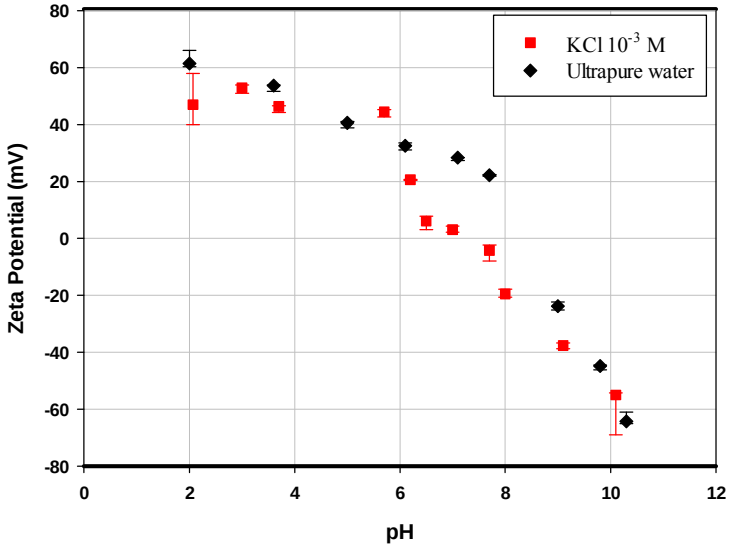

Figure 2.6. Zeta potential of Al_2O_3 powder in 10^{-3} M KCl solution and ultrapure water

2.4.5. FTIR Measurements

Fourier transform infrared (FTIR) spectroscopy is a measurement technique for collecting infrared spectra. The FTIR spectra of the powders were measured by Shimadzu 8400-S FTIR. Figure 2.7 shows that the FTIR spectra of silica powder. In the 1200-400 cm^{-1} region of the spectrum have two main peaks. They are due to the decrease in the following modes: (Si-O) in Si-OH surface groups, -(OH) of the Si-O-H

angle, and (O-Si-OH) of the O-Si-OH angle. In other words, absence of other peaks shows the purity of silica powder (Yelken, 2011).

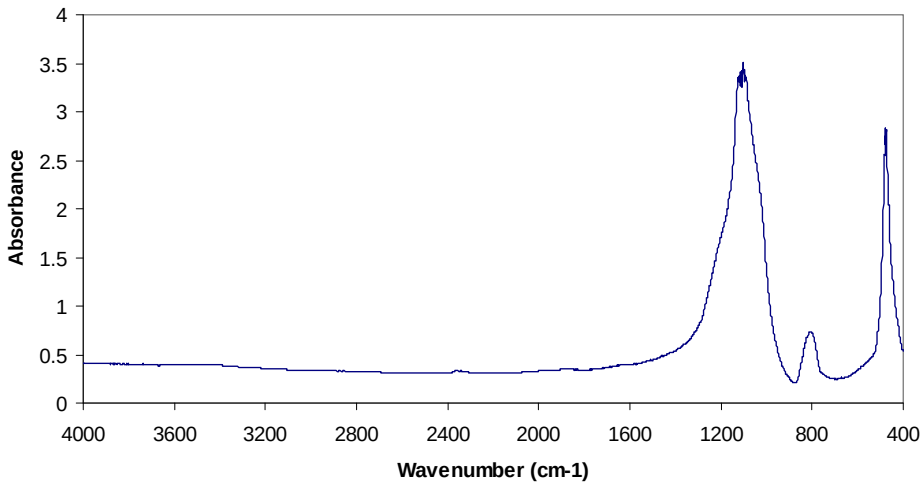

Figure 2.7. The FTIR spectra of silica powder SiO_2
(Source: Yelken, 2011)

The weak bands observed at 1132 cm^{-1} were produced by the Al-O bonds (Figure 2.8). It showed bands at 830,603 and 455 cm^{-1}, which probably were produced by vibrations of Al-O bonds corresponding to alumina ions with tetrahedral symmetry. The stretching vibration of the OH ions of residual water has a very intense broadband at 3200-3700 cm^{-1} (Yelken, 2011).

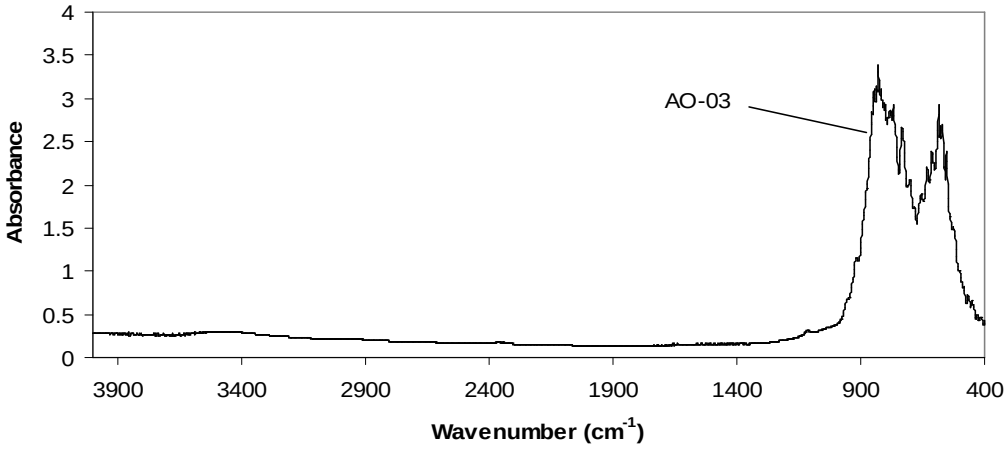

Figure 2.8. The FTIR spectra of alumina powder Al_2O_3
(Source: Yelken, 2011)

2.4.6. XRD Scans

X-ray diffraction techniques are family of non-destructive analytical techniques which reveal information about crystallographic structure and physical properties of materials and thin films.these techniques are based on observing the scattered intensity of an X-ray beam hitting a sample as a function of incident and scattered angle, polarization and wavelength or energy. X-ray diffraction of the powders were investigated by Phillips X'Pert Pro. The X-ray diffraction of silica powder showed in Figure 2.9. The X-ray pattern confirm amorphous silicon dioxide.

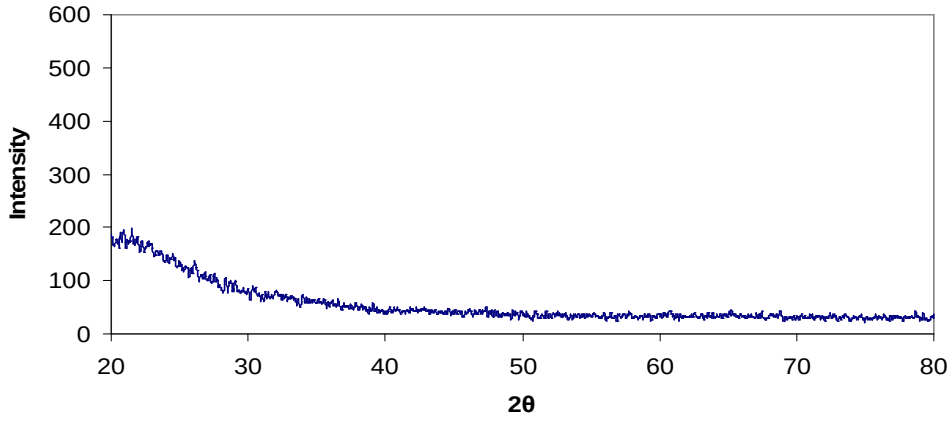

Figure 2.9. XRD patterns of silica powder (SiO_2)
(Source: Yelken, 2011)

X-ray diffraction pattern of alumina powderis given in Figure 2.10. Powder showed mixed phases of alpha and gamma alumina.

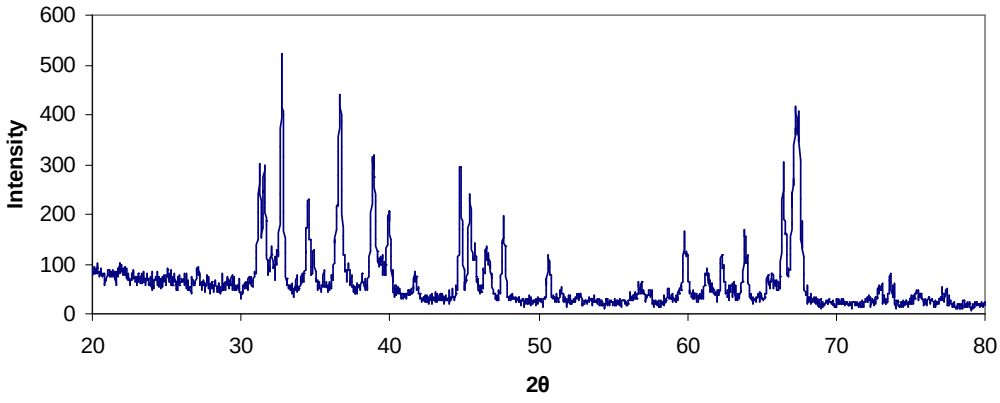

Figure 2.10. XRD patterns of alumina (Al_2O_3)
(Source: Yelken, 2011)

CHAPTER 3

EXPERIMENTAL METHODS

In this study, Atomic Force Measurements were applied between sapphire surface and spherical silica colloid prob which has atomically smooth surface. Do these measurements were isolated from the theoretical analysis of electrical double layer forces, through the use of the electrical double layer theory, the electrical force component of surface charge at that point was be obtained. This analysis on multiple points such as sapphire and quartz oxide surfaces the surface charge or potential distribution graph (charge or potential map) can be obtained. Measurements were repeated at different pH conditions. The results were compared with the zeta potential results.

3.1. Cleaning of Metal Oxide Surfaces

The aim of this work is to measure force used by AFM and detection charge mapping on sapphire and quartz surfaces for that reason these surfaces must be smooth at the atomic level. In other words, the surface roughness and cleanliness are assumed to be perfect.

Cleaning method of oxide surface is:

1) cleaned at 80 °C ultra-pure water for 5 minutes,
2) cooled to room temperature and subsequently washed with copious amounts of ultra-pure water,
3) cleaned ultrasonically in a glass cell and then washed with ultra-pure ethanol and ultra-pure water copiously,
4) dried under vacuum,
5) exposed to UV radiation for 10 minutes,
6) washed ultra-pure ethanol and ultra-pure water again in copiously and kept in a desiccator under vacuum.

Surface, liquid cell, tweezer and other materials must be subjected to the same cleaning procedure before each experiment. Force measurements start after the optical microscope AFM surface control for the last time. Scanning electron microscope (SEM) and Atomic force microscope (AFM) tests confirmed the accuracy of the surface cleaning procedures. SEM studies were carried out by Philips XL 30 SFEG and AFM measurements were perfomed by Digital Instrument, MMSPM-NanoScope IV in Materials Research Center, IZTECH. SEM images of quartz and sapphire surfaces are displayed in Figure 3.1 and 3.2. These SEM images confirm the success of the cleaning method.

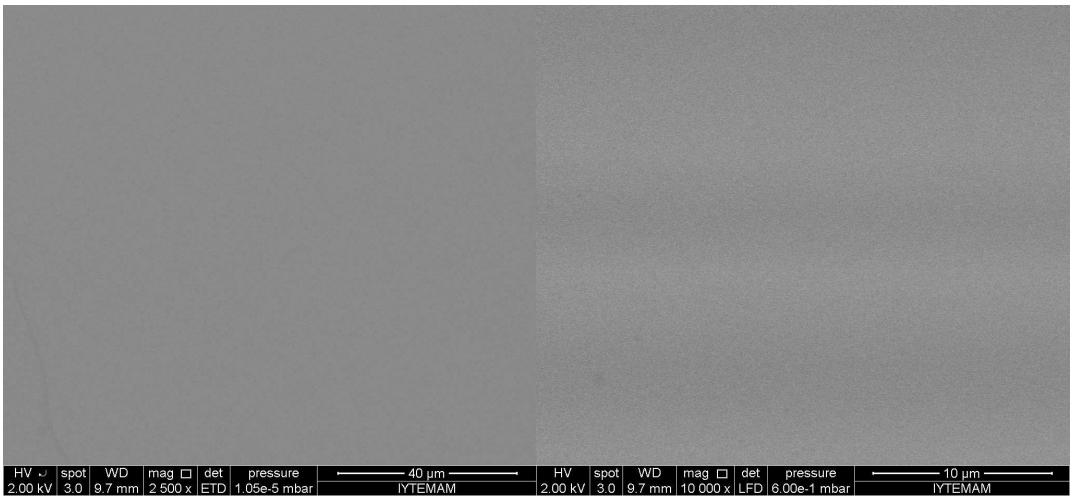

Figure 3.1. SEM migrograph of Z-cut quartz single crystal (SiO_2)

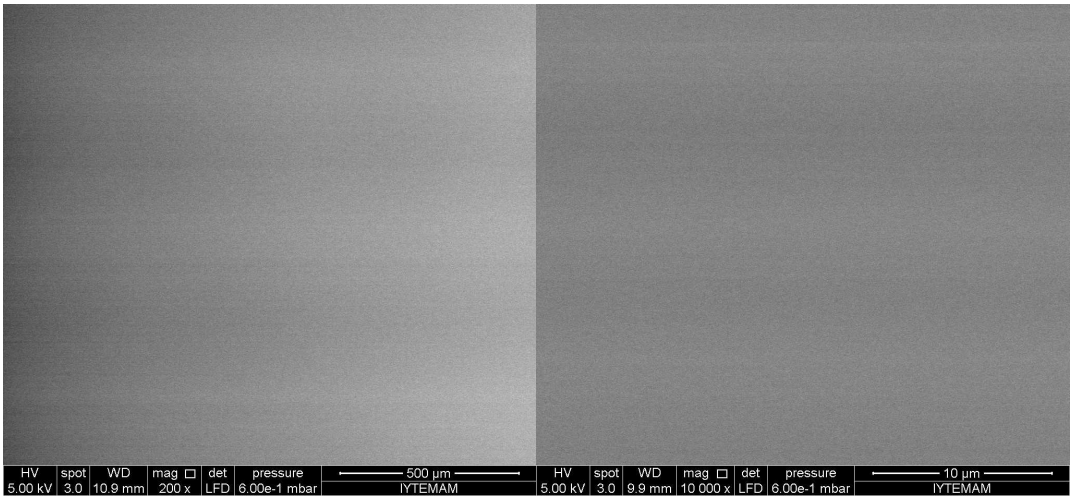

Figure 3.2. SEM migrograph of 0001 sapphire crystal surface (Al_2O_3)

The AFM was used to collect numerical data of levels of roughness and scan silica and alumina surface at atomic level. It is expected to be smooth to obtain high-resolution images (topographic scan). AFM images of quartz and sapphire surfaces were shown in Figures 3.3 and 3.4. These pictures were made in various fields on surfaces 5x5 micrometers in size and were selected as representative of a large number of screening.

Surface topoghrapy images of SiO_2 surface are shown in Figure 3.3. The surface was smooth with a surface roughness of 0.160 nm. Similarly, the average surface roughness value of Al_2O_3 was found (Ra) 0.129 nm (Figure 3.4). These values are compatible with the values of given by the company Ra <1.0 nm and Ra <0.5 nm.

These measurements show that both crystal surfaces are smooth at the atomic level,and this measurementsb confirm the cleaning process.

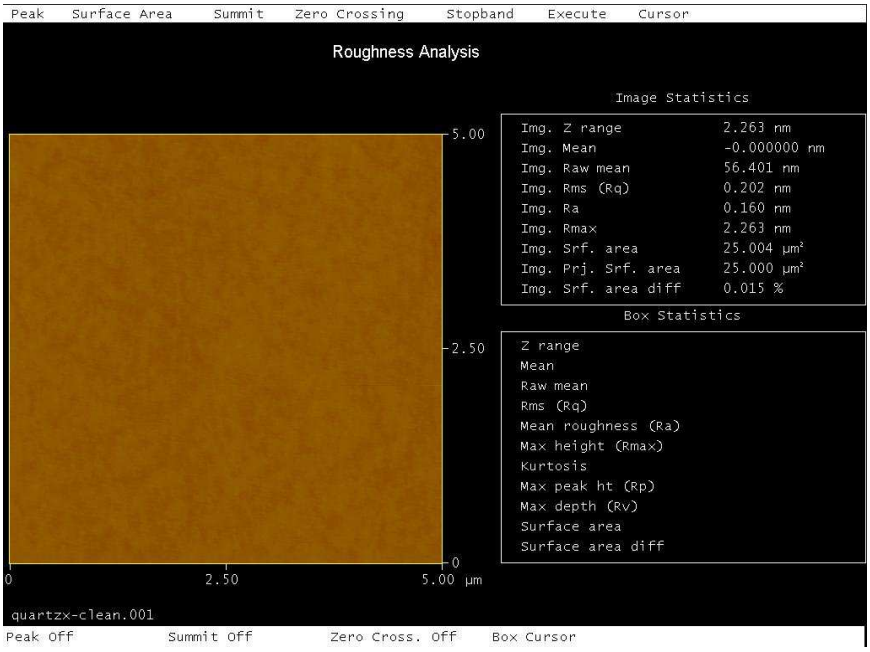

Figure 3.3. Surface topography image of Z-cut quartz crystal surface (SiO_2) using AFM

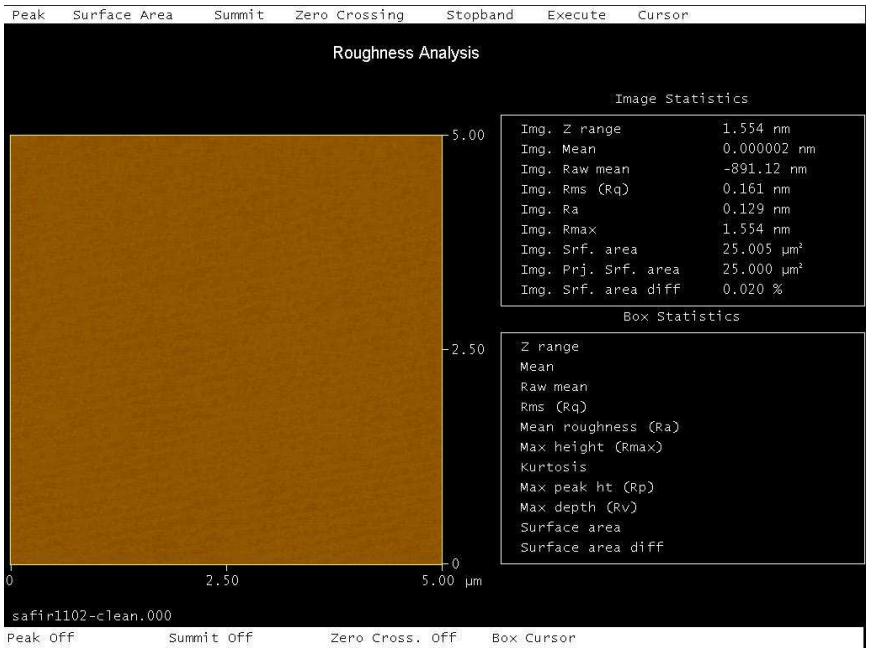

Figure 3.4. Surface topography image of 0001 sapphire crystal surface (Al_2O_3) using AFM

3.2. Preparation and Surface Cleaning of Colloid Probe Particles

According to particle size analysis, the silica powder has a wide particle size range (more than 90% from 0.1 to 10 mm), and the average powder grain size is about 2µm. The size distribution of powder can be seen in the SEM images (Figure 3.1). Particle size distribution of silica powder arise from nano to micrometer in diameter. Therefore, to obtain particle which is used as a probe, the range of the particles sizes must be near 5µm and the nanoparticle are not attached on surface.

The following operations were applied to obtain clean particles. Particles must be;

1) distributed using physico-chemical methods (dispersion),
2) classified on a narrow range size,
3) immobilized so as to allow particles to be classified,

3.2.1. Dispersion of Colloid Probe Particles

Air dispersion of particles in this size is not possible due to the extremely strong van der Waals, electrostatic, and capillary forces. Silica particles which have a very high

hamaker constant about $10x10^{-20}$ J on air are expected to show a strong agglomeration due to capillary forces (Lennard Bergström, 1997). The effective Hamaker constant of silica particles dispersed in water is less then approximately %90 of air. Therefore, the only way to obtain individual particles is distribute silica powder in an aqueous solution with a suitable chemical properties. However, to reduce the effective Hamaker constant of the particles is not sufficient to disperse. Besides, electrical repulsion should overcome van der Waals attraction. Neutral pH water (pH = 7) provide high surface charge (-50 mV), and gives a strong repulsion to silica particles according to the results of the zeta potential. Depending on the concentration of electrolyte, Van der Waals attractive force is calculated as a function of the distance between two silica particles which have 2 μm mean size in aqueous solution at pH=7. The chart of Distance-Interaction energy is shown in Figure 3.5.

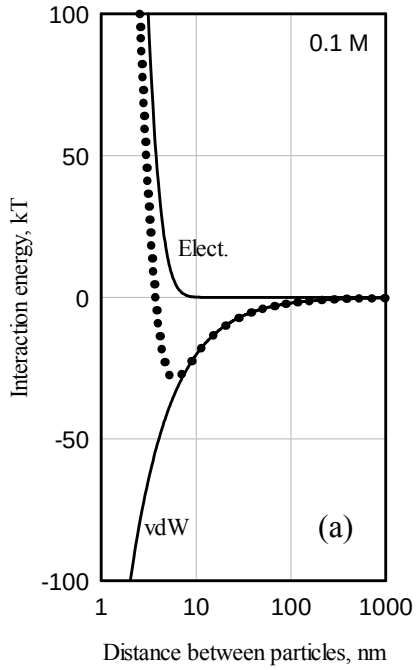

Figure 3.5. The interaction energy between 2 μm silica particles in different solution conditions . (*Dotted line shows the total interaction energy (van der Waals + Electrostatic). Particles has a 50 mV surface potential at pH = 7. Hamaker constant of water is taken as 1x10-20 J. Electrolyte concentration a) 0.1 M KCl; b) 0.01 M KCl; c) 0.001 M KCl)*

(cont. on next page)

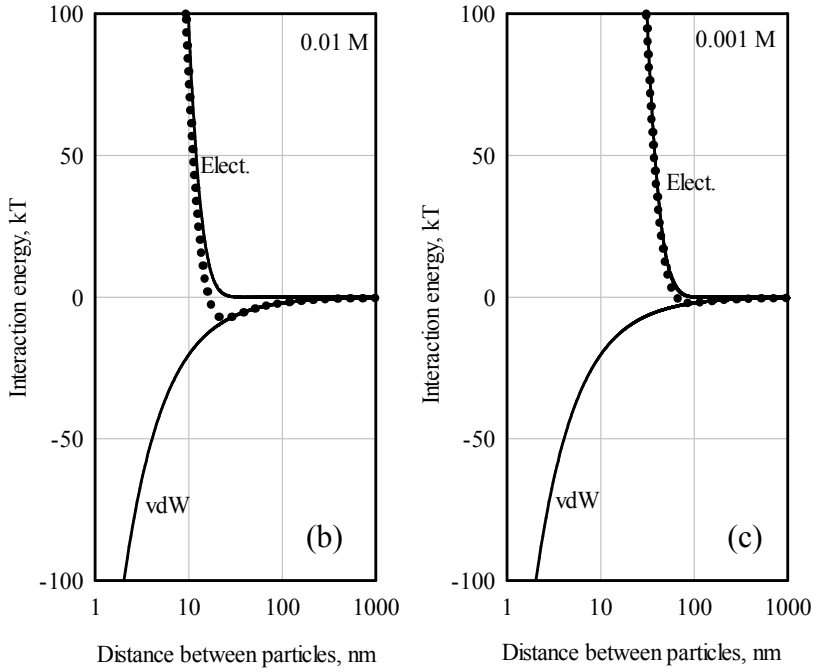

Figure 3.5. (cont.)

As can be seen in figure, when the particles are closer to 10 nm, they feel attraction intensity of about 30 kT at 0.1M KCl electrolyte concentration,

Attraction force decreases with the decreasing electrolyte concentration. Therefore,silica particles have 50 mV potential profile in pure water and they strongly push each other. Thus, as a first step in the preparation of colloidal particles of silica used as the probe, 1 g silica powder, with 1 liter of pH 7 in distilled water (0.1 wt%) were distributed using ultrasonic treatment for 10 min. Particles are not interact with each other was observed under the microscope.

3.2.2. Classification of Colloid Probe Particles

Dispersion of silica particles is not enough to achieve colloidal probe particles. Distributed particles should be classified in a narrow size range using a suitable procedure. The method used for this purpose has been to provide decantation of particles in the water. 0.1% silica solution prepared as described in the paragraph above, was allowed to settle for 20 minutes with a height of 30 cm long phial. After 20 minutes the upper side of the solution was carefully separated with the bottom of the suspended using vacuum. Then, the bottom and the "coarse" particles completed to 1

liter with water again, and solution was settled for 5 minutes. In this way, the suspension containing particles 5 and 10 μm as a result of five times decantation was obtained. These particles were stored in water until they are used again. Settling rate should be determined as a function of particle size. For this purpose, Stoke's equation that gives excelllent results for small size of 10 μm was used.

$$V = \frac{g d^2 (\rho_p - \rho_w)}{18 \mu_w} \tag{3.1}$$

In this equation, g is the gravitational acceleration (m/s^2), d is the particle size (m), ρ_p and ρ_w is the density of particles and water respectively (kg/m^3), and μ_w is the viscosity of the water (kg/m.s). The comparision of the Stoke's equation with Concha equation is shown in Figure 3.6. According to the results, settling rates of 2, 5 and 10 μm diameter particles are 0.20, 1.25 and 5.00 mm/min respectively. This difference in sedimentation rates allows classification of particles with different size by using decantation process.

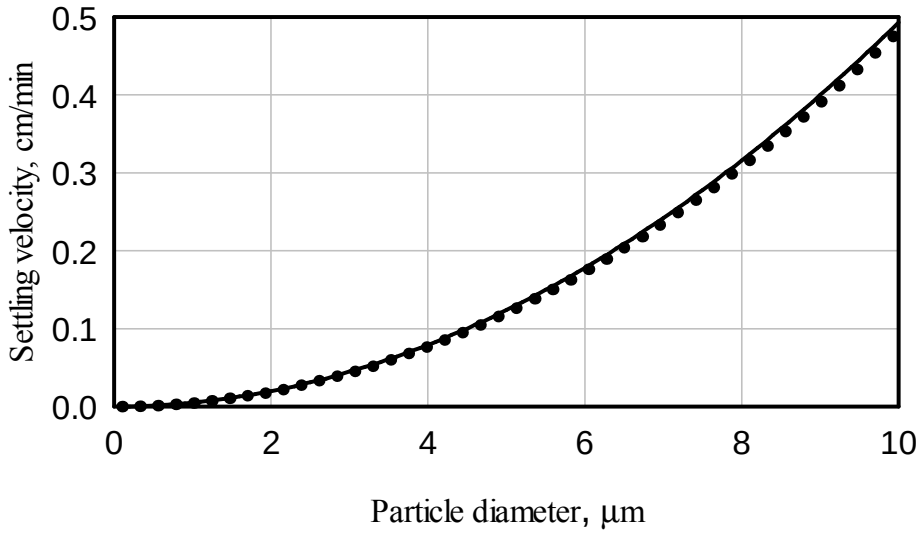

Figure 3.6. Settling rate of particles in the size range of 0-10 μm (Points calculated by Stoke's equation, the solid line shows the empirical values of the calculated actual precipitation).

Silica particles are dispersed on physico-chemical conditions and classified using decantation process. Figure 3.7-a and Figure 3.7-b shows the optical microscope photos.

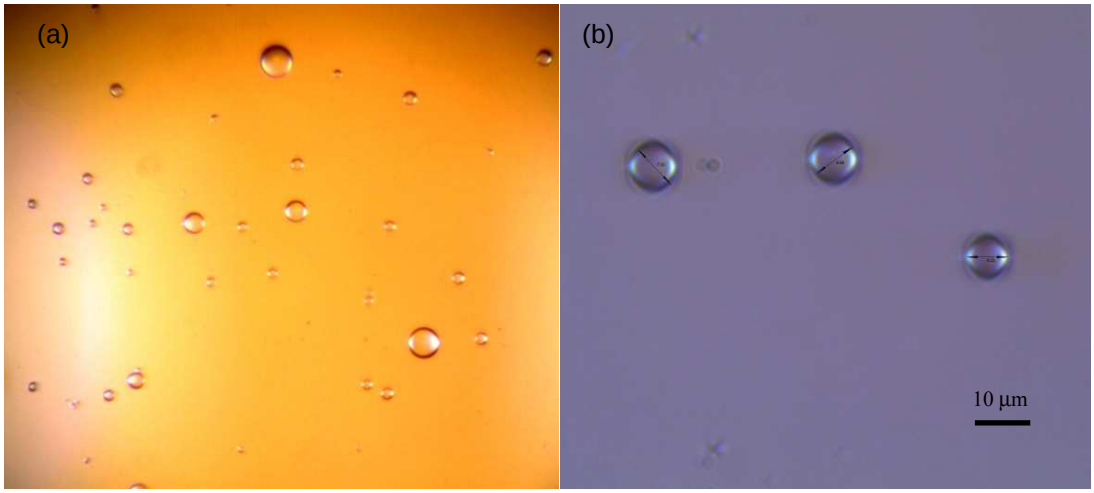

Figure 3.7. Distributed (dispersed) silica particles a) before decantation b) after decantation

3.2.3. Immobilization and Storage of Colloid Probe Particles

Silica particles in the solution (Figure 3.7) immobilized on the 47 mm diameter 0.2 µm membrane filter. Immobilized on a membrane filter of particles photographs displayed in Figure 3.8. The success of the dispersion process is obtained from the photographs in which the surfaces of particles is quite clear and does not contain small grains on the surface. This particles are ready to be used as a colloid probe. These particles keep in an oven under vacuum until used.

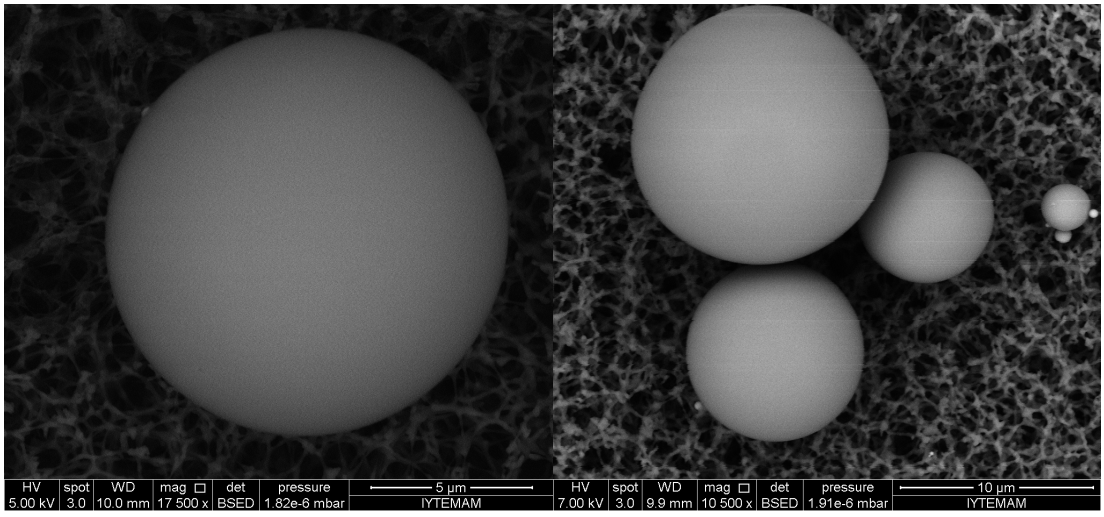

Figure 3.8. Silica particles immobilized on the membrane filter

3.3. Determination of Spring Constants of Cantilevers

The force measurement by using Atomic Force Microscopy requires a lot of detail. Most important point of them is determining the cantilever spring constant accurately.

According to Hooke's law, firstly the spring constants values of the cantilever must be known to convert the amount of curvature to the actual (absolute) values of the force. The force is equal F=kx (Figure 3.9). Where F, the interaction force between the surface and the sharp tip (Newton), x, observed bending (m), and k is the spring constant of cantilever (Newton / meter).

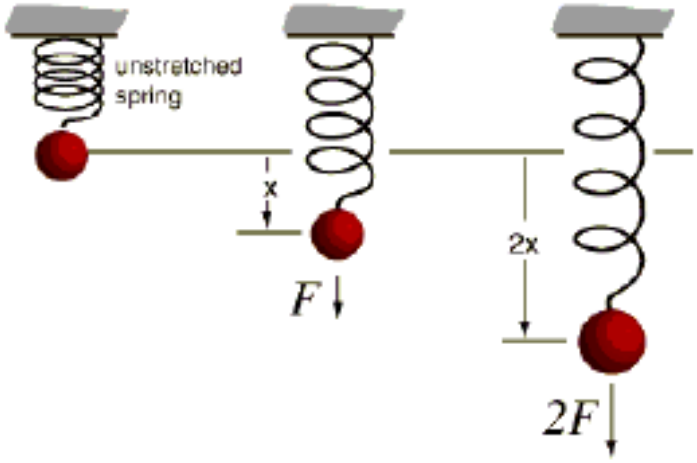

Figure 3.9. According to Hooke's law , the relationship between force and elongation of spring.(Source:http://www.ndted.org/EducationResources/CommunityCollege/Ultrasonics/Physics/elasticsolids.htm)

The correct calculation of each spring constant of cantilever is very important to obtain force measurements quantitatively. Using average spring constants mentioned in the box by the company that can be misleading. These values are not accurate enough for the present study and should be confirmed. In summary,the calculation of the spring constant for each cantilever is important for accuracy. Different methods are used to calculate the spring constant of the cantilever. These methods was listed in Table 3.1 (Ohler, 2007).

Table 3.1. Methods of calculation spring constant and Margins of error for each method (Source: Ohler, 2007)

Method	**Uncertainty**	**Main source of error**
Simple Beam	~%16	Cantilever thickness
PBA	~%26	Elastic modulus of SiN
Frequency Scaling	~%9	Si density
Reference cantilever	~%9	Deflection sensitivity
Added mass (Cleveland method)	~%15-30	Particle diameter
Sader	~%4	Cantilever width
Thermal tune	~%8	Deflection sensitivity

Sader method calculate the spring constant by using finite element analysis. According to Table 3.1. Sader method has 4% margin of error with at least approach. Sader method which was held with the rectangular cantilevers used in this study. Width and length values of the rectangular cantilever are required as well as the natural resonant frequency and oscillator factor (quality factor) values to determine the spring constant of rectangular cantilever with Sader method at liquid or air condition.
Accordingly, the spring constant is given by the following equation:

$$k_n = 7.5246\,\rho_f\, b^2\, L\, Q_f\, \omega_f{}^2\, \Gamma_i \tag{3.2}$$

Here;

ρ_f: the density of the fluid (air; 1.23 kg/m^3)

b: width of cantilever(m)

L: length of cantilever(m)

Q_f: oscillator factor

ω_f : natural resonant frequency (Hz)

Γ_i: imaginary part of hydrodynamic function (a function of Re; for example for Re=10 to $\Gamma_i = 0.2$)

Reynold number is given by following equation:

$$\mathrm{Re} = \frac{\rho_f \, \omega_f \, b^2}{4 \mu_f} \tag{3.3}$$

Here, μ_f viscosity of the fluid (air; 1.79×10^{-5} kg/m.sn).

Though Γi was proposed for the complex functions,in this study, an empirical function of Re was developed for Γi.

$$\Gamma_i = \frac{1.225\text{x}10^{-3} + 0.208\mathrm{Re} + 3.28\mathrm{Re}^2 + 5.04\mathrm{Re}^3 + 0.509\mathrm{Re}^4 + 1.111\text{x}10^{-3}\mathrm{Re}^5}{10^{-6} + 0.0055\mathrm{Re} + 0.554\mathrm{Re}^2 + 4.36\mathrm{Re}^3 + 2.09\mathrm{Re}^4 + 0.033\mathrm{Re}^5} \tag{3.3}$$

Width and length of cantilevers was determined using image tool program. The resonant frequency and oscillator factor value of cantilevers was calculated by using Atomic Force Microscopy for each cantilever as well. All measurements were repeated by 5 times and error intervals were determined for each calculation. Length,width, resonant frequency, oscillation factor values are given in terms of the mean values and error ranges in Figure 3.10-a, Figure 3.10-b, Figure 3.10-c and Figure 3.10-d, respectively.

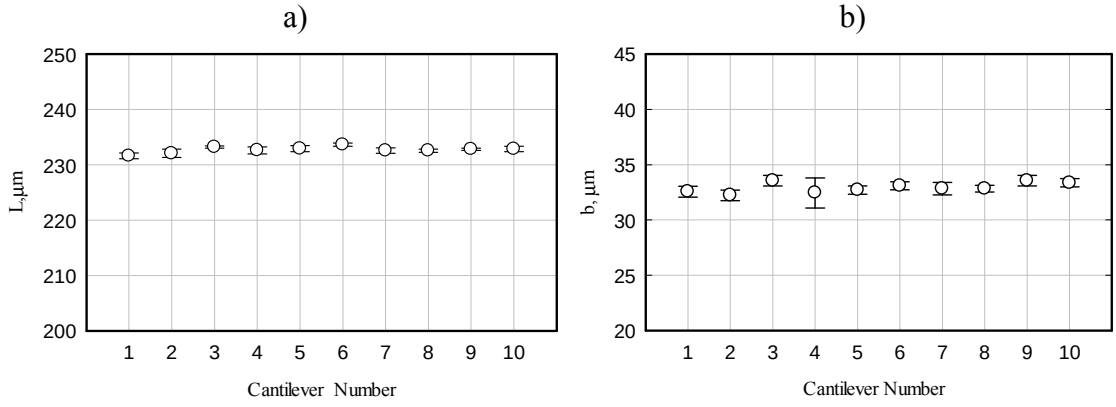

Figure 3.10. Cantilevers used in the test a) length, b) width, c) resonant frequency and d) oscillator factor

(cont. on next page)

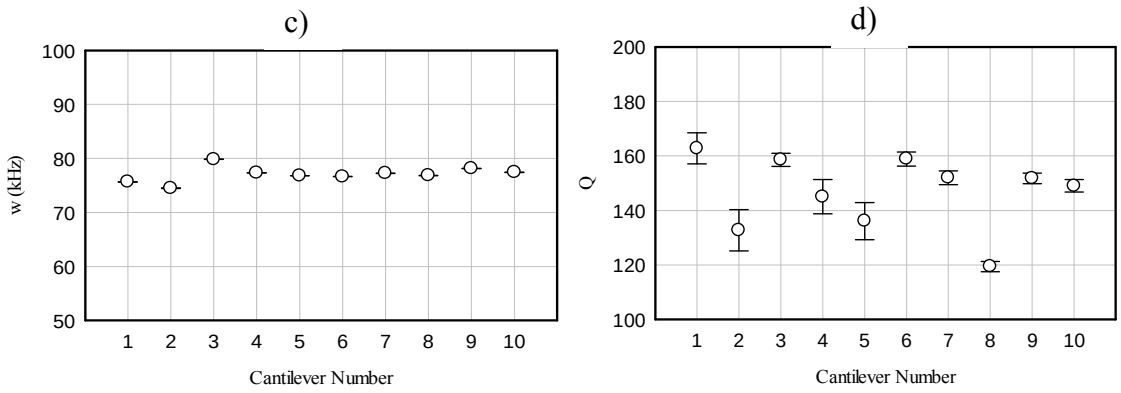

Figure 3.10. (cont.)

An example of calculation the spring constant of cantilever is as follows :

$$\rho_a := 1.23 \cdot \frac{kg}{m^3} \qquad \mu_a := 1.79 \cdot 10^{-5} \cdot \frac{kg}{m \cdot sec}$$

$$b := 33.36\,10^{-6} \cdot m \qquad L := 232.87\,10^{-6} \cdot m \qquad \varpi := 77.45\,10^{3} \cdot Hz \qquad Q := 149$$

$$Re := \frac{\rho_a \cdot \varpi \cdot b^2}{4 \cdot \mu_a} \qquad Re = 1.481$$

$$\Gamma(Re) := \frac{1.225\,10^{-3} + .208 \cdot Re + 3.28 \cdot Re^2 + 5.04 \cdot Re^3 + 0.509 \cdot Re^4 + 1.111 \cdot 10^{-3} \cdot Re^5}{1.0 \cdot 10^{-6} + .0055 \cdot Re + .554 \cdot Re^2 + 4.36 \cdot Re^3 + 2.09 \cdot Re^4 + 0.033 \cdot Re^5}$$

$$\Gamma(Re) = 1.026$$

$$k := (2 \cdot \pi)^2 \cdot 0.1906 \rho_a \cdot b^2 \cdot L \cdot Q \cdot \varpi^2 \cdot \Gamma(Re) \qquad k = 2.20 \frac{N}{m}$$

10 cantilevers are selected and calculated spring constant. The length, width, resonant frequency and oscillation factors of cantilevers are given in Table 3.2.

Table 3.2. Spring constant were calculated for 10 cantilevers

Cantilever Number	Length, μm	Width μm	ω_f (kHz)	Q	k_n, N/m
#01	231.60	32.56	75.68	162.79	2.26
#02	232.13	32.23	74.48	132.75	1.79
#03	233.23	33.55	79.85	158.62	2.46
#04	232.60	32.45	77.33	145.03	2.08
#05	232.92	32.69	76.81	136.11	1.95
#06	233.64	33.09	76.65	158.90	2.30
#07	232.56	32.82	77.25	152.02	2.20
#08	232.56	32.82	76.84	119.44	1.72
#09	232.82	33.55	78.14	151.80	2.28
#10	232.87	33.36	77.45	149.00	2.20

Spring constants were calculated for each cantilever (Figure 3.11)

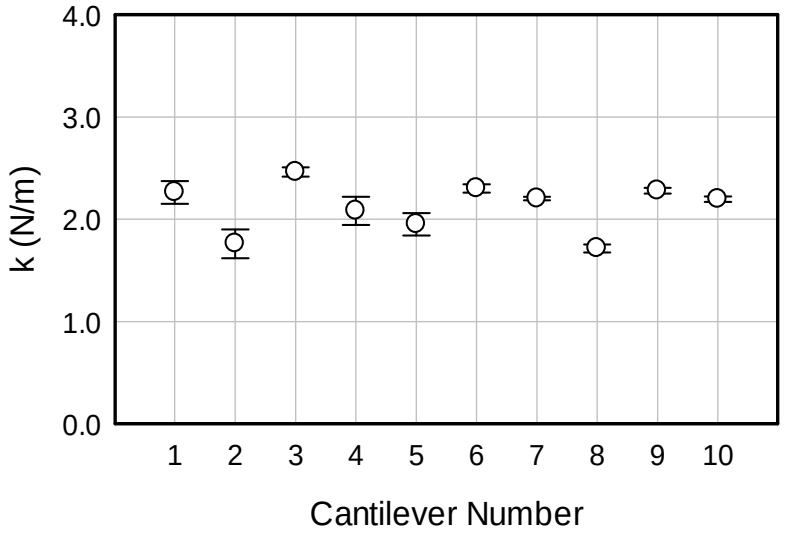

Figure 3.11. The spring constants of the cantilevers used in the studies

3.4. Preparation of Colloid Probes

3.4.1. Nanomanipulator

Silica colloid probes used for the surface charge measurement studies on sapphire and quartz surface. To achieve these probes, 5-10 μm diameter colloidal particles were required fixing on cantilever which is about 230 μm in length and 32 μm in width. It is difficult to see particles in this size even under a high-class microscope. The extremely high resolution of a special device are needed both optical and mechanical in its ability for determination whether it has intended properties (sphericity, smooth surface, no pollution), manipulation and fixing on cantilever.

This device:

a) must contain a high-magnification microscope and this magnification must be possible to switch to the form continuous (continuous zoom),
b) must have a high depth of focus,
c) must contain two arms which be able to move the XYZ directions nanometer level motion and must have contain two arms that the micro-capillary tubes can be mounted for manipulation of particles,
d) the stage should have moving nanometer level on XY directions, and sample can be placed on the stage,
e) Should be control by the computer completely,

Colloid prob preperation was running on the Nanomanipulator. Nanomagnetic Scientific Instruments Company which is in Hacettepe Technopark was tasked with a production of nanomanipulator by project coordinator and M.S. student. This device was maden with a supporting of TUBITAK. The Nanomanipulator also was put on product list of the company. Some of the important features of the device shown in Table 3.3 are as follows:

Table 3.3. Specifications of Nanomanipulator.

1. Camera

2. Microscope unit

Continuous magnification x100-X1400

Resolution 0.85 μm

5MP camera with image processing program

3. Lens with a long focal depth

4. The left arm of XYZ / 5. The right arm of XYZ

Independent or at the same time XYZ axis movement on 45 mm motion field

Move smoothly with the theoretical sensitivity of 1 nm step

The encoder reads the action, position identification, storage location information

6. The sample mount

7. Motorized XY table

XY axis movements with a 50mm field of action

Move smoothly with a resolution of 42nm

8. Body

Vibration absorption table

Note: The electronic unit and software with USB 2.0 connection to a computer with dual screen computer allows control of all the menus.

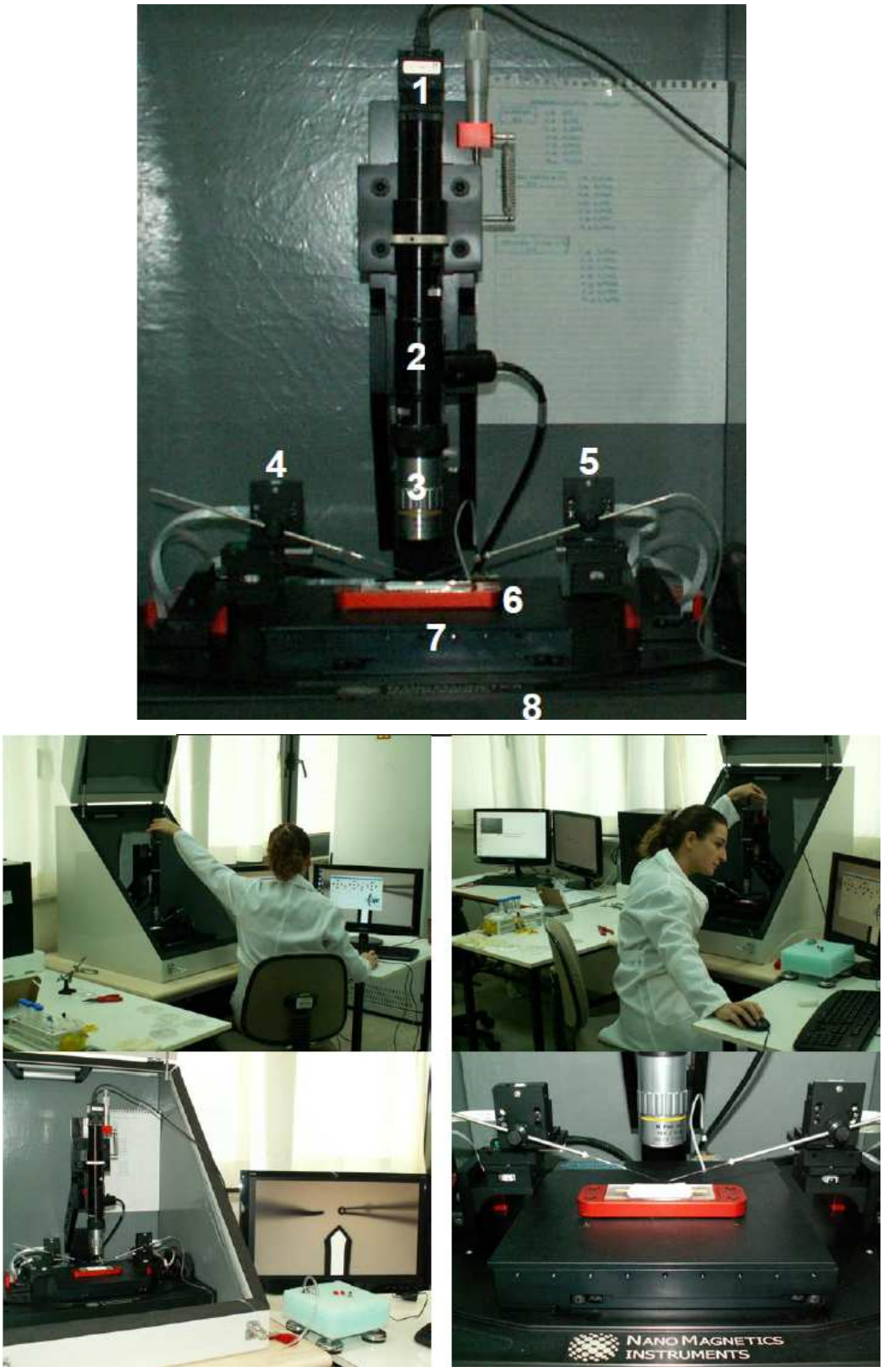

Figure 3.12. Nanomanipulator used to make colloidal probes

3.4.2. Procedure of Colloid Probe Preparation

Colloid probes were prepared by fixing colloidal-sized particles on tippless cantilever using nanomanipulator. The materials used in the preperation of colloid prob is shown in Figure 3.13.

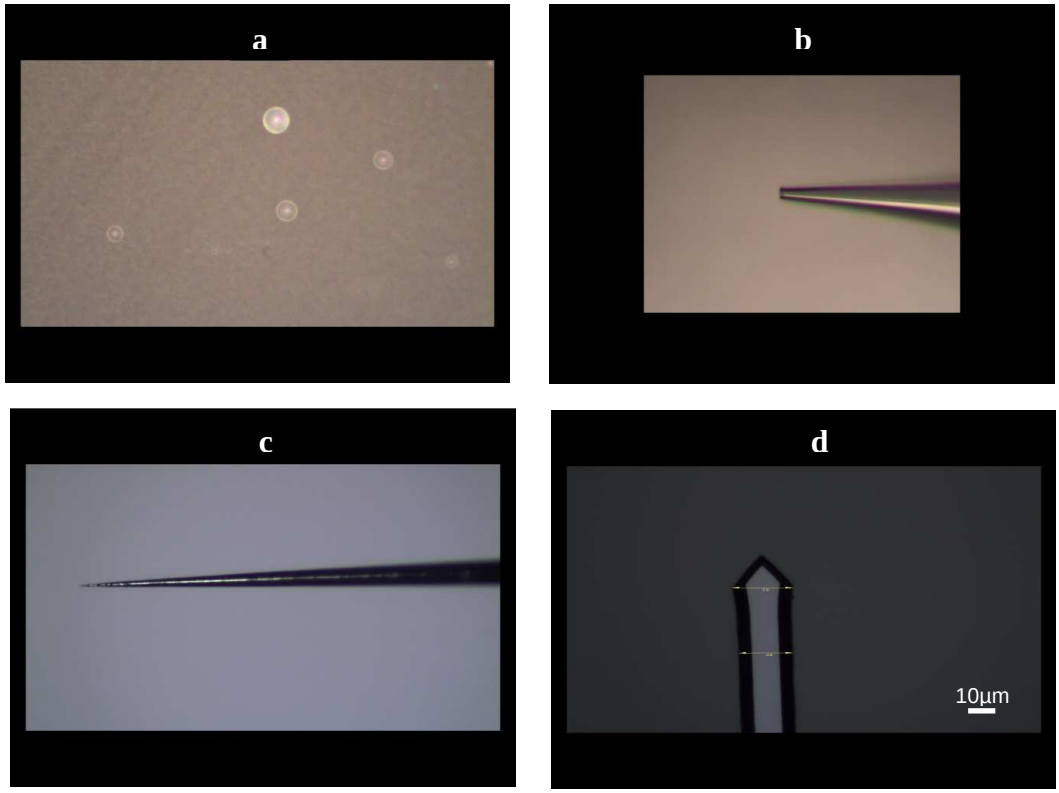

Figure 3.13. Materials used in the preperation of probe: a) Colloid probe particles, b) micro pipettes used to capture the colloidal particles have 5 micrometers inner diameter, c) tungsten needle was used to apply adhesive on cantilever with 1 micron tip, d) silicone tippless cantilever

Microscope of nanomanipulator was used to watch all the manipulation process in detail. In addition, the high working space needed for the manipulation achieved due to the depth of focus of the microscope. Steps of the preperation of the colloid probe as follows:

a) was approached of the to the surface,
b) glass capillary tube was continued to approach in a controlled way (please note that dispersed particles completely isolated on the membrane filter),
c) particle was adsorped with the help of micro-vacuum pump,

d) particle was captured by capillary tube,
e) particle was approximated to the cantilever,
f) the adhesive to be taken with tungsten needle,
g) approximation of particle and needle to the cantilever,
h) adhesive was applied end of the cantilever,
i) particle was left on cantilever,
j) back side of cantilever(a some of the adhesive is located on the back end of cantilever),
k) image of coloid probe,
l) SEM image of a colloid probe,

The steps were shown in Figure 3.14. Completed colloid probes immediately put on the desiccator under vacuum until measurement of the force. It is important to note that, the colloid prob which is prepared by nanomanipulator was come in third in the competation of SEM, which was organized by Materials Research Center, IZTECH.

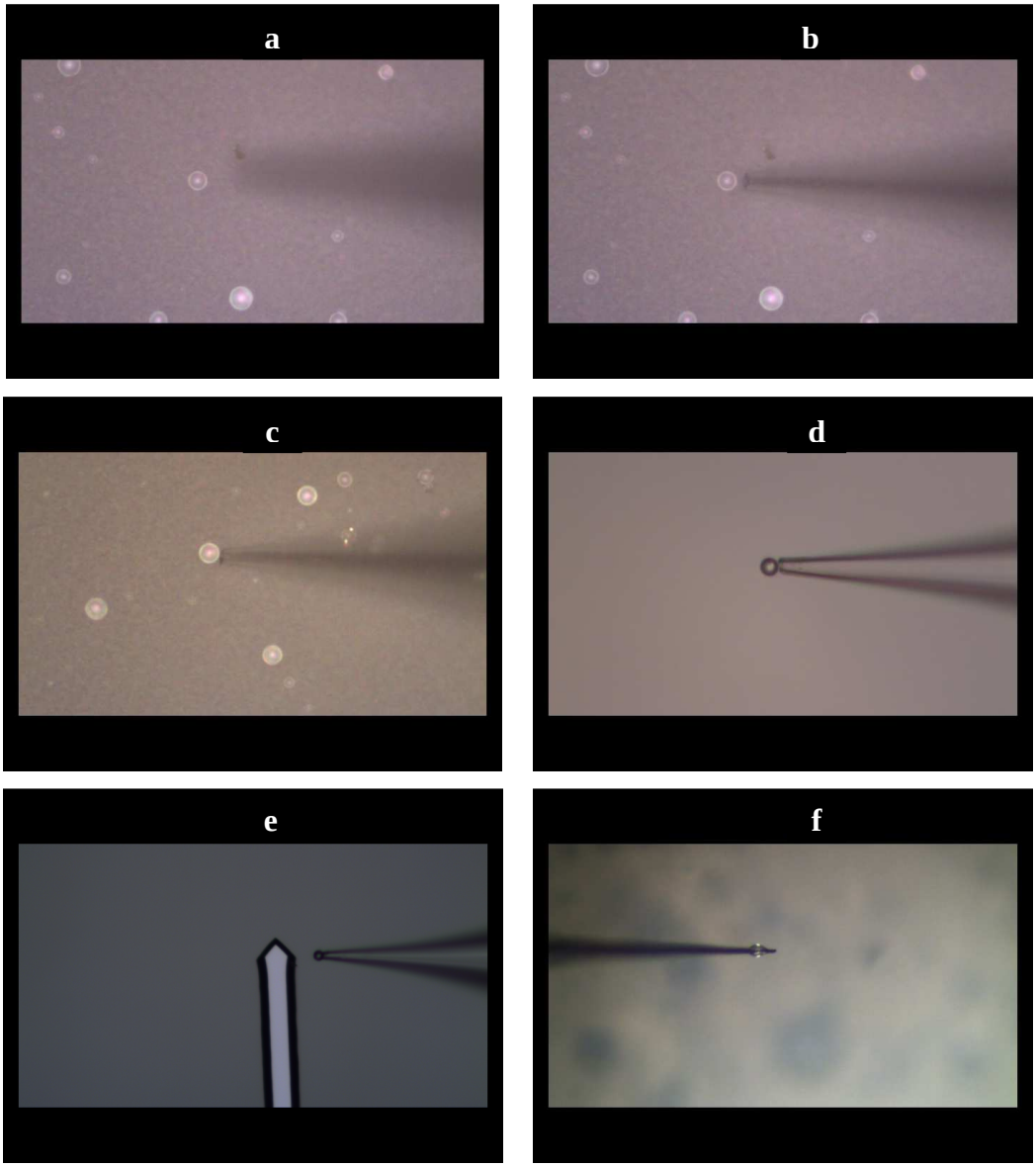

Figure 3.14. The steps of the preperation of the colloid probe

(cont. on next page)

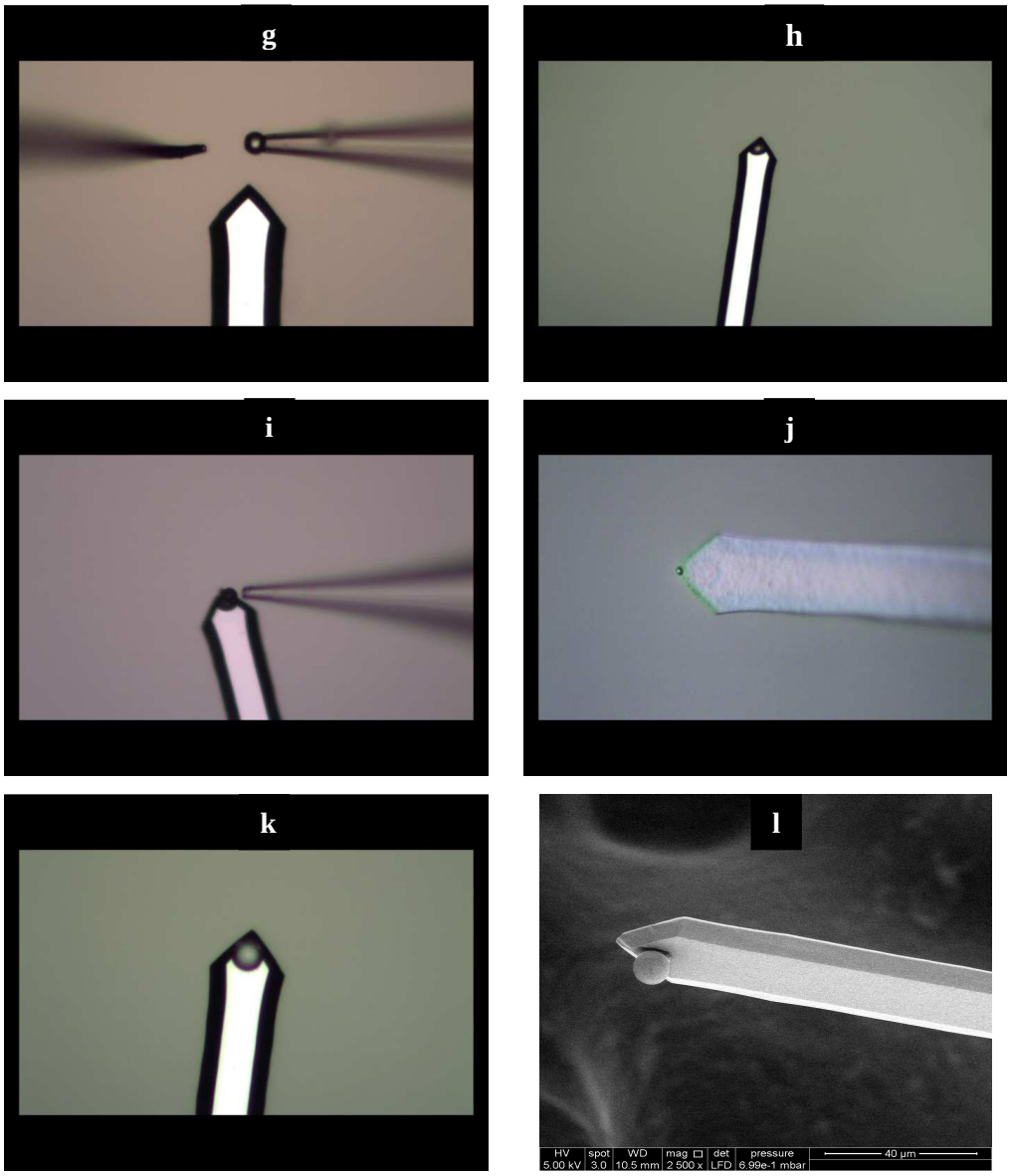

Figure 3.14. (cont.)

3.5. Force Measurements

In this study, Atomic Force Microscopy (AFM) which is generally used in determining the overall topography of the surface was used for direct measurement of the atomic forces in a solution between two solid surfaces (one of the scanned surface and colloid probe). Force measurements was running on AFM, Nanomagnetic of Scientific Instruments Company in Department of Chemical Engineering, IZTECH.

Theory and equations used in the analysis of van der Waals and Electrostatic forces between the colloid probe and the surface. In this section, the force measured between the colloid probe and the surface. Raw signals were converted to force-distance curves. The force-distance curves were analyzed by the theory. Potential profile of surface were obtained. As a result, surface charge distributions obtained by means of analysis of force measurements on different conditions were given.

3.5.1. Atomic Force Microscopy

The force measurement by using Atomic Force Microscopy requires a lot of detail. Therefore, princible of Atomic Force Microscopy should be analyzed. The basic principle of the atomic force microscope is quantify the interaction between the atoms at the end of a cantilever (Figure 3.15) and atoms on the surface. This interaction depends on the distance between the tip and the surface. Thus, the sample surface is placed on the piezoelectronic scanner and interactions begins at a distance during approximation in a controlled manner. Depending on the strength of the interaction, a bending has been observed on the cantilever which is maden a very thin silicon or silicon nitride. The deflection of the spring is measured using a laser beam. The laser beam reflect on cantilever and changes of laser beam was detected by photodetector (photodiode) (Figure 3.16). In this way, measuring force is possible even under nanonewton magnitude.

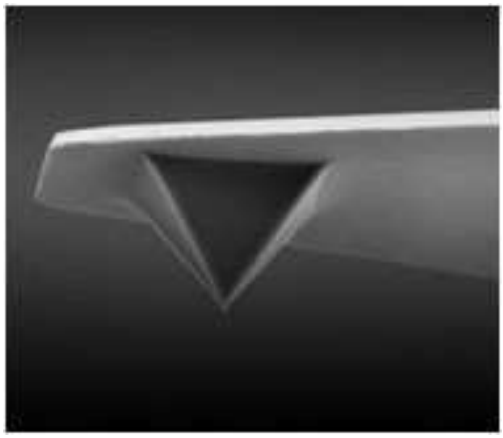

Figure 3.15. The tip of Atomic Force Microscopy
(Source: Nanoworld Catalog 2011)

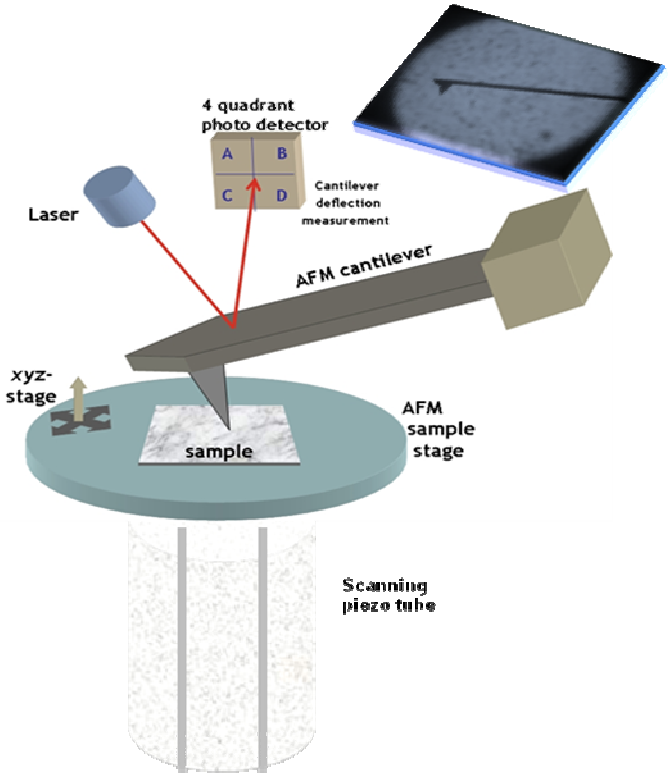

Figure 3.16. The principle of force measurement
(Source: Wikipedia 2012)

3.5.2. Force Measurement with Atomic Force Microscopy

Cantilever is approximated to the closest surface point that surface and cantilever has not started interaction yet (a few hundred nanometers). During the measurement, cantilever is approximated to the surface at a certain speed, when the surface and prob contact with each other then retracted and returns to the first point (Figure 3.17-a) (Polat et al., 2006). Interaction force varies during cantilever approach or move away from the surface, due to the change of the distance amount between surface and cantilever. This force manifests itself as the bending of the cantilever. Bending that formed due to the interaction of surface and cantilever is measured by a laser-photo-detector system. As a result, the vertical displacements change the cantilever signal which is detected by photodetector and then raw data is obtained (Figure 3.17-b).

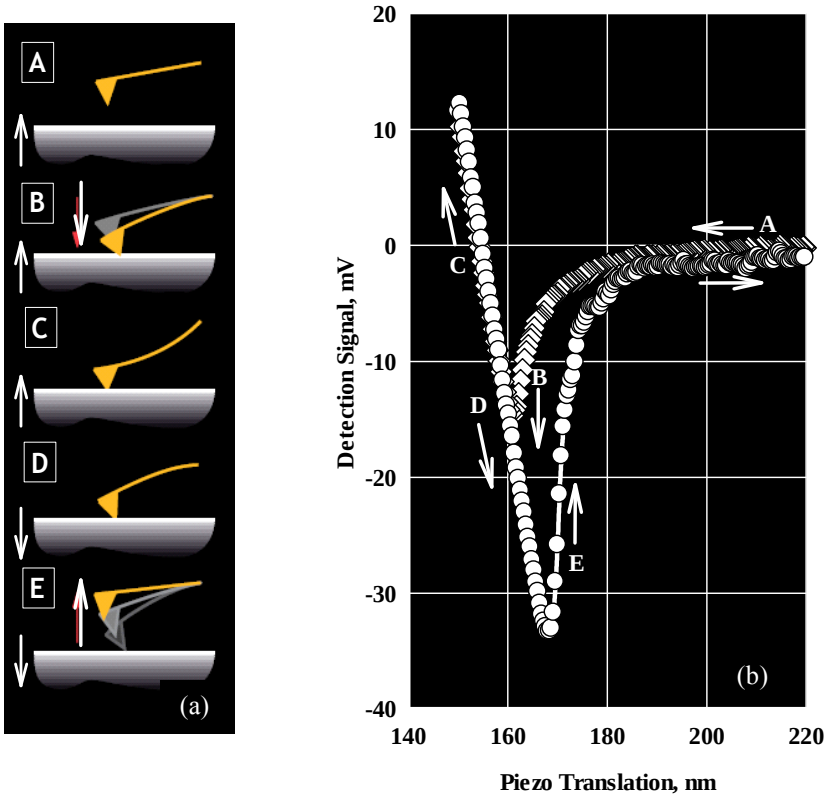

Figure 3.17. Principles of obtaining force curves from AFM
(Source: Polat et al., 2006)

3.5.3. Preparation for Force Measurements with Colloid Probes in Liquid Media

The most important detail is to make sure the surface (silica or sapphire substrates), and the probe colloid (colloidal silica particles used in this study) are clean at atomic levels , before starting force measurement. The colloid probes used in the thesis, in order to avoid any pollution or chemical imbalance problem, should be subjected to a cleaning and conditioning process.

According to this prosedure colloid probe:

1) kept for a short period of time (30 seconds) in 50°C ultra-pure water
2) washed with copious amounts of ultra-pure water,
3) cleaned with ultrasonic treatment (10-20 seconds) washed with ultra-pure and ethanol copiously,
4) dried under vacuum oven and exposed to UV radiation at 10 minutes,

5) washed again ultra-pure ethanol and ultra-pure water in abundance and kept in a desiccators under vacuum.

During UV treatment (Figure 3.18), laser light reflects back side of cantilever and this light must not subject to any blackout on cantilever. In order to make sure of that, 5 were cantilever taken as an example and were exposed to radiation under the UV lamp increasing periods of time. Following, the power of reflected laser light was measured in different points of cantilever by the AFM photodiode. The results shown in Figure 3.19 reveal that UV radiation affect the capacity of the laser light reflection even the least bit, although this effect even after a 40 minute radiation experiments is not sufficient to affect. Thus, the UV cleaning method can be safely used for colloid probes.

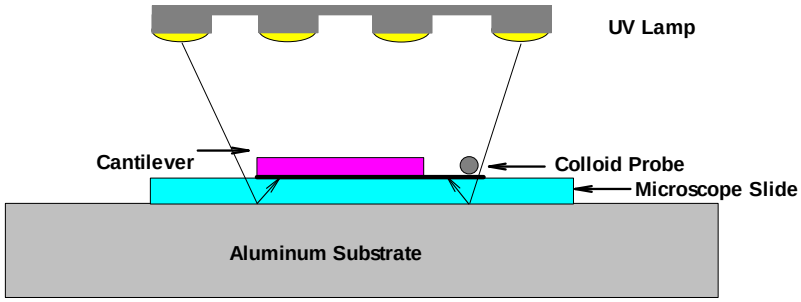

Figure 3.18. Colloid probe placed in UV lamp cell

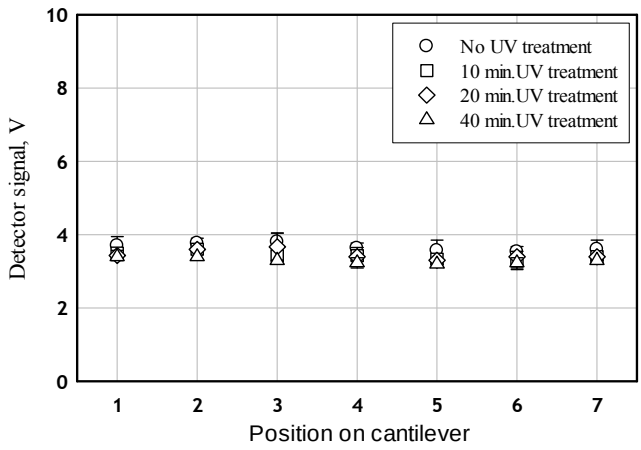

Figure 3.19. The effect of UV radiation on cantilever of the capacity of the laser light reflection

Another important point is that colloid probes and surface must wash with chemical solution before starting the experiment. Then, colloid prob cantilever washed with pure

water copiously and a solution of media respectively and subsequently is placed in the AFM apparatus. Surface and cantilever immersed in experimental solution completely. Both colloid prob and surface kept in this solution for 10 minutes to stabilize the whole system. The colloid prob was used for force measurement.

3.5.4. Force Measurements with Colloid Probes and Acquisition of Raw Force Signals

The force measurement between silica colloid probe and quartz or sapphire surface was be measured by AFM. All measurement was applied with a liquid cell. Force measurement was performed to determine attractive and repulsive forces between probe and surface. Measurements were carried out at sixteen different point on 40x40μm part of quartz surface. Same procedure was repeated several times to check reproducibility. All these experiments was repeated various pH conditions and different surface. An AFM force-distance curve is a plot of deflection vs. tip-sample distance (Figure 3.20).

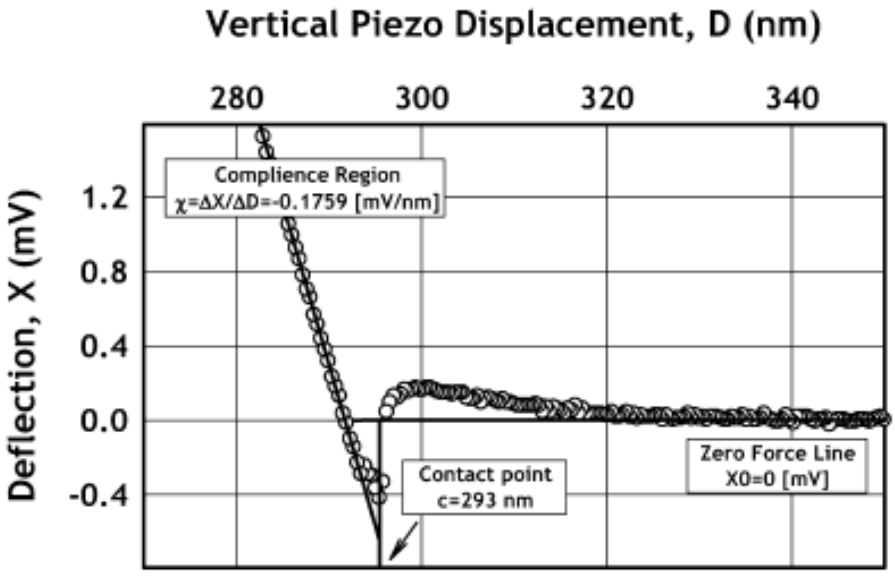

Figure 3.20. An example of raw force curve data
(Source: Polat et al., 2006)

3.5.5. Conversion of the Raw Force Signals to Real Force-Distance Curves

The curve in Figure 3.20 was obtained from the raw data of AFM, and only gives the change in the laser signal caused by bending of cantilever due to interaction forces between probe and surface. Distance D between surface and probe was not actual sample-probe distance h. This two distance differ because of piezo displacement D and cantilever deflection x. Therefore AFM force-displacement curve does not dublicate probe-surface interaction. This raw curves must be converted real force-distance curves.For this purpose some mathematical manipulations as spring constant is necessary to use. The algorithm to convert the Piezo Translation-Detection Signal Data to Real Force-Distance Curves is summarizes as follows:

Cantilever deflection: $x = (X - X_0) / (\Delta X / \Delta D)$

Probe-Surface seperation: $h - (D - c) / x$

Force (F_{AFM}): $F_{AFM} = k_n x$

These equations;

X, the amount of the reflected laser beam (Volt),

X_0, the amount of the reflected laser beam on based (Volt),

D, the amount of vertical piezo displacement (meter),

c, contact point(meter),

x, cantilever deflection (meter),

h, surface-probe distance (meter),

k_n, spring constant (Newton/meter),

F_{AFM}, interaction force obtained from AFM (Newton),

After colloid probe contact with the surface, the signal change (ΔX) caused by cantilever bending is directly proportional to the position change (ΔD) caused by vertical movement of piezo. This region is called as contact area and the slope of Δx/ΔD is used to calibration of cantilever signal. The procedure is illustrated in Fig. 3.21 and the algorithm used for raw force signal to actual force curve conversion.

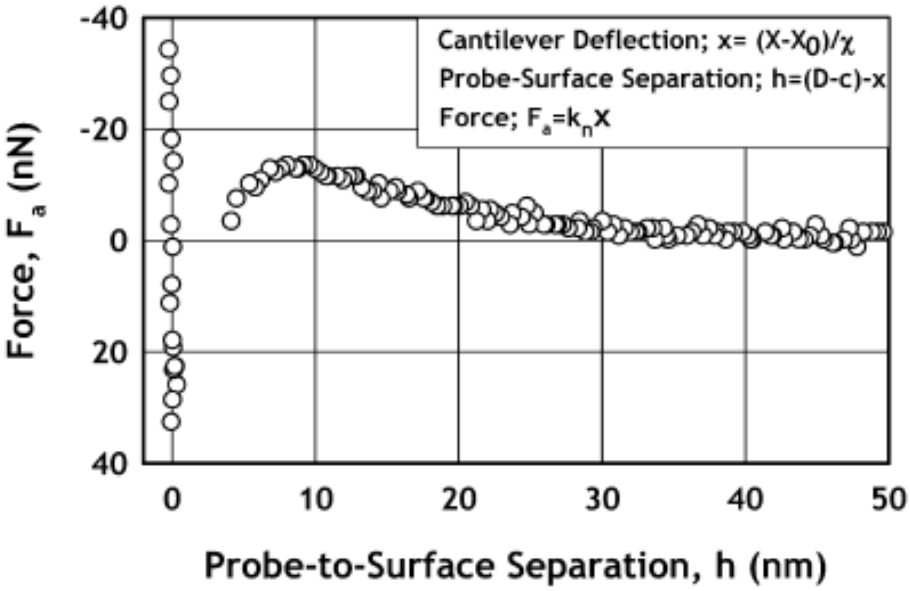

Figure 3.21. An example of conversion of raw force curve data to actual force curve (Source: Polat et al., 2006)

3.5.6. Theoretical Force-Distance Curves

Figure 3.21 shows that net interaction force F_{AFM} (nN) which occur depending on the distance between the surface and probe during the approach of colloid probe to the surface. This net force of interaction consists of van der Waals and electrostatic force interaction between the probe and surface. Thus, it is possible to obtain information about qualifications of the interacting surfaces when compared to the van der Waals (F_{vdw}) and electrostatic (F_{cp} and F_{cc}) pressures was given in below:

$$F_{vdw} = \frac{A_{12}}{6\pi h^3} \tag{3.1}$$

$$F_{cp}(h) = \frac{-\varepsilon\varepsilon_0\kappa^2}{2}\left[\frac{\psi_1^2 + \psi_2^2 - 2\psi_1\psi_2\cosh(\kappa h)}{\cosh(\kappa h)^2 - 1}\right] \tag{3.2}$$

$$F_{cc}(h) = \frac{-1}{2\varepsilon\varepsilon_0}\left[\frac{2\sigma_1\sigma_2\cosh(\kappa h) + (\sigma_1^2 + \sigma_2^2)}{\sinh(\kappa h)^2}\right]$$

The net force of interaction (F_{DLVO}) per unit area of the interacting plates:

$$F_{DLVO}(h) = F_{cc/cp}(h) + F_{vdW}(h) \tag{3.3}$$

Total pressure (F_{DLVO}) which is component of van der Waals (F_{vdw}) and electrostatic (F_{el}) interaction was converted to force ($F_{AFM)}$ through Derjaguin approximation. Details of calculation of theoretical force were given in Appendix C.

$$F_{AFM}(h) = 2\pi r \int_{h}^{\infty} F_{DLVO}(h)dh \tag{3.4}$$

3.5.7. Comparison of Real Force-Distance Curves with Theoretical Force-Distance Curves to Determine Surface Charge

Interaction force measured by AFM is compared the theoretical pressure curves by using 'curve fitting' method that is statistically the best fit curve. The only parameter of potential was changed to match the theoretical curve with experimental curve. The best potential profile was found by changing charge or potential in therotical force measurement. Therefore, the best fit curve was determined by using 'curve fitting' method. The only parameter of potential was changed to match the theoretical curve with experimental curve. Surface charge distribution was achieved through the analysis of force measurements with different points.

Force measurement were repeated at 16 different points as given below at constant solution conditions. These 16 points are away 10 μm from each other on x and y directions.

CHAPTER 4

RESULTS

4.1. Raw Force Data

Force measurement result between quartz surface and silica colloid probe (10^{-3} M KCl solution at pH=6.0 and T=20 °C) is given in Figure 4.1. These measurements were repeated 3 times at the same point to confirm the signal value and the average of these three values is taken.

Curve in Figure 4.1 was obtained in the same way with representatively shown in Figure 3.17-b, and this graph shows Piezo Translation (nm) versus cantilever detection signal (mV). As can be seen from graph, piezo starts closer to the surface on 300 nm. In the meantime,there was no bending and signal was zero because of no interaction due to colloid probe was too far away from the surface. However, interaction began between surface and colloid probe when piezo comes close to 150 nm approximately, at this point cantilever was bending and photodiode read a signal.

According to figure, the interaction is repulsive and increases with while piezo close to surface. Despite the presence of the driving force, colloid probe continued to close to the surface and colloidal probe contacted with surface below 100 nm. This area was referred to as contact point and colloid prob flushed to the surface. Therefore, cantilever bent in proportion with continuing to approach and linear signal was generated below 100 nm. Change of signal was determined with the slope of this curve. In other words, the cantilever signal is calibrated in this region, and spring constant is used to convert the raw force signals to the real force distance curves.

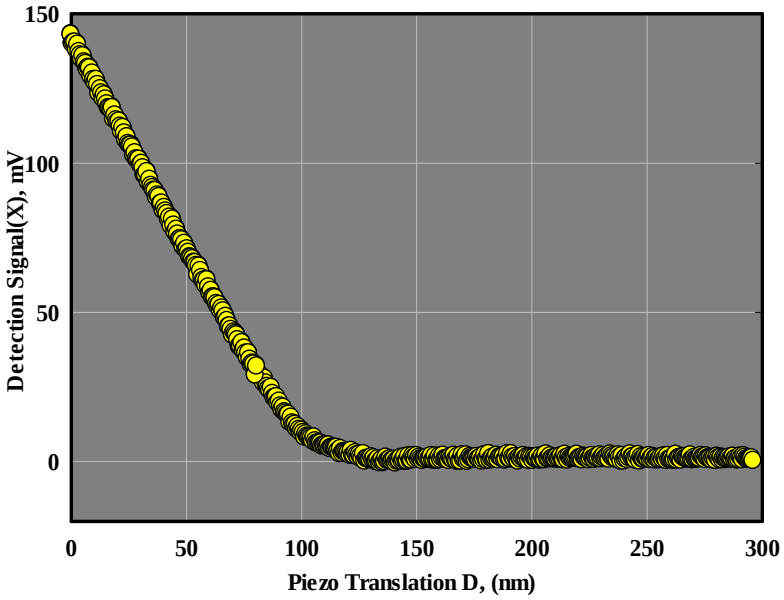

Figure 4.1. The raw force measurement results obtained from the AFM (Quartz surface-quartz colloid prob; 10^{-3} M KCl solution; pH=6.0; T=20 ^{o}C)

4.2. Conversion of Raw Force Data to Real Force-Distance Curves

The raw force signal in Figure 4.1 was converted to force-distance curve was showed in Figure 4.2 by using transformations. Probe was 80 nm away to surface initially and there was no interaction between the probe and the surface. However, when probe was close to 40 nm, repulsive interaction began between colloid probe and surface. The value of this force continued to increase until the probe contacted with the surface.

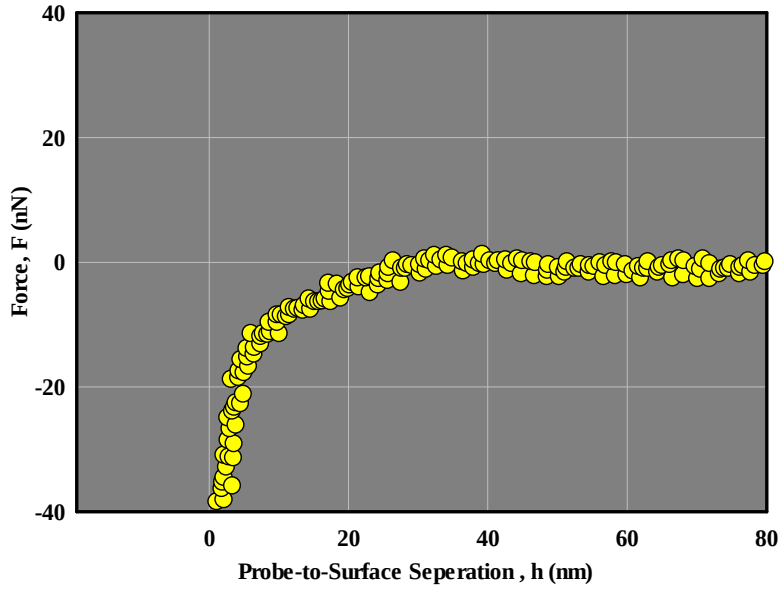

Figure 4.2. Force-Distance curve obtained by transformation of raw force measurement (Quartz surface-quartz colloid probe; spring constant k=2.06 N/m; 10^{-3} M KCl solution; pH=6.0; T=20 ^{o}C)

Surface potential of silica powder was approximately -35 mV at pH = 6 (Figure 2.5). The surface had a negative potential at this pH value, which was an expected value. In this case, despite the presence of van der Waals forces, a strong repulsive force occured between probe and surface. Figure 4.2 show that probe has a strong repulsive force which excess the van der Waals force until it starts to contact with surface.

4.3. Theoretical Force-Distance Curves Superimposed Real Force-Distance Curves

Interaction force measured by AFM in Figure 4.2 was compared with the theoretical force curves plotted in Figure 4.3. The best potential profile was found by changing the charge or potential in therotical force measurement. Therefore,the best fit curve was determined by using the 'curve fitting' method. A dark colored line is achieved, if the surface has constant charge. Similarly, the light-colored lines are obtained if surfaces have constant potential while they approached to each other.

All of the parameters used in the statistical analysis were the actual values of the experiment (Spring Constant k=2.06 N/m; 10^{-3} M KCl solution; pH=6.0; T=20 ^{o}C; charge of colloid prob=-35 mV; Hamaker constant of Quartz was 1.02×10^{-20} Joule

[Bergström, 1997]). The only parameter of potential was changed to match the theoretical curve with experimental curve. According to this analysis, the surface potential should be around -46 mV and was calculated to match the theoretical curve with experimental curve in Figure 4.3. As can be seen from the figure theoretical curve and experimental force (F_{AFM}) are almost the same in case of surface potential is -46 mV. Analysis also show that surface behaved like constant surface charge. This results are expected for quartz-quartz system under this conditions.

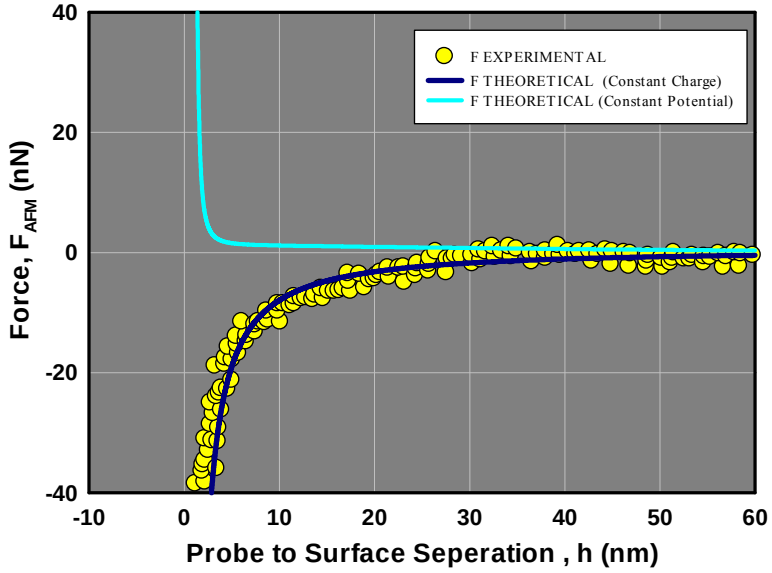

Figure 4.3. Comparison of force-distance curves with theoretical curves (Quartz yüzey-quartz colloid prob; spring constant k=2.06 N/m; 10^{-3} M KCl solution; pH=6.0;T=20^{o}C)

4.4. Surface Charge Maps

Surface charge distribution was achieved through the analysis of force measurements with different points. Force measurement were repeated at 16 different points as given below at constant solution conditions. These 16 points are 10 µm away from each other on x and y directions (Figure 4.4).

16	**15**	**14**	**13**
9	**10**	**11**	**12**
8	**7**	**6**	**5**
1	**2**	**3**	**4**

Figure 4.4. Schematic representation of 16 points on the sample surface

Each measurement for every point on this experiment was repeated 3 times and were averaged. Figure 4.1 shows raw force signal as a function of the vertical piezo displacement based on these measurements.

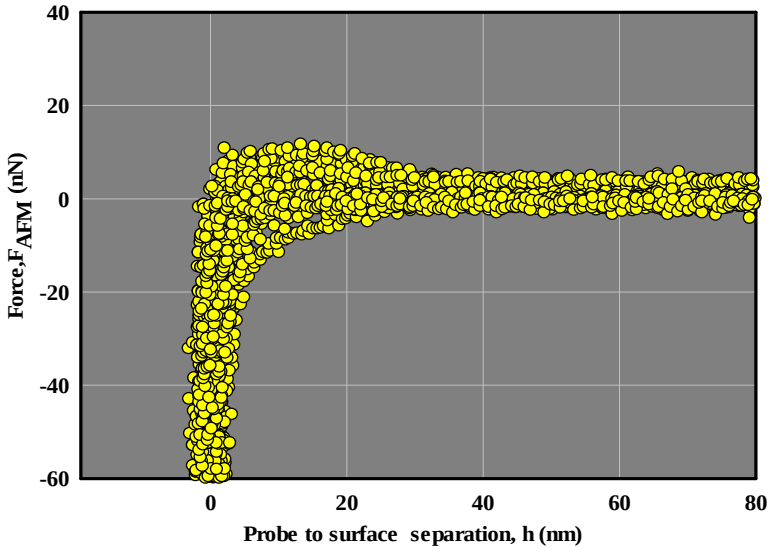

Figure 4.5. Force –Distance curves obtained from selected 16 different points on surface (Quartz surface-quartz colloid prob; spring constant k=2.06 N/m; 10^{-3}M KCl solution; pH=6.0; T=20 ^{o}C)

In the next step, the raw force signals were converted into a real force curves at each point as described in detail above. The surface potential was determined by the comparison experimental results with the theory for each point. The forces in Figure 4.5

were obtained between silica colloid probe and the quartz surface at pH=6. The value of the spring constant is k=2.06 N/m.

The surface of a potentials of 16 point on surface are displayed in Figure 4.6 as a result of analysis of the forces in Figure 4.5. Figure 4.7 also shows potential profile of the same surfaces,10^{-3}M KCl solution at T =20 °C with different pH=10.

According to these results, the average potential of quartz surface was obtained -31mV in pH = 6.0 solution (Figure 4.6). This value was in full agreement with the zeta potential measurements ranging from -20 mV to -40 mV (Figure 4.8). However, Figure 4.6 shows large differences in the values of the surface potential between 0 mV and -78 mV.

Similarly, the average potential of the quartz surface was close to -86 mV at pH = 10.0 solution (Figure 4.7). This value, is very close to the zeta potential measurements ranging from -80 mV to -100 mV (Figure 4.8). According to Figure 4.7, the potential of quartz surface varies from -109 mV to -58 mV at pH 10.

Figure 4.8 shows that, quartz surface at pH 10 has a more negative and homogeneous distribution than pH 6. As a result, the average surface potential values consistent with the conventional methods (electrophoretic potential measurement) are illustrated in Figure 4.6 and 4.7. But the developed method provides a detail far beyond the average surface potential, and quantitative information about the distribution of the surface potential. Knowledge of the distribution of the surface potential at the surface compared to the average potential is extremely important to explain adsorption phenomena (for example, how a negative surface also allow adsorption of negative ions).

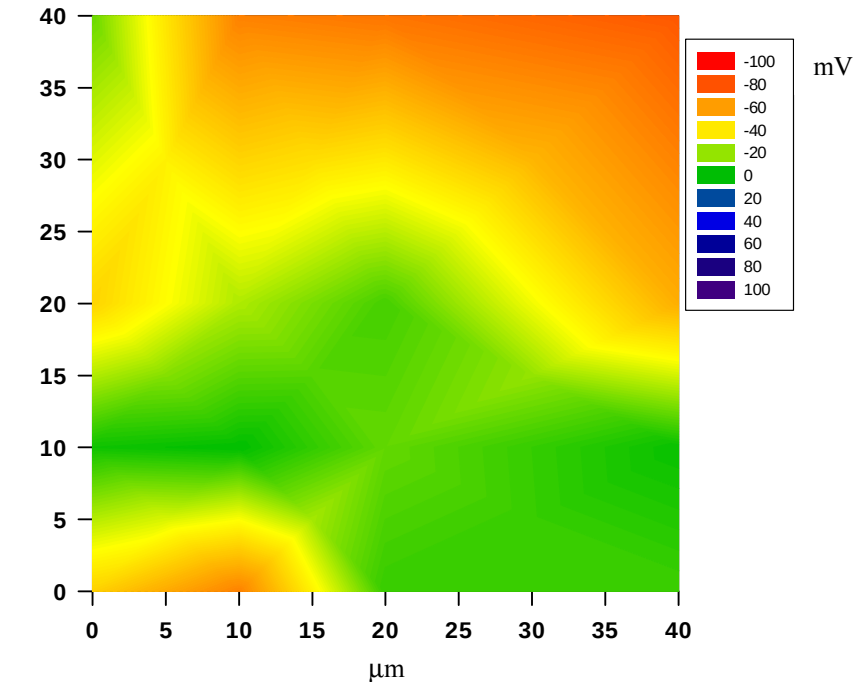

Figure 4.6. Surface potential was calculated by analysis of force-distance curves (Quartz surface-quartz colloid probe; spring constant k=2.06 N/m; 10^{-3} M KCl solution; pH=6.0; T=20 ^{o}C)

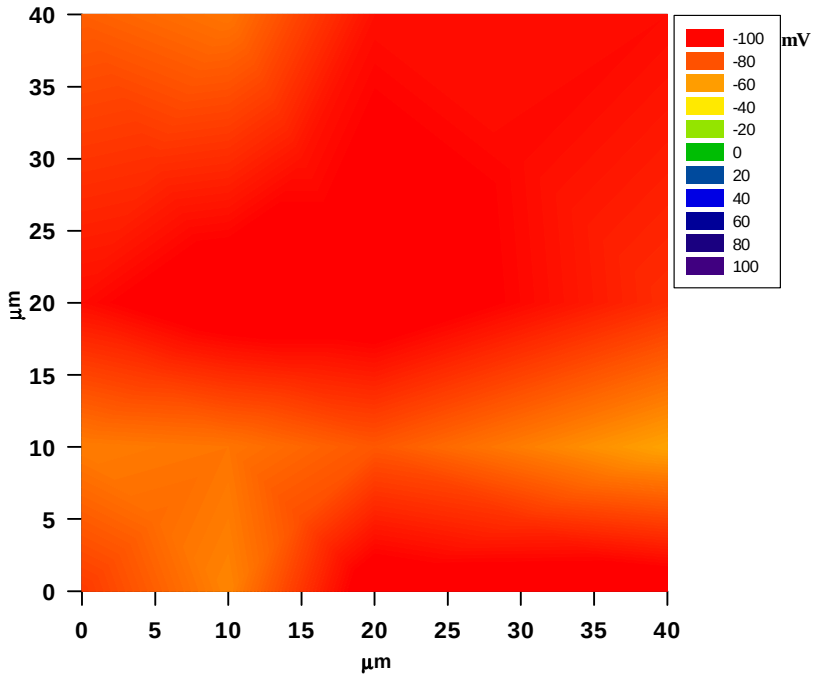

Figure 4.7. Surface potential was calculated by analysis of force-distance curves (Quartz surface-quartz colloid probe; spring constant k=2.06 N/m; 10^{-3} M KCl solution; pH=10; T=20 ^{o}C)

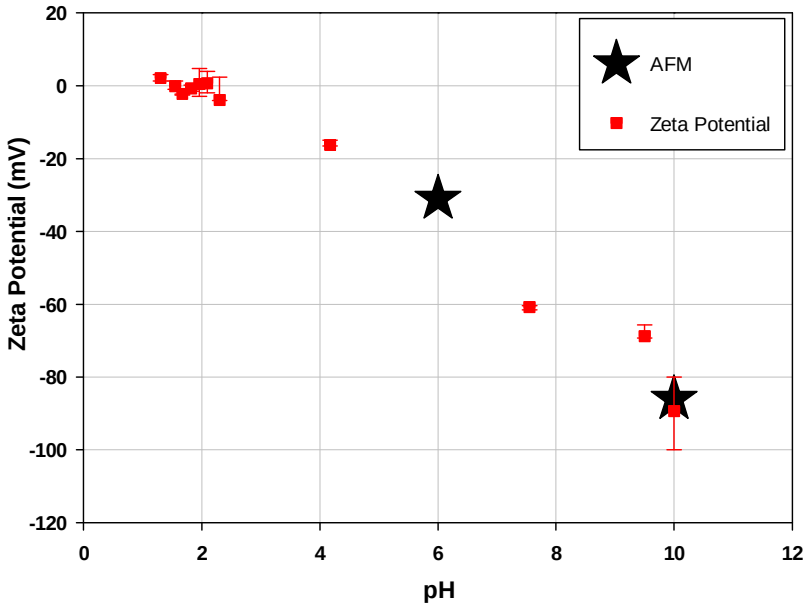

Figure 4.8. Comparison of average surface charges from quartz surface charge maps with zeta potential measurements

Figure 4.9 and 4.10 show the potential distribution of sapphire surface .This analysis was occurred between quartz colloid probe and sapphire surface at pH = 2.0 and pH = 10.

Accordingly, the average potential of the sapphire surface in an acidic environment (pH = 2.0) is +46 mV and this value compatible with zeta potential measurements range from +40 mV to +55 mV (Figure 4.11). The distribution of the surface potential values are between +19 mV to +55 mV (Figure 4.9).

The average surface potential of sapphire surface at pH 10 condition was -61 mV (Figure 4.10) and the potential distribution was observed between -49 mV and -70 mV. These values are compatible with zeta potential measurement results ranging from -55 mV to -70 mV (Figure 4.11).

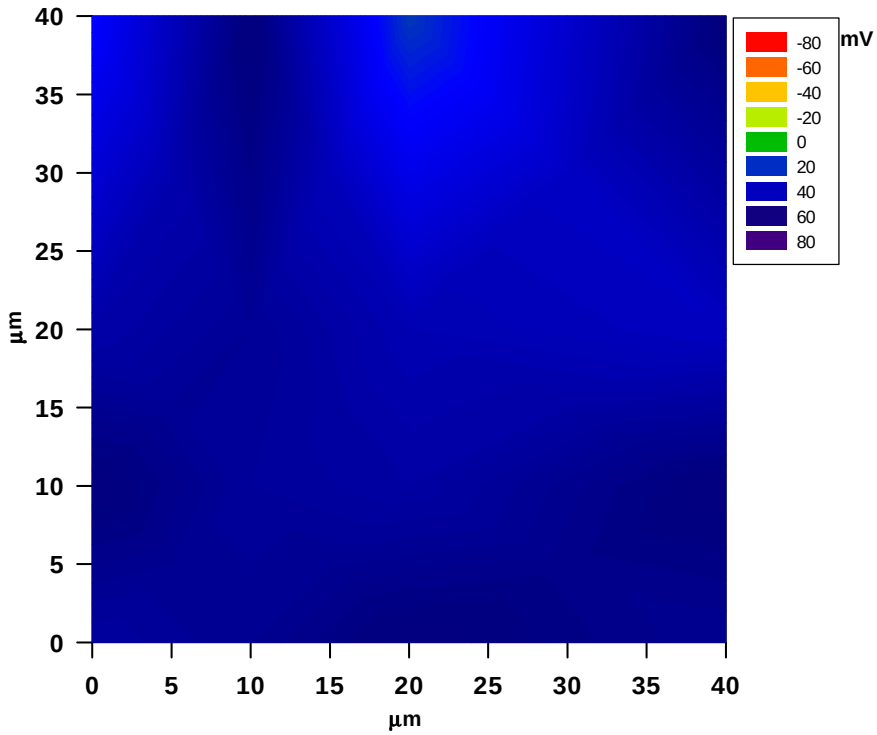

Figure 4.9. Surface potential was calculated by analysis of force-distance curves (Sapphire surface-quartz colloid probe; k=2.06 N/m; 10^{-3} M KCl solution; pH=2.0; T=20 ^{o}C)

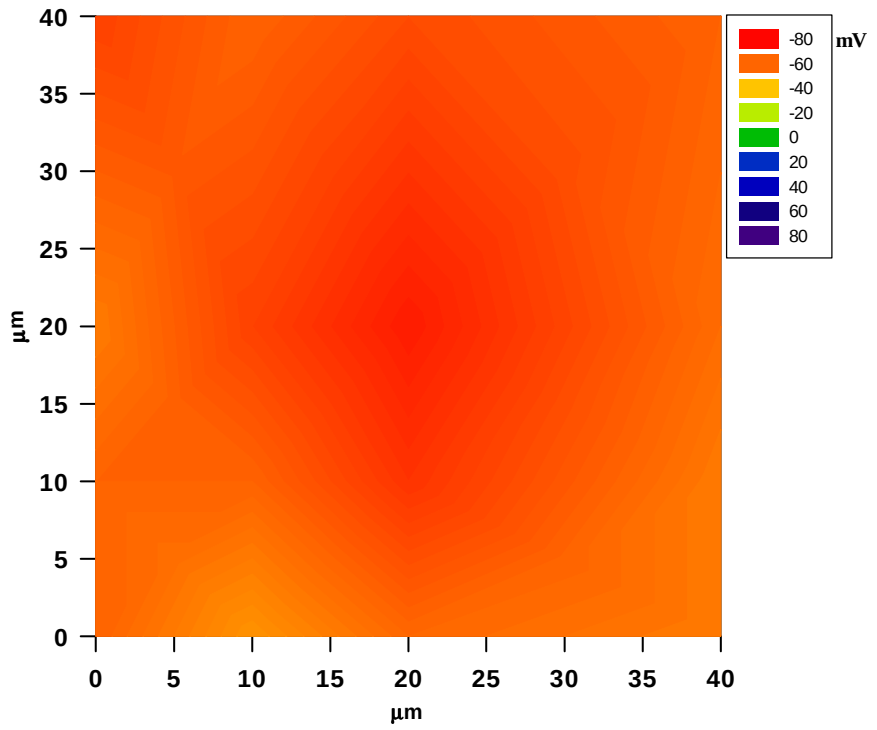

Figure 4.10. Surface potential was calculated by analysis of force-distance curves (Sapphire surface-quartz colloid probe; k=2.06 N/m; 10^{-3} M KCl solution; pH=10; T=20 ^{o}C)

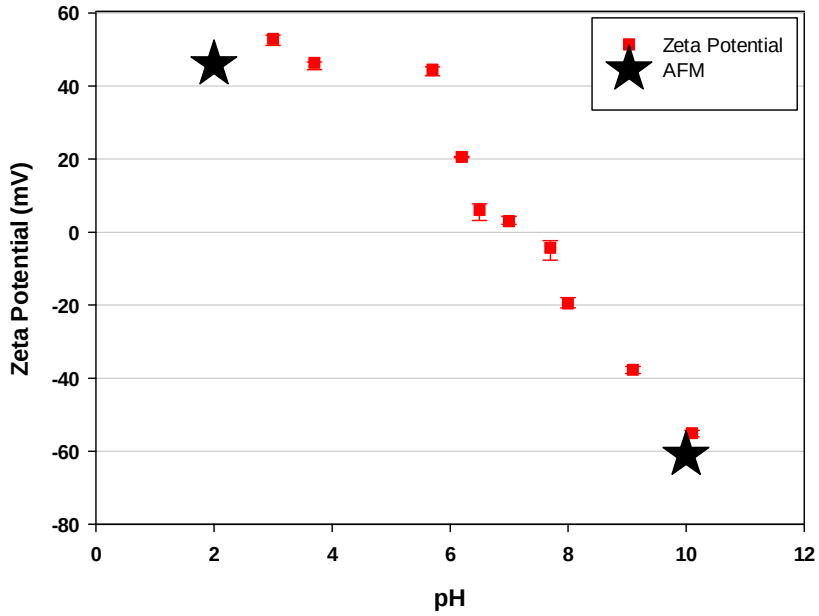

Figure 4.11. Comparison of average surface charges from sapphire surface charge maps with zeta potential measurements

CHAPTER 5

CONCLUSION

In this study, Atomic Force Microscopy (AFM) which is generally used in determining the overall topography of the surface was used in order to develop a potential map of the surfaces. One of the surfaces was the substrate whose potential was aimed to be determined. The other was a colloid probe particle created as part of this work from a spherical particle of any material of interest. In this work, quartz and sapphire single crystals were used as substrates. Spherical silica particles were employed as colloid probes.

AFM was used to measure the actual nanonewton level forces between the substrates and colloid probes. The measured force curves between the substrate and the colloid probe particle were then employed to determine the potential of surface at the points of measurement by a careful analysis of the present theories. When the force measurement was repeated on selected grid points on the surface, a potential map of the surface can be obtained after carrying out necessary analysis.

The actual act of measurement of the the force between the substrate and the colloid prob is possible only after a very long and tedious preparation processes which had to be followed in order to prove that such a potential map could be obtained. Characterization of the surfaces and powders to be used as substrates and colloid probes, isolation of colloid probe particles, preparationof colloid probes using a custom-made nanomanipulation system, a very through cleaning of the substrates and colloid probes, determining spring sonstant of cantilevers, developing of of transformation techniques to convert raw force signals to actual force-distance curves and developing and running the analytical solutions to analyze the measured force-distance curves were among in the details obtaining the surface potential maps.

The results show that the method was quite succesful in predicting the potential distribution on the alumina and quartz substrate surfaces at various solution conditions using quartz colloid probes. The experiments carried out at pH of 6 and 10 for the quartz-quartz case creates surface potential maps consistent with the known cases and aggree well with the surface-average zeta potential measurements. The same is true for

the sapphire-quartz system where the measured surface potential maps showed good aggrement with the surface-average zeta potential measurements.

This work showed that the potential distribution of flat metal oxide surfaces immersed in solution could be succesfully determined using selected probe material (colloid probes).

REFERENCES

Admatechs, http://www.admatechs.co.jp, **2011.**

Atkins, D.T., Ninham, B.W., Surface and structural forces measured between silica surfaces in 1,2-ethanediol, *Colloids and Surfaces A*, **1997**, 129-130, 23-32.

Bradley, R. S., The Cohesive Force between Solid Surfaces and the Surface Energy of Solids, *Philosophical Magazine*, **1932**, 13, 853-862.

Bhattacharjee, S., M. Elimelech, Surface Element Integration: A Novel Technique for Evoluation of DLVO Interaction between a Particle and a Flat Plate. *J. of Colloid and Interface Science*, **1997**, 193, 273-285.

Bhattacharjee, S., J. Chen, M. Elimelech, DLVO Interaction Energy between Spheroidal Particles and Flat Surface, *Colloids and Surfaces*, **2000**, 165, 143-156.

Barouch, E. and Matijevic, E., Double-layer interactions of unequal spheres. Part 1.The effect of electrostatic attraction with particles of like sign of potential, *J. of Chemical Society Faraday Trans. I.*, **1985**, 81, 1797-1817.

Chapman, D.L., A Contribution to the Theory Electrocapillarity, *The London, Edinburgh, and Dublin Philosophical Magazine and Journal of Science*, **1913**, 25, 475-481.

Casimir, H.B.G., Polder, D., The Influence of Retardation on the London- van der Waals Forces, *Physical Review*., **1948**, 73, 360-372.

Chan, D.Y.C, Pashley, R.M and White, L.R., A simple algorithm for the calculation of the electrostatic repulsion between identical charged surfaces in electrolyte, *J. Colloid Interface Science*, **1980**, 77, 283-285.

Chan, D.Y.C., Mitchell, D.J.J., The Free Energy of an Electrical Double Layer, *J. of Colloid and Interface Science*, **1983**, 95, 193-197.

Debye, P.J.W., van der Waals' Cohesive Forces, *Phys. Z.*, **1920**, 21, 178-187.

Debye, P.J.W., Hückel, E., Zur Theorie der Electrolyte. 1. Gefrierpunktserniedrigung und verwandte Erscheinugen, *Phys. Z.,* **1923**, 24, 185-206.

Derjaguin, B.V., Friction and adhesion. IV. The theroy of adhesion of small particles, *Kolloid-Z.* **1934**, 69, 155-164.

Derjaguin, B.V., L. Landau, Theory of the stability of strongly charged lyophobic sols and the adhesion of strongly charged particles in solution of electrolytes, *Physicochim USSR*, **1941**, 14, 633-662.

De Boer, J.H., The influence of van der Waals' forces and primary bonds on binding energy, strength and orientation, with special reference to some artificial resins, *Trans. Faraday Soc*., **1936**, 32, 10-37.

Dzyaloshinskii, I.E., Liftshitz, E.M., Pitaevski, L.P., The general theory of van der Waals forces, *Advances in Physics*, **1961**, 10, 165-209.

Dzombak, D.A. and Morel, F.M.M., Surface complexation modeling: Hydrous ferric oxide, **1990**, John Wiley and Sons, New York.

Eisenchitz, R. and London, F., U ber das Verhaltnis der van der Waalsschen Krafte zu den homöopolaren Bindungskraften, *Phys. Z*., **1930**, 60,491-527.

Franks, G.V., Meagher, L., The Isoelectric Points of Sapphire Crystals and Alpha-Alumina Powder, *Colloids and Surfaces A*, **2003**, 214, 99-110.

Fowkes, F.M., Surfaces and Interfaces, **1967**, Ed. J.J. Burke, Syracuse Univ. Press, New York

Gregory, J., The Calculation of Hamaker Constant, *Advances in Colloid Interface Science*, **1969**, 2, 396-417.

Gouy, L.G., Sur la constitution de la charge electrique a la `surface d'un electrolyte, *J. of Physics Radium*, **1910**, 9, 457-468.

Gouy G., Sur la constitution de la charge electrique a la `surface d'un electrolyte, *Comptes Rendus of the French Academy of Sciences*, **1910**, 149, 654-657.

Yelken, G., Estimation of the Surface Charge Distribution of Solids in Liquids by using Atomic Force Microscopy, **2011**, Izmir Institude of Technology, Departmant of Chemical Engineering, Izmir

Hamaker, H.C., The London – van der Waals attraction between spherical particles, *Physica,* **1937**, 4, 1058-1072.

Holmberg K., Surfactants and polymers in aqueous solution, **2002**, John Wiley and Sons, New York.

Hogg, R., Healy, T.W., Fuerstenau, D.W., Mutual coagulation of colloidal dispersions, Trans. Faraday Soc., **1966**, 62, 1638-1651.

Israelachvili, J.N., D. Tabor, The Measurement of Van der Waals Dispersion Forces in Range 1.5 to 130nm, *Proceeeding of the Royal Society A*, **1972**, 331, 19-38.

Israelachvili, J.N. and Ninham, B.W., Intermolecular forces-the long and short of it, *J. of Colloid Interface Science*, **1977**, 58, 14-25.

Keesom, W.H., Die van der waalsschen Kohäsionskräfte, *Phys. Z.,* **1921**, 22, 129-643.

Kosmulski, M., Surface Charging and Point Zero Charge, **2009**, CRC Press Taylor and Francis group., Florida.

Krupp, H., Particle Adhesion: Theory and Experiment, *Advan. Colloid Interface Sci.*, **1967**, 1, 111-239.

Levine, I.A, Physical Chemistry, 4th Ed., **1995**, McGraw Hill, Inc., New York.

Liftshitz, E.M., The Theory of Moleculer Attractive Forces between Solids, *Soviet Physics*, **1956**, 2, 73-83.

Lennart Bergström, Hamaker constants of inorganic materials, *Advances in Colloid and Interface Science*, **1997**, 70, 125-169.

Moelwyn-Hughes, E.A., Physical Chemistry, **1961**, 2nd Ed., Pergamon Press, London.

Mtixtl, MTI Corparation, http://mtixtl.com/crystalssubstratesa-z.aspx, **2011**.

Nanoworld Catalog, http://www.nanoworld.com/silicon-nitride-afm-tips, **2011.**

Ohler, B, Cantilever spring constant calibration using laser Doppler vibrometry, *Rewiew of Scientific Instruments*, **2007**, 78, 063701

Overbeek, J. Th. G., in Colloid Science., **1952**, Ed. H.R. Kruyt,1, Elsevier, Amsterdam

Polat, M. A Review of the Interactions between Particles Dispersed in Aqueous Media, I: The Electrical Double Layer. *J. of Ore Dressing*, **1999**, 2, 7-35.

Polat, M., Polat H., A Review of the Theory of Interactions between Particles Dispersed in Aqueous Media, II. Van der Waals Interactions, *J. of Ore Dressing*, **2000-a**, 3, 21-48.

Polat, M., Polat H., A Review of the Theory of Interactions between Particles Dispersed in Aqueous Media, III. Electrostatic and Structural Interactions and the DLVO Theory. *J. of Ore Dressing*, **2000-b**, 4, 1-21.

Polat M., Sato K., Nagaoka T., Watari K., Effect of pH and Hydration on the Normal and Lateral Interaction Forces between Alumina Surfaces, *Journal of Colloid and Interface Science*, **2006**, 304, 378–387.

Polat H., Kes M., Kelesoglu S., Polat M., Aksoy G., Determination of the particle interactions, rheology and the surface roughness relationship for dental restorative ceramics, *Journal of the European Ceramic Society*, **2009**, 29, 2959–2967.

Polat,M., Polat H., Analytical solution of Poisson-Boltzmann equation for interacting plates of arbitrary potentials and same sign, *Journal of Colloidal and Interface Science*, **2010**, 341, 1, 178-185.

Pugh, R. J., Bergstrom, L., Surface and colloid chemistry in advanced ceramic processing, **1994**, 51,363, Marcel Dekker Inc. New York.

Renne, M.J., Nijboer, B.R.A., Microscopic derivation of macroscopic Van der Waals forces, Chem. Phys. Letters, **1967**, 1, 317-320.

Slater, J.C. and Kirkwood, J.G., The van der waals Forces in Gases, *Physical Review*., **1931**, 37, 682-697.

Verwey, E.J.W., J.T.G. Overbeek, Theory of Stability of Lyophobic Colloids, **1948**, Elsevier, Amsterdam.

Visser, J., On Hamaker constants: Comparison between Hamaker constants and Lifshitz-van der Waals constants, *Advances in Colloid and Interface Science*., **1972**, 3, 331-363.

Wikipedia, http://simple.wikipedia.org/wiki/Atomic_force_microscope, **2012**.

APPENDIX A

A COMPILATION OF HAMAKER CONSTANTS

Table A.1. A Compilation of Hamaker Constants ($x10^{-20}$ J)
(Source: Polat and Polat, 2000-a)

Material	Hamaker Constant	Reference	Method
Water	5.47 $^{(1v1)*}$	Visser, 1975	L
	4.38 $^{(1v1)}$	Krupp et al., 1972	L
	4.35 $^{(1v1)}$	Bargeman and Voorst Vader, 1972	
	3.70 $^{(1v1)}$	Hunter, 1992	L
Ionic compounds			
Sb_2S_3	18-24 $^{(1w1)}$	Daluya and Srivastava, 1967	CC
AgI	15.8 $^{(1v1)}$/2.75 $^{(1w1)}$	Lyklema, 1967	MicA
	3.1-4.4 $^{(1w1)}$	Mathai and Ottewill, 1966	CC
ThO_2	10 $^{(1w1)}$	Rastogi and Srivastava, 1969	
Kaolinite	20 $^{(1w1)}$	Hunter and Alexander, 1973	CC
	10-70 $^{(1w1)}$	Ottewill and Rastogi, 1960	
MgO	11.6 $^{(1v1)}$/1.80 $^{(1w1)}$	Visser, 1975	L
	10.6 $^{(1v1)}$	Böhme et al., 1969	L
	1.76 $^{(1w1)}$	Krupp, et al., 1972	L
Al_2O_3	17.91 $^{(1v1)}$/4.44 $^{(1w1)}$	Visser, 1975	L
	15.5 $^{(1v1)}$	Böhme et al., 1969	L
	15.4 $^{(1v1)}$	Bargeman and Voorst Vader, 1972	
	4.17 $^{(1w1)}$	Krupp, et al., 1972	L
$Al(OH)_3$	12.6 $^{(1w1)}$	Zimon, 1969	
SiO_2	8.55 $^{(1v1)}$	Büttner and Gerlach, 1970	MacA
	16.4 $^{(1v1)}$	Fowkes, 1967	ST
	50 $^{(1v1)}$	Jongh, 1958	MicA
	0.2-0.94 $^{(1w1)}$	Watillon and Gerard, 1964	MicA
	1.7 $^{(1w1)}$	Fowkes, 1967	ST
Quartz	8.0-18.6 $^{(1v1)}$	Gregory, 1970	MacA
	8.83 $^{(1v1)}$/1.70$^{(1w1)}$	Hunter, 1992	MacA
	1.2-5.6 $^{(1w1)}$	Gregory, 1970	MacA
Mica	2.0-2.1 (1w1)	Hunter, 1992	MacA
Sapphire	15.6 (1v1)/5.32 (1w1)	Hunter, 1992	MacA
Calcite	10.1 (1v1)/2.23 (1w1)	Hunter, 1992	MacA
CaF	7.20 (1v1)/1.04 (1w1)	Hunter, 1992	MacA
TiO2 (anatase)	19.7 (1v1)	Fowkes, 1967	ST
	2.5 (1w1)	Fowkes, 1967	ST
TiO2 (rutile)	31.0 (1v1)	Fowkes, 1967	ST
	5.9 (1w1)	Fowkes, 1967	ST

The values in the table for a given material are listed from more reliable ones down to less accurate ones. (1v1): Interaction in vacuum; (1w1): Interaction in water; CC: Colloid Chemistry; MicA: Microscopic Approach; MacA: Macroscopic Approach; ST: Surface Tension; L: Liftshitz Formula

(cont. on next page)

Table A.1. (cont.)

Material	Hamaker Constant	Reference	Method
Fe2O3	23.2 (1v1)/3.4 (1w1)	Fowkes, 1967	ST
Fe(OH)3	65 (1v1) 180 (1v1) 17.7-20.0 (1w1)	Jain and Srivastava, 1969 Jain and Srivastava, 1969 Zimon, 1969	MicA MicA
CdS	16.8 (1v1)/ 5.24 (1w1) 15.3 (1v1) 4.85 (1w1)	Visser, 1975 Böhme et al., 1969 Krupp, et al., 1972	L L L
SnO2	25.6 (1v1)/4.3 (1w1)	Fowkes, 1967	ST
KCl	6.2 (1v1) 0.31 (1w1)	Böhme et al., 1969 Krupp, et al., 1972	L L
KBr	7.15 (1v1)/0.69 (1w1) 6.7 (1v1) 0.54 (1w1)	Visser, 1975 Böhme et al., 1969 Krupp, et al., 1972	L L L
CaO	12.4 (1v1)	Büttner and Gerlach, 1970	MacA
KI	6.3 (1v1)	Böhme et al., 1969	L
CaF2	6.55 (1v1)	Büttner and Gerlach, 1970	MacA
BaSO4	16.4 (1v1)/1.7 (1w1)	Fowkes, 1967	ST
Elements			
Carbon	21.7 (1v1)	Marshall, 1964	MicA
Graphite	47.0 (1v1) 3.7 (1w1)	Böhme et al., 1969 Fowkes, 1967	L ST
Diamond	32.9 (1v1)/ 15.1 (1w1) 28.4 (1v1) 13.9 (1w1)	Visser, 1975 Böhme et al., 1969 Krupp, et al., 1972	L L L
Hg	43.4 $^{(1v1)}$/10.5 $^{(1w1)}$	Fowkes, 1967	ST
Pt	8-16 $^{(1w1)}$	Derjaguin et al., 1969	CC
Au	54.7 $^{(1v1)}$/ 37.7 $^{(1w1)}$ 45.5 $^{(1v1)}$ 45.3 $^{(1v1)}$ 33.4 $^{(1w1)}$	Visser, 1975 Böhme et al., 1969 Bergeman and Voorst Vader, 1972 Krupp, et al., 1972	L L L
Ag	44.7 $^{(1v1)}$/ 29.7 $^{(1w1)}$ 40 $^{(1v1)}$ 39.8 $^{(1v1)}$	Visser, 1975 Krupp, et al., 1972 Bargeman and Voorst Vader, 1972	L L
Cu	30.7 $^{(1v1)}$/ 17.9 $^{(1w1)}$ 28.4 $^{(1v1)}$/17.5 $^{(1w1)}$	Visser, 1975 Krupp, et al., 1972	L L
Si	25.9 $^{(1v1)}$/ 13.4 $^{(1w1)}$ 25.6 $^{(1v1)}$/13.4 $^{(1w1)}$	Visser, 1975 Krupp, et al., 1972	L L
Ge	32.0 $^{(1v1)}$/ 17.8 $^{(1w1)}$ 30.0 $^{(1v1)}$/17.7 $^{(1w1)}$	Visser, 1975 Krupp, et al., 1972	L L
Te	14.0 $^{(1v1)}$/5.38 $^{(1w1)}$	Krupp, et al., 1972	L

The values in the table for a given material are listed from more reliable ones down to less accurate ones. (1v1): Interaction in vacuum; (1w1): Interaction in water; CC: Colloid Chemistry; MicA: Microscopic Approach; MacA: Macroscopic Approach; ST: Surface Tension; L: Liftshitz Formula

(cont. on next page)

Table A.1. (cont.)

Material	Hamaker Constant	Reference	Method
Fe	21.2 $^{(1v1)}$/29 $^{(1w1)}$	Fowkes, 1967	ST
Pb	21.4 $^{(1v1)}$/30 $^{(1w1)}$	Fowkes, 1967	ST
Sn	21.8 $^{(1v1)}$/31 $^{(1w1)}$	Fowkes, 1967	ST
Hydrocarbons			
Pentane	3.75 $^{(1v1)}$/0.34 $^{(1w1)}$	Hunter, 1992	MacA
Hexane	4.07 $^{(1v1)}$/0.36 $^{(1w1)}$	Hunter, 1992	MacA
Heptane	4.32 $^{(1v1)}$/ 0.39 $^{(1w1)}$ 3.6 $^{(1v1)}$	Hunter, 1992 Crowl, 1967	MacA MicA
Octane	4.50 $^{(1v1)}$/ 0.41 $^{(1w1)}$ 4.6 $^{(1v1)}$ 0.69 $^{(1w1)}$	Hunter, 1992 Duyvis, 1962 Sonntag, 1967	MacA CC CC
Nonane	4.66 $^{(1v1)}$/0.44$^{(1w1)}$	Hunter, 1992	MacA
Decane	4.82 $^{(1v1)}$/ 0.46 $^{(1w1)}$ 5.0 $^{(1v1)}$ 4.6 $^{(1v1)}$ 5.8 $^{(1v1)}$ .0.4 $^{(1w1)}$ 0.55-0.61 $^{(1w1)}$	Hunter, 1992 Crowl, 1967 Walbridge and Waters, 1966 Gregory, 1970; Clunie et al., 1970 Visser, 1972 Parsegian and Ninham, 1971	MacA MicA MicA MicA CC MacA
Undecane	4.88 $^{(1v1)}$/0.47 $^{(1w1)}$	Hunter, 1992	MacA
Dodecane	5.04 $^{(1v1)}$/0.50 $^{(1w1)}$	Hunter, 1992	MacA
Tridecane	5.05 $^{(1v1)}$/0.50 $^{(1w1)}$	Hunter, 1992	MacA
Tetradecane	5.10 $^{(1v1)}$/0.51 $^{(1w1)}$	Hunter, 1992	MacA
Pentadecane	5.16 $^{(1v1)}$/0.53 $^{(1w1)}$	Hunter, 1992	MacA
Hexadecane	5.23 $^{(1v1)}$/0.54 $^{(1w1)}$	Hunter, 1992	MacA
Octadecane	0.4 $^{(1w1)}$	Visser, 1972	CC
Benzene	23 $^{(1v1)}$ 0.04 $^{(1w1)}$	Parfitt and Willis, 1966 Albers and Overbeek, 1960	MicA
Toluene	10 (1v1) 5.4 (1v1)	Jain and Srivastava, 1969 Croucher and Hair, 1977	MicA
Chlorobenzene	58 (1v1)	Sheludko et al., 1965	ST
CCl_4	37.7-57.0 (1v1)	Sheludko et al., 1965	CC,ST
Acetone	4.2 (1v1)	Croucher and Hair, 1977.	
Aniline	66.0 (1v1)	Sheludko1966, Sheludko et al., 1965	CC
Polymers			
PVC	7.78 (1v1)/1.30 (1w1)	Hunter, 1992	MacA
PVA	8.84 (1v1)/0.54 (1w1)	Dunn, 1970	MicA
PMMA	6.3 (1v1) 7.11 (1v1)/ 1.05 (1w1) 0.72-6.2 (1w1)	Dunn, 1970 Hunter, 1992 Friend and Hunter, 1971	MicA MacA
Polystyrene	7.31 (1v1)/ 0.42 (1w1) 6.58 (1v1)/0.95 (1w1) 6.5 (1v1)/ 0.35 (1w1) 7.8-9.8 (1v1)	Visser, 1975 Hunter, 1992 Krupp et al., 1972 Croucher and Hair, 1977	L L MacA

The values in the table for a given material are listed from more reliable ones down to less accurate ones. (1v1): Interaction in vacuum; (1w1): Interaction in water; CC: Colloid Chemistry; MicA: Microscopic Approach; MacA: Macroscopic Approach; ST: Surface Tension; L: Liftshitz Formula

(cont. on next page)

Table A.1. (cont.)

Material	Hamaker Constant	Reference	Method
PVF	21.8 (1v1)	Marshall, 1964	MicA
PE	10.0 (1v1)/0.4 (1w1)	Fowkes, 1967	ST
PTFE	3.80 (1v1)/ 0.33 (1w1) 5.6 (1v1)/0.04 (1w1)	Hunter, 1992 Fowkes, 1967	MacA ST
Various Resins	6.4-7.5 (1v1)	Crowl, 1967	
DMMA	9-10 (1w1)	Neiman et al., 1969	CC
Cellophane	45.4 (1v1)	Marshall, 1964	MicA

The values in the table for a given material are listed from more reliable ones down to less accurate ones. (1v1): Interaction in vacuum; (1w1): Interaction in water; CC: Colloid Chemistry; MicA: Microscopic Approach; MacA: Macroscopic Approach; ST: Surface Tension; L: Liftshitz Formula

APPENDIX B

ANALIYTICAL FORCE CALCULATIONS FOR CONSTANT SURFACE POTENTIAL AND CONSTANT CHARGE SYSTEM

B.1. Arbitrarily Charged Plates of Same Sign-Constant Potential

Co: solution electrolyte concentration,

ψ_{1i}: solid surface zeta potential (potential on the solid surface at infinite separation between the probe and the surface),

ψ_{2i}: probe surface zeta potential (potential on the probe surface at infinite separation between the probe and the surface),

A_{123}: Hamaker constant between the probe and the surface separated by water,

z: electrolyte valence taken as 1 for a simple electrolye of type KCl,

Real constant in equations:

$$\varepsilon = 78$$

$$\varepsilon = (8.854.10^{-12}\frac{C^2}{J.m})$$

$$T = 293K$$

$$F = 96484.5\frac{C}{mol}$$

$$R = 8.31441\frac{J}{mol.K}$$

Constants entered in equations:

$$z = 1$$

$$C_0 = 0.1\frac{mol}{m^3}$$

$$\kappa = (\frac{2z^2F^2C_0}{\varepsilon\varepsilon_0 RT})^{0.5}$$

Setting the parameters for a specific point on the surface (Ψ_{01} is varied to correct charge on the solid surface).

Enter the relevent parameters for that location.

$$\psi_{1i} = 0.055V$$

$$\psi_{2i} = 0.03V$$

$$A_{121} = 1.02.10^{-20} J$$

$$r = 6.10^{-6} m$$

Outputs:

$$Y_{1i} = \frac{zF\psi_{1i}}{RT}$$

$$Y_{2i} = \frac{zF\psi_{2i}}{RT}$$

$$S_{1i} = (2\cosh.(Y_{1i}) - 2)^{0.5}$$

$$S_{2i} = (2\cosh.(Y_{2i}) - 2)^{0.5}$$

$$\sigma_{1i} = \sqrt{2\varepsilon\varepsilon_0 RTC_0}.S_1$$

$$\sigma_{2i} = \sqrt{2\varepsilon\varepsilon_0 RTC_0}.S_2$$

$$\sigma_{1i} = \sqrt{8C_0 RT\varepsilon\varepsilon_0}(\cosh.(\frac{zF\psi_{1i}}{RT}) - 1)$$

$$\sigma_{2i} = \sqrt{8C_0 RT\varepsilon\varepsilon_0}(\cosh.(\frac{zF\psi_{2i}}{RT}) - 1)$$

$$p = 2RTC_0(\cosh.(\frac{zF\psi_{2i}}{RT}) - 1)$$

$$P = \frac{p}{2RTC_0}$$

Procedure:

1-Initially specific location on the surface is selected for probing and probe is located at that point.

2-The probe potential Ψ_{2i} is set to the zeta potential at that pH for the probe particles.

3-Solid surface potential Ψ_{1i} is varied by the user for that location until theoretical and experimental curves coincide.

4- Thus Ψ_{1i} is the surface potential of the solid at that location.

5-The probe is moved to a new location and 1-4 is repeated T.

Notes:

i) Hamaker constant is assumed the same in all calculations.

ii) Probe surface potential Ψ_{2i} considered constant at zeta potential the particle probes different parts of the surface for constant potential surfaces (σ_{2i} is considered unchanged for constant charge surfaces).

Running the algorithm to find S vs H and P vs H curves for the selected location.

Vary S_2 from S_{2f} to calculate corresponding H values (S_{2f} is a sufficiently large value).

$$S_{2f} = -20$$

$$\delta = \frac{S_{2i} - S_{2f}}{300}$$

$$S_2 = S_{2i} - \delta, S_{2i} - 2\delta .. S_{2f}$$

Calculate S_2.

$$\phi(Y_2) = S_2^{\,2} - 2\cosh(Y_{2i})$$

$$S_1(S_2) = (2\cosh(Y_{1i}) + \phi(S_2))^{0.5}$$

Calculate the X_m, X_{mp} and H values (S_2).

Note that the H is calculate from the distance of the left (X_m) and right (X_{mp}) hand surfaces from the middle point.

$$X_{mp}(S_z) = \mathrm{Re}\left[\int_0^1 \frac{S_2}{\sqrt{u\left[(S_2^{\,2}u - \phi(S_2))^2 - 4\right]}}\right].du$$

$$X_m(S_z) = \mathrm{Re}\left[\int_0^1 \frac{S_2}{\sqrt{u\left[(S_2{}^2 u - \phi(S_2))^2 - 4\right]}}\right].du$$

$$H(S_2) = X_m(S_2) + X_{mp}(S_2)$$

Calculate the electrostatic pressure.

$$P_e(S_2) = \cosh(Y_{2i}) - 1 - 0.5S_2^2$$

$$p_e(S_2) = 2RTC_0 P_e(S_2)$$

$$\sigma_2(S_2) = \sqrt{2\varepsilon\varepsilon_0 RTC_0}.S_2$$

$$\sigma_1(S_2) = \sqrt{2\varepsilon\varepsilon_0 RTC_0}.S_1(S_2)$$

$$h(S_2) = \frac{H(S_2)}{\kappa}$$

Calculate the van der Waals pressure.

$$p_{vdW}(S_2) = \frac{-A_{121}}{6\pi h(S_2)^3}$$

Calculate the overall pressure curve as a function of plate separation.

$$p_T(S_2) = p_{vdW}(S_2) + p_e(S_2)$$

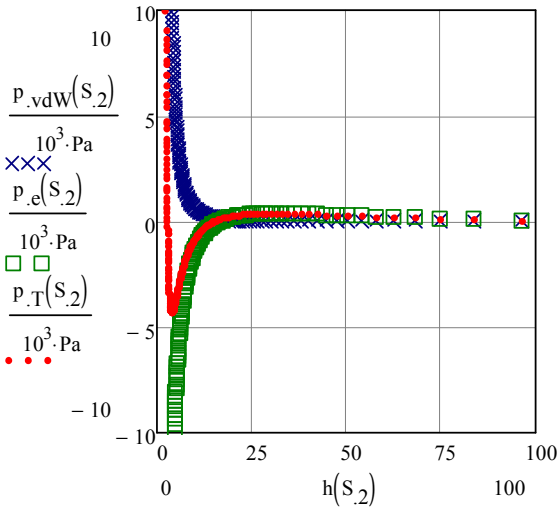

Convert from pressure to force using Derjaguin Approach.

$$F_T(S_2) = 2\pi r \int_{h(S_2)}^{100h(S_2)} p_T(S_2)dh(S_2)$$

B.2. Arbitrarily Charged Plates of Same Sign-Constant Charge

Enter the surface potentials at finite seperation for both the solid and the probe surface (zeta potential).

Note that for constant charge case, these potentials will be different for diffrent h values.

$Y_{1i} = 2.178$

$Y_{2i} = 1.188$

Calculate the surface charges at infinite separation.

Note that for constant charge case, these charges will be constant for all h values.

$S_{1i} = 2.635$

$S_{2i} = 1.259$

Start varying the Y values from an initial to a final surface potential to calculate corresponding H values. Note that the initial surface potential is equal to the surface potential at infinite separation. The final surface potential is sufficiently large value.

$Y_{2f} = -20$

$$\delta = \frac{Y_{2i} - Y_{2f}}{300}$$

$$Y_2 = Y_{2i} - \delta, Y_{2i} - 2\delta..Y_{2f}$$

Calculate f (Y_2)

$$\phi(Y_2) = S_{2i}{}^2 - 2\cosh(Y_2)$$

$$Y_1(Y_2) = a\cosh(\frac{S_{1i}{}^2}{2} - \frac{S_{2i}{}^2}{2} + \cosh(Y_2))$$

Calculate the X_m, X_{mp} and H values (Y_2)

Note that the H is calculate from the distance of the left (X_m) and right (X_{mp}) hand surfaces from the middle point.

$$X_m(Y_z) = \mathrm{Re}\left[\int_0^1 \frac{S_{1i}}{\sqrt{u\left[(S_{1i}{}^2 u - \phi(Y_2))^2 - 4\right]}}\right].du$$

$$X_{mp}(Y_z) = \mathrm{Re}\left[\int_0^1 \frac{S_{2i}}{\sqrt{u\left[(S_{2i}{}^2 u - \phi(Y_2))^2 - 4\right]}}\right].du$$

$$H(Y_2) = X_m(Y_2) + X_{mp}(Y_2)$$

Calculate the dimensionless electrostatic pressure.

$$P_e(Y_2) = \cosh(Y_2) - 1 - 0.5S_{2i}{}^2$$

Calculate the real potentials, charges and electrostatic pressure.

$$\sigma_{1i} = 4.041.10^{-3}\frac{C}{m^2}$$

$$\sigma_{2i} = 9.229.10^{-4}\frac{C}{m^2}$$

$$\psi_1(Y_2) = \frac{Y_1(Y_2)RT}{zF}$$

$$\psi_2(Y_2) = \frac{Y_2 RT}{zF}$$

$$P_e(Y_2) = 2RTC_0P_e(Y_2)$$

$$h(Y_2) = \frac{H(Y_2)}{\kappa}$$

8-Calculate the van der Waals pressure.

$$p_{vdW}(Y_2) = \frac{-A_{121}}{6\pi h(Y_2)^3}$$

9-Calculate the overall pressure curve as a function of plate separation.

$$p_T(Y_2) = p_{vdW}(Y_2) + p_e(Y_2)$$

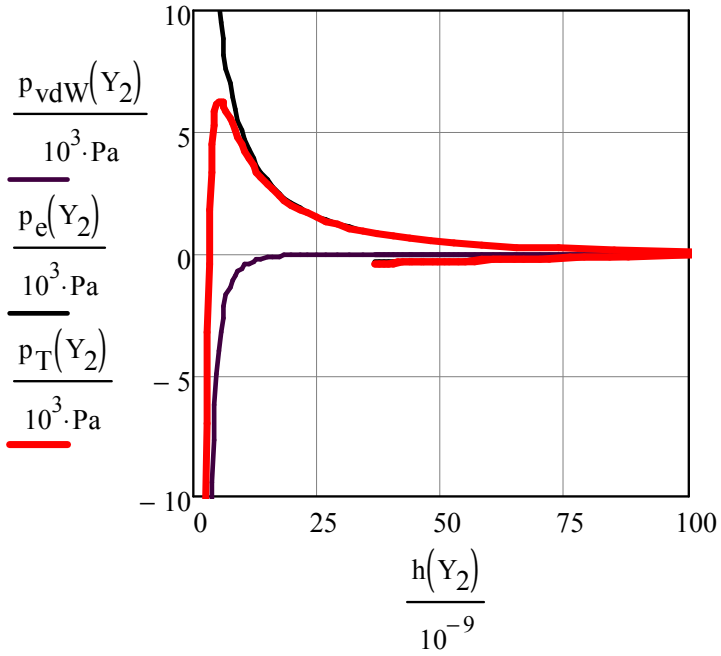

10-Convert from pressure to force using Derjaguin Approach

$$F(Y_2) = 2\pi r \int_{h(Y_2)}^{100h(Y_2)} p_T(Y_2)dh(Y_2)$$

APPENDIX C

THEORETICAL FORCE CALCULATION FOR CONSTANT SURFACE POTENTIAL / CHARGE SYSTEM FOR LOW POTENTIAL CASE

$$R = 8.31441 \frac{J}{mol.K}$$

$$C_0 = 0.1 \frac{mol}{m^3}$$

$$A_{121} = 1.02.10^{-20} J$$

$$r = 6.10^{-6} m$$

$$\kappa = (\frac{2z^2F^2C_0}{\varepsilon\varepsilon_0 RT})^{0.5}$$

$$h = .1.10^{-9}.m,.2.10^{-9}\, m..H$$

$$H = 100.10^{-9}\, m$$

$$\sigma_1 = \varepsilon\varepsilon_0 \kappa\psi_1$$

$$\sigma_2 = \varepsilon\varepsilon_0 \kappa\psi_2$$

$$\mathrm{F_{cp}(h)} = \frac{-\varepsilon\varepsilon_0 \kappa^2}{2}\left(\frac{\psi_1^2 + \psi_2^2 - 2\psi_1\psi_2 \cosh(\kappa h)}{\cosh(\kappa h)^2 - 1}\right)$$

$$\mathrm{F_{cc}(h)} = \frac{-1}{2\varepsilon\varepsilon_0}\left(\frac{2\sigma_1\sigma_2 \cosh(\kappa h) + (\sigma_1^2 + \sigma_2^2)}{\sinh(\kappa h)^2}\right)$$

$$F_{vdW}(h) = \frac{A}{6\pi h^3}$$

$$F_{Tcp}(h) = F_{cp}(h) + F_{vdW}(h)$$

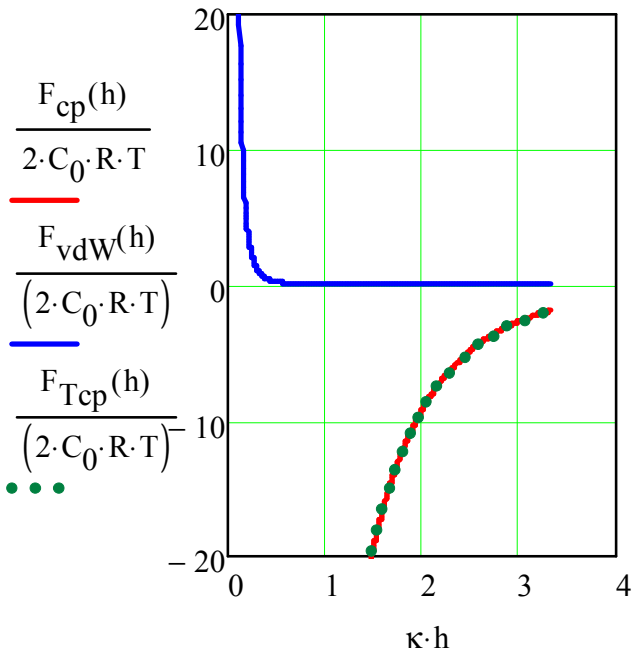

$$F_{Tcc}(h) = F_{cc}(h) + F_{vdW}(h)$$

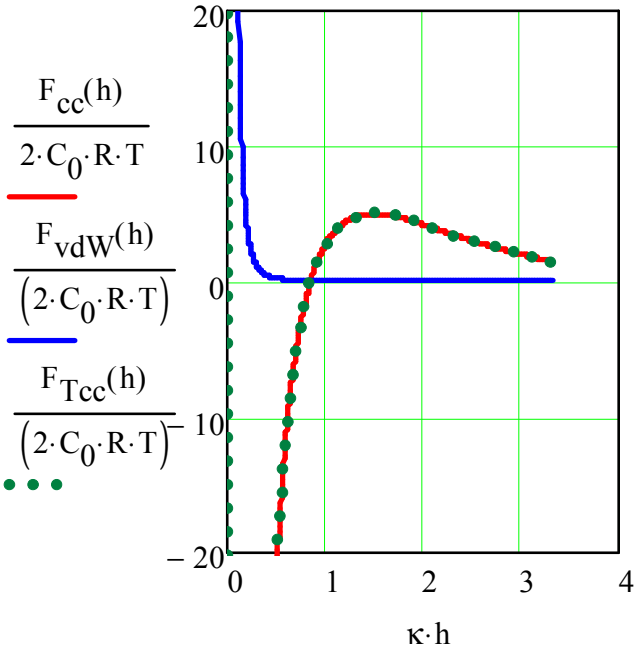

$$F_{TCP}(h) = 2\pi r \int_{h}^{100h} F_{Tcp}(h)dh$$

$$F_{TCC}(h) = 2\pi r \int_{h}^{100h} F_{Tcc}(h)dh$$